Functional and Structural Analysis of the *C. elegans* PAXT-1 – XRN2 Complex

Inauguraldissertation

zur

Erlangung der Würde eines Doktors der Philosophie vorgelegt der

Philosophisch-Naturwissenschaftlichen Fakultät

der Universität Basel

von

Hannes Richter

aus Tettau, Deutschland

Basel, 2015

Genehmigt von der Philosophisch-Naturwissenschaftlichen Fakultät

auf Antrag von Prof. Dr. Mihaela Zavolan, Dr. Helge Großhans, Prof. Dr. Gunter Meister

Basel, den 21.04.2015

Prof. Dr. Jörg Schibler
Dekan

Namensnennung-Keine kommerzielle Nutzung-Keine Bearbeitung 3.0 Schweiz
(CC BY-NC-ND 3.0 CH)

Sie dürfen: **Teilen** — den Inhalt kopieren, verbreiten und zugänglich machen

Unter den folgenden Bedingungen:

Namensnennung — Sie müssen den Namen des Autors/Rechteinhabers in der von ihm festgelegten Weise nennen.

Keine kommerzielle Nutzung — Sie dürfen diesen Inhalt nicht für kommerzielle Zwecke nutzen.

Keine Bearbeitung erlaubt — Sie dürfen diesen Inhalt nicht bearbeiten, abwandeln oder in anderer Weise verändern.

Wobei gilt:

- **Verzichtserklärung —** Jede der vorgenannten Bedingungen kann **aufgehoben** werden, sofern Sie die ausdrückliche Einwilligung des Rechteinhabers dazu erhalten.
- **Public Domain (gemeinfreie oder nicht-schützbare Inhalte) —** Soweit das Werk, der Inhalt oder irgendein Teil davon zur Public Domain der jeweiligen Rechtsordnung gehört, wird dieser Status von der Lizenz in keiner Weise berührt.
- **Sonstige Rechte —** Die Lizenz hat keinerlei Einfluss auf die folgenden Rechte:
    - Die Rechte, die jedermann wegen der Schranken des Urheberrechts oder aufgrund gesetzlicher Erlaubnisse zustehen (in einigen Ländern als grundsätzliche Doktrin des **fair use** bekannt);
    - Die **Persönlichkeitsrechte** des Urhebers;
    - Rechte anderer Personen, entweder am Lizenzgegenstand selber oder bezüglich seiner Verwendung, zum Beispiel für **Werbung** oder Privatsphärenschutz.
- **Hinweis —** Bei jeder Nutzung oder Verbreitung müssen Sie anderen alle Lizenzbedingungen mitteilen, die für diesen Inhalt gelten. Am einfachsten ist es, an entsprechender Stelle einen Link auf diese Seite einzubinden.

Quelle: http://creativecommons.org/licenses/by-nc-nd/3.0/ch/ Datum: 12.11.2013

Acknowledgement

I thank my girlfriend Anna for her continuous support during the ups and downs of PhD life. Her love and kindness energizes and motivates me in pursuing challenging projects.

I would express my deep gratitude to my PhD advisor Dr. Helge Großhans for giving me the opportunity to grow as an independent scientist, offering freedom and support to pursue own ideas as well as challenge obtained results to excel in my field of study.

I am very grateful to Dr. Heinz Gut for introducing me to the secrets of protein crystallography, his personal and scientific motivation as well as his support to push me and my project to make a contribution to the protein crystallography community.

I would like to thank Dr. Iskra Katic and the worm facility to help me with the genetic manipulations of *C. elegans* in the last stages of my project as well as her support during the paper writing process.

I thank Jeremy Keusch for his support and help with protein purification and handling of the facility equipment.

I wish to thank Dr. Daniel Hess for the many mass spectrometry runs he conducted, especially one run, which helped to identify a protease cleavage site in XRN2, which subsequently led to a crystallizable construct design.

I thank my parents, my family and my friends for their love and support and to be there in difficult moments as well as sharing wonderful happy times. Furthermore I would like to thank my brother Stephan for proof reading my thesis manuscript.

Finally, I thank my lab mates for the enjoyable lab atmosphere, the FMI support infrastructure and the IT department for the opportunity to help setting up cloud-based services.

Abstract

XRN2 is an essential nuclear 5′→ 3′ exoribonuclease that is involved in quality control, processing and degradation of RNAs, such as rRNA, snRNA and miRNAs. Recently, *C. elegans* XRN2 was discovered to exist in a stable complex with PAXT-1. Binding to XRN2 is mediated by PAXT-1's DUF3469/XRN2 binding domain (XTBD). Whereas binding of the XTBD confers stability on XRN2 similar to observations made for yeast Rai1 – Rat1 complexes, kinetic analysis using the Michaelis-Menten model does not show any contributions to catalytic activity by PAXT-1. However, XRN2 alone processively degrades small RNAs, like its paralog XRN1, but shows no release activity for miRNAs off AGO, even when bound to PAXT-1. Here we show the XTBD to be a general binding domain for 5′→ 3′ exoribonucleases 2 and present the crystal structure of the XTBD – XRN2 complex. Whereas the XTBD serves as a general adapter to XRN2, XRN1 binding is excluded due to sterical hindrance. Strikingly, a single point mutation in PAXT-1 Tyr56 completely abrogates binding to XRN2 *in vitro* and *in vivo*. Using CRISPR to generate endogenous PAXT-1 Tyr56 to Ala mutations, phenotypes identical to *paxt-1* null mutant worms are observed. Remarkably, *paxt-1*null mutant worms can be rescued by an unrelated XTBD-containing protein from humans, CDKN2AIPNL, which confers stability to XRN2 by formation of a chimeric complex *in vivo*. We conclude that XRN2 uses a similar mechanism for substrate binding and processive degradation as XRN1 and that PAXT-1 confers stability to the nuclease complex by binding through its XTB domain. Moreover, the XTBD serves as a general binding adapter for the XRN2 nuclease family, yet excluding XRN1 binding.

Contents

I Introduction

1 RNA metabolism

Ribonucleic acids (RNA) are molecules that play an important role in crucial metabolic functions such as protein synthesis and its regulation. The molecule itself is built by a multiple of connected mononucleotides. These consist of a ribofuranose moiety linked with one of four bases on the 1′ carbon, assembling to adenosine (A), cytidine (C), guanosine (G) and uridine (U) and a phosphate group at the 5′ carbon (Westheimer, 1987). Unlike deoxyribonucleic acid (DNA), RNA mostly exists as a single strand, however forms secondary structures by base-pairing with itself (Holley et al., 1965; Mathews et al., 2004; Tinoco and Bustamante, 1999). In certain circumstances RNAs also form intermolecular duplexes, e.g. miRNA – mRNA or miRNA passenger – guide duplexes (Bushati and Cohen, 2007; Krol et al., 2010). Until two decades ago the RNA field was mainly focused on RNA molecules supporting and facilitating protein synthesis. Five major RNA species play a crucial role, messenger RNA (mRNA), ribosomal RNA (rRNA), small nuclear RNA (snRNA), transfer RNA (tRNA) and ribozymes/RNase P. However, with the discovery of previously unknown non-coding RNAs (ncRNA) such as micro-/small interfering- and Piwi-interacting RNAs (miRNA/siRNA/piRNA) as well as long non-coding RNAs (lncRNA), the field of RNA rapidly gained attention (Brosius and Tiedge, 2004; Girard et al., 2006). This is because only about 2% of the genome codes for protein-coding mRNAs and until recently the remainder was considered "junk DNA" (Frith et al., 2005; Mattick, 2001; Ohno, 1972). Remarkably, with new RNA species emerging it becomes evident, that some of the so called "junk DNA" serves coding for functional RNAs yet do not code for proteins (Kapranov et al., 2010).

While RNAs execute many important functions, their biogenesis, processing and decay is dependent on RNA nucleases (RNases) (Miki and Großhans, 2013; Nagarajan et al., 2013; Yang, 2011; Yang et al., 2006). This class of enzymes cleaves phosphodiester bonds of the ribonucleic phosphate backbone and can be regarded as molecular machines that solely degrade the RNA polymer (Yang, 2011). However such a simplified view does not account for the many essential biological tasks RNases are involved in, such as rRNA maturation, splicing, gene silencing, and viral defense (Krol et al., 2010; Li et al., 2015; Miki and Großhans, 2013). Thus, understanding RNases and their functional relationship with RNAs as well as the underlying molecular mechanism are important to understand fundamental processes of life. Expression of a gene, meaning the transformation of the genetic code into functional molecules, is such a fundamental process and illustrates the functional complexity of RNAs and RNA nucleases (Figure 1). It starts with transcription, generating the nascent mRNA, and RNA nucleases CPSF as well as XRN2 make important contributions in mRNA cleavage and transcription termination, respectively (Hsin and Manley, 2012). Concomitantly, introns are excised through a process called splicing, which involves ribozymes exhibiting RNase activity to support

maturation of the mRNA (Wachtel and Manley, 2009; Will and Lührmann, 2011). Subsequently, the ribosome, a molecular machine consisting of rRNAs and proteins, translates the mRNA sequence to synthesize a polypeptide chain, which then assumes a functional three-dimensional fold (Ben-Shem et al., 2011; Klinge et al., 2011; Rabl et al., 2011). rRNAs themselves heavily depend on, for example, small nucleolar RNAs (snoRNA) and various RNases, such as XRN2, to fully mature to functional molecules (Gerbi et al., 2001). Finally the mRNA is degraded by the exosome and/or XRN1, which is initiated by various mechanisms such as decapping, deadenylation, non-sense mediated decay (NMD) or RNA interference (RNAi) (Figure 1) (Garneau et al., 2007; Krol et al., 2010; Schoenberg, 2011). Thus RNases are more specialized and appear more versatile than pure scavenger RNA nucleases would suggest. Especially the RNase XRN2 acts on various different, yet important RNAs and understanding this molecular machine on a functional and molecular level will thus expand our understanding of many key biological processes (Miki and Großhans, 2013; Nagarajan et al., 2013).

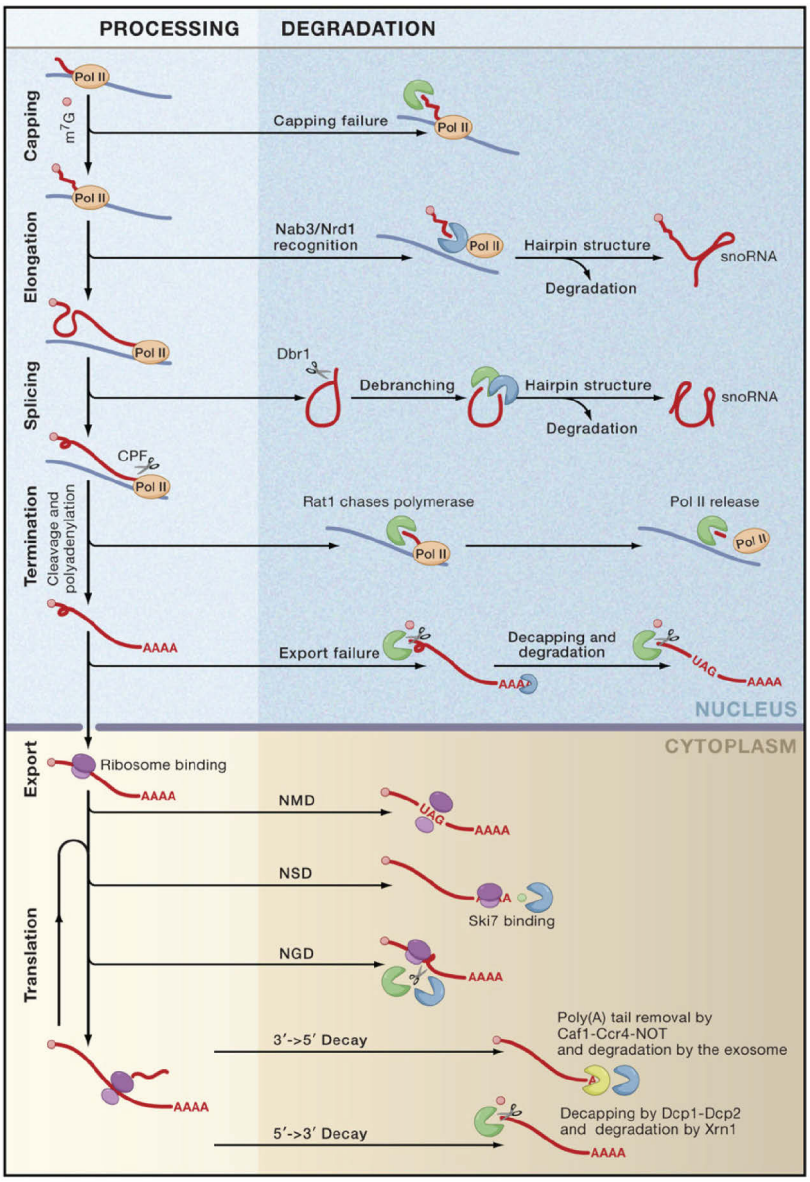

Figure 1: The scheme shows the various different stages of transcription and translation, in which RNases are involved (drawing taken from Houseley and Tollervey, 2009).

1.1 RNases and Their Role in Eukaryotic Gene Expression of Proteins

The messenger RNA conveys the genetic information from the nucleus to the cytoplasm and serves as a blueprint for protein synthesis (Carmody and Wente, 2009; Khorana et al., 1966; Nirenberg et al., 1966). Its biogenesis starts with the transcription of DNA by RNA polymerase II (RNAP II) (Bentley, 1999; Maniatis and Reed, 2002). Transcription is initiated by formation of a pre-initation complex (PIC), harboring transcription factors, co-activators and chromatin-remodeling complexes, at the promoter of a gene, upstream of transcribed DNA (Kim et al., 1997). This complex forms the transcription bubble, so that RNAP II binds the DNA and synthetizes an RNA polymer (Holstege et al., 1997; Kim et al., 2000; Wang et al., 1992). RNAP II, a nucleotidyltransferse with 12 subunits, then synthesizes a polynucleotide chain by using nucleoside triphosphate substrates (Gnatt et al., 2001; Kershnar et al., 1998; Myer and Young, 1998). Moreover, the largest subunit RPB1 of the RNAP II holoenzyme contains a carboxy terminal domain (CTD) and RNAP II activity is regulated through the CTD phosphorylation state (Hsin and Manley, 2012). For example, transcription factor TFIIH associated cyclin-dependent kinase 7 (CDK7) phosphorylates Ser5 of the CTD and releases RNAP II from the promoter region to start elongation (Akoulitchev et al., 1995; Feaver et al., 1991; Lu et al., 1992). Co-transcriptionally, the pre-mRNA is processed by factors loaded onto RNAP II's CTD as soon as it emerges from the RNA exit channel. Its 5'- end is capped with a methylated guanine monophosphate (m^7GMP), which is linked by a 5' – 5' triphosphate bridge to the pre-mRNA to protect it from nucleolytic degradation (Garneau et al., 2007; Shatkin, 1976). Furthermore, introns, non-coding sequences, are excised from the pre-mRNA and flanking exons are joined together in a process referred to as splicing (Wachtel and Manley, 2009; Will and Lührmann, 2011). The complex process of splicing is carried out by the spliceosome, made up by protein complexes containing non-coding snRNAs U1, U2, U4, U5 and U6, called small ribonucleic proteins (snRNPs). These snRNPs transiently interact with each other, dependent on the specific splicing step. In a first step the intronically encoded splice site is recognized, followed by the nucleophilic attack of the branch point adenosine forming the intron lariat. Subsequently, the lariat is cleaved and flanking exons end-joined. This reaction is catalyzed by the snRNAs U2 and U6, as they show Mg^{2+} dependent endonuclease activity and are referred to as ribozymes (Valadkhan et al., 2007). U2 and U6 form a complex through extensive base-pairing and the AGC triad as well as the adjacent ACAGAGA box of U6 are crucial for catalysis (Dayie and Padgett, 2008; Hilliker and Staley, 2004; Lesser and Guthrie, 1993; Wachtel and Manley, 2009). However protein-free splicing reactions are slow, suggesting that proteins must be involved in catalysis or at least stimulate ribozyme activity (Valadkhan et al., 2007).

Remarkably, the crystal structure of a domain of Prp8, interacting with U2 and U6 at the core of splicing catalysis, revealed an RNase H-like fold and Mg^{2+} binding capabilities (Pena et al., 2008; Ritchie et al., 2008; Yang et al., 2008). Even though the RNase H-like domain is truncated and lacks some key catalytic residues, point mutations at Prp8's active site have severe viability defects, suggesting a direct engagement in catalysis (Pena et al., 2008). To guarantee for a correct exon sequence, splicing is carried out co-transcriptionally and the RNAP II CTD in part recruits splicing factors to do so. In a final step, the capped- and spliced- pre-mRNA is endonucleolytically excised off the RNAP II – DNA complex and polyadenylated at its 3'-end by CPSF (cleavage/polyadenylation specificity factor) and polyadenylate polymerase (PAP), respectively (Balbo and Bohm, 2007; Murthy and Manley, 1995). The CPSF is a tetrameric protein complex with subunit CPSF-160 recognizing and binding the polyadenylation signal (AAUAAA) and CPSF-73 mediating cleavage (Mandel et al., 2006). CPSF-73 belongs to the β-CASP nucleases adapting a metallo-β-lactamase fold and hydrolyzes phosphodiester bonds in RNA or DNA. Remarkably, hydrolysis depends on two Zn^{2+} ions and works either endo- or 5'- exoribonucleolytically. Unique zinc-dependency of the β-lactamase class enzymes is probably mediated by a high number of histidines in the catalytic center (Mandel et al., 2006; Yang, 2011). Subsequently, the acquired poly(A) tail is bound by different poly(A)-binding proteins (PABP), which modulates PAP activity (nuclear PABPN1) (Kerwitz et al., 2003; Kühn et al., 2009; Wahle, 1991) and translation (cytoplasmic PABPC) (Gray et al., 2000; Imataka et al., 1998; Otero et al., 1999) as well as protecting the 3'- tail from exonucleolytic degradation *in vitro* (PABPC) (Bernstein et al., 1989; Ford et al., 1997; Körner and Wahle, 1997; Wormington et al., 1996). Finally, transcription is terminated through a yet not well understood mechanism, however an increasing number of reports indicate XRN2 to play an important role (see below) (Brannan et al., 2012; Dengl and Cramer, 2009; El Hage et al., 2008; Kim et al., 2004; Luo et al., 2006; Wagschal et al., 2012; West et al., 2004).

The final transcript is then exported to the cytoplasm and used as a template for translation to generate functional proteins (Carmody and Wente, 2009). Accordingly, tRNAs, which are covalently bound to one of the 21 amino acids at the 3'-end, pair to the template mRNA with their corresponding anti-codon and thus deliver substrates for protein synthesis (Schimmel et al., 1993). tRNAs themselves interact with RNases such as RNase Z, RNase P and XRN2 for maturation and quality control, respectively (Wichtowska et al., 2013). RNase Z cleave the 3' trailer and RNase P the 5' leader sequence of the pre-tRNA endonucleolytically. Whereas RNase Z depends on two Zn^{2+} ions and shares similarities to the β-lactamase fold, RNase P is a classical ribozyme using two Mg^{2+} ions for hydrolysis (Kirsebom, 2007; de la Sierra-Gallay et al., 2005).

Translation, similarly to transcription, follows a heavily regulated and complex initiation-, elongation- and termination process (Schmeing and Ramakrishnan, 2009) mainly driven by the ribosome. The ribosome, with its major 60 S and 40 S subunits, is a 3.2 MDa RNP and both subunits

in turn are complexes of mature rRNAs and various protein subunits. It catalyzes the peptidyl transferase reaction by which a polypeptide chain is formed (Ben-Shem et al., 2011; Klinge et al., 2011; Rabl et al., 2011). The 28 S ribosomal RNA, with its enzymatic activity, is a prime example of a ribozyme, which was believed to be an exclusive function of proteins for decades (Kruger et al., 1982; Nissen et al., 2000; Voorhees et al., 2009). As such, rRNAs are crucial for protein synthesis and their biogenesis as well as quality control is driven by RNases such as XRN2 (see below) (Miki and Großhans, 2013; Nagarajan et al., 2013).

1.2 Regulation of Gene Expression Through small RNAs and RNases

Whereas mRNAs convey information for protein synthesis as described above, non-coding RNA (ncRNA) function as scaffolds, guides or exhibit enzymatic activity (Mattick and Makunin, 2006). This class of RNA is roughly divided by size into small- and long- ncRNAs (Guttman and Rinn, 2012; Kim et al., 2009), with small ncRNAs being capable to regulate gene expression post-transcriptionally (Fabian and Sonenberg, 2012; Krol et al., 2010; Peters and Meister, 2007).

RNA induced gene silencing is a post-transcriptional process by which translation is inhibited and/or mRNA degradation is induced (Ecker and Davis, 1986; Fire et al., 1998; Ratcliff et al., 1997). This process is driven by small 20 to 25 nt long single stranded RNA molecules, derived from endogenous or exogenous RNA precursors. For siRNAs, RNA precursors originate from viral RNA material and serve as an antiviral defense mechanism or can be taken up from the environment (*C. elegans* RNAi by feeding) (Hamilton and Baulcombe, 1999; Timmons and Fire, 1998). For miRNAs these precursors are RNAP II transcripts, containing a cap-structure as well as a poly(A) tail, that are referred to as primary micro RNA (pri-miRNA) (Lee et al., 2002).

An enzyme complex consisting of DGCR8, a RNA binding protein, and endonuclease Drosha (for details see below) bind and cleave the pri-miRNA to a shorter, approx. 70 nt long hairpin RNA called precursor miRNA (pre-miRNA) (Denli et al., 2004; Gregory et al., 2004; Lee et al., 2003). Bound by exportin 5, the pre-miRNA is exported to the cytoplasm (Bohnsack et al., 2004; Lund et al., 2004; Yi et al., 2005) and undergoes its final maturation step by cleavage through Dicer. The endoribonuclease Dicer processes not only pre-miRNAs but also exogenous RNA fragments to produce dsRNA fragments consisting of a guide-/passenger- or 5p-/3p- strand for siRNA and miRNA, respectively (Bernstein et al., 2001; Grishok et al., 2001; Hutvágner et al., 2001; Knight and Bass, 2001). Dicer and Drosha are eukaryotic homologs of bacterial RNase III and comprise two active centers to produce double stranded RNA fragments. This class of enzymes depend on two metal ions for sequence independent cleavage and the catalytic event is thus similar to that of RNase H (Gan et al., 2006). The two active sites, built by two aspartates and a glutamate, are aligned to the substrate such that

cleavage occurs symmetrically to produce a 2 nt overhang at each strand's 3' end. Whereas substrate binding is facilitated by a dsRNA binding domain, analysis of the Dicer crystal structure revealed additional RNA binding domains. These domains mediate length and structure specificity for cleavable substrates to produce Dicer typical dsRNAs with a usual length of approx. 20 nt (Gan et al., 2006; Macrae et al., 2006; MacRae et al., 2007). Of note, miRNA duplexes contain a bulge, a locus of unpaired nucleotides, whereas siRNA duplexes are usually fully complementary. One strand is then selected and loaded to an argonaute protein (Aza-Blanc et al., 2003; Khvorova et al., 2003; Schwarz et al., 2003).

The argonaute protein family (AGO) is grouped in three subfamilies, the AGO clade, the Piwi clade and the worm specific WAGO clade, with each clade and their respective proteins serving different specialized functions (Ender and Meister, 2010; Peters and Meister, 2007). Argonautes have a well conserved domain architecture. Whereas its PAZ domain recognizes and binds the 3'- end of the selected RNA (Lingel et al., 2003; Yan et al., 2003), its MID domain binds the 5'- phosphate. The Piwi domain adopts an RNase H fold, which is – depending on the specific AGO – active and exhibits endonuclease activity towards an RNA – RNA duplex (Elkayam et al., 2012; MacRae et al., 2008; Schirle and MacRae, 2012; Song et al., 2004). This enzymatic activity relies on the catalytic DEDH motif, which coordinates three metal ions similar to transposases (Rivas et al., 2005). Interestingly, human Ago3 (hAgo3) harbors this catalytic motif, but exhibits no endonucleolytic activity. As the DEDH motif is a prerequisite for activity, the presence of two unstructured loops in the N-terminal domain, absent in hAgo3, are required to determine an AGO protein to be cleavage-competent, at least in humans (Faehnle et al., 2013; Hauptmann et al., 2013; Schürmann et al., 2013). The varying number of different AGO proteins reflect the importance of their functional role and different small RNA species may be loaded to certain AGOs. Whereas siRNAs are preferably loaded to cleavage-competent AGOs, miRNAs are loaded to catalytically inactive forms (Chekulaeva et al., 2011; Fabian et al., 2012; Förstemann et al., 2007; Jannot et al., 2008; Mathys et al., 2014; Mi et al., 2008; Okamura et al., 2009; Steiner et al., 2007). MiRNA-loaded AGOs bind to the 3' untranslated region (UTR) of an mRNA by imperfect base pairing. Precisely, the miRNA seed-sequence (nt 2 – 8), located on its 5'-end, binds the 3' UTR fully complementary, whereas some nucleotides within its 3'-end do not match the target sequence (Lai, 2002; Lee et al., 1993; Lewis et al., 2003; Lim et al., 2005; Wightman et al., 1991). Upon binding to the 3' UTR, the RNA-induced silencing complex (RISC) is formed, including miRNA-AGO complex and GW182 protein (AIN-1/2 in *C. elegans*) mediating translation inhibition and mRNA degradation (Chekulaeva et al., 2011; Hammond et al., 2000; Li et al., 2008; Meister et al., 2005; Rehwinkel et al., 2005). GW182 is a scaffold protein and recruits the CCR4/NOT effector complex through its multiple tryptophan repeats (Braun et al., 2011; Chekulaeva et al., 2011). The deadenylase CCR4/NOT acts on the targeted mRNA by translationally repressing it and subsequently initiating its

degradation by the exosome due to the loss of the mRNA's poly(A)- tail (see details below) (Behm-Ansmant et al., 2006; Chen et al., 2009; Piao et al., 2010). For siRNAs bound by slicing AGO2 however, mRNAs are endonucleolytically cleaved and therefore form a suitable substrate for exoribonucleases (see details below).

Taken together, RNPs consisting of argonaute proteins and small non-coding RNAs, fine tune gene expression post-transcriptionally and 50% of all mRNAs are predicted to be controlled by this mechanism, which is supported by various RNases (Figure 2) (Krol et al., 2010).

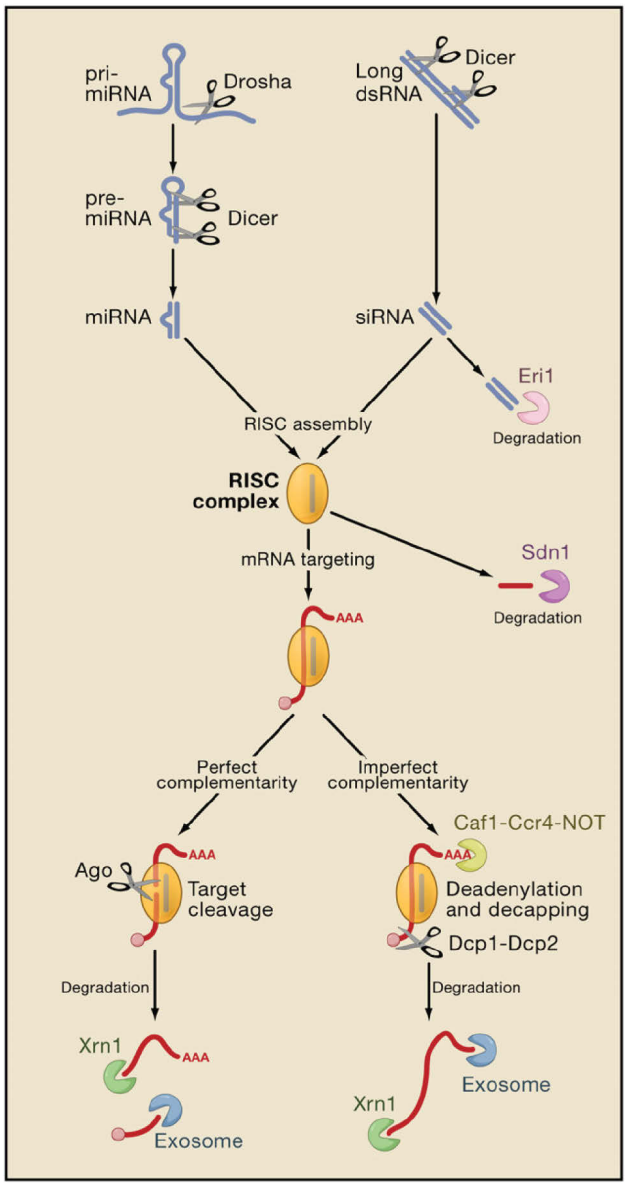

Figure 2: The scheme illustrates the multiple steps of miRNAs and siRNAs maturation mediated by Drosha and Dicer as well as RNase activity triggered by the RNA-induced gene silencing mechanism (drawing taken from Houseley and Tollervey, 2009).

2 RNA Degradation by Exoribonucleases

RNA nucleases are enzymes that execute many vital tasks to ensure cellular viability and protection (Yang, 2011). They can be grouped by their mode of action as endoribonucleases cleaving within an RNA molecule or as exoribonuclease cleaving from either the 5′- or 3′-end. Alternatively, RNases can be grouped by their metal-ion dependencies, which is the requirement of one, two or no metal ion for catalysis, reflecting the molecular mechanism underlying the cleavage process. Exoribonucleases belong to the two-metal-ion dependent nucleases and this catalysis mechanism is the most abundant (Chang et al., 2011a; Yang, 2011).

2.1 5′ → 3′ Exoribonucleases

The family of 5′ → 3′ Exoribonucleases (XRN) are made up of XRN1 (PACMAN in *D. melanogaster*) and its paralog XRN2 (Rat1p in yeast). Both enzymes share a high sequence identity of approx. 40 – 50% in their N-terminal nuclease region (Chang et al., 2011a; Miki and Großhans, 2013) and act on various RNA substrates such as mRNA for XRN1 and miRNA and rRNA for XRN2 (see details below). Eukaryotes have usually both XRN1 and -2, which predominantly locate to the cytoplasm and nucleus, respectively (Heyer et al., 1995; Johnson, 1997). As plants lack an XRN1 ortholog, the XRN2 homolog XRN4 takes over its function as it is localized in the cytoplasm (Kastenmayer and Green, 2000). Due to this separation, XRN1 and -2 have access to different RNA substrates, resulting in different tasks. In yeast, XRN2 is essential, whereas deletion of XRN1 causes phenotypes such as growth reduction (Amberg et al., 1992; Larimer and Stevens, 1990). In contrast loss of XRN1 causes defects in ventral closing and thorax formation in *D. melanogaster* (Grima et al., 2008) and absence of XRN2 leads to phenotypes such as growth delay, sterility and larval molting defects in *C. elegans* (Chatterjee and Grosshans, 2009; Frand et al., 2005; Miki et al., 2014a).

XRN's molecular organization is divided into an N-terminal nuclease segment comprising two conserved regions CR1 and CR2 connected by an unconserved unstructured part and a C-terminal segment. Whereas in XRN1 this C-terminal segment comprises additional well conserved domains connected to an unstructured and poorly conserved C-terminal tail, XRN2 lacks these additional C-terminal domains (Chang et al., 2011b; Jinek et al., 2011; Xiang et al., 2009). XRNs belong to 5′-phosphomonoesters producing hydrolases (EC 3.1.13) and use two divalent cations such as Mg^{2+} or Mn^{2+} for catalysis (Jinek et al., 2011; Kenna et al., 1993; Stevens and Poole, 1995; Xiang et al., 2009). By this, XRNs have distant relations with other Mg^{2+}- dependent nucleases such as flap-endonuclease FEN-1 and bacteriophage T4 RNase H (Jinek et al., 2011; Yang, 2011). Despite similarities with endoribonucleases, XRNs exclusively bind to 5′- monophosphorylated single stranded nucleic acids, with high preference for RNA and an approx. 10-fold reduced affinity for DNA (Kenna et al., 1993;

Poole and Stevens, 1995; Stevens and Poole, 1995). Recently, the structure of XRN1 in complex with a trinucleotide substrate was solved and explains the molecular mechanism of substrate binding. Steric hindrance in front of the nuclease cleft formed by helix α1 and a conserved loop (~ residues Leu515 – Asp550) prevents double stranded substrate access. Efficient substrate binding is achieved by a minimum of three unpaired nucleotides which are bound by XRN through a π – π base stacking with His41 and Trp540 in XRN1. Moreover the basic pocket is made up by highly conserved Lys93, Gln97, Arg100 and Arg101 residues and the latter two form hydrogen bonds with the 5′ phosphate bound oxygens (Jinek et al., 2011). This explains XRN's preference for 5′ phosphorylated RNAs and excludes larger 5′ terminal groups due to electrostatic and sterical limitations. XRNs degrade their substrate in a processive manner, by binding an RNA polymer, fully degrading it to mononucleotides without release of intermediate products (Jinek et al., 2011; Kenna et al., 1993; Stevens and Poole, 1995; Xiang et al., 2009). Two metal ion dependent nucleases usually employ two Mg^{2+} ions, coordinated by 8 highly conserved acidic residues, which coordinate the scissile phosphate (3′ phosphate) of the RNA phosphate backbone and drive the hydrolytic reaction, which is based on a nucleophile substitution S_n2 mechanism. One Mg^{2+} ion supports the formation of a nucleophile, a hydroxide ion, followed by the in-line nucleophilic attack and the second Mg^{2+} stabilizes the pentacovalent phosphate intermediate, which then creates the single 3′ OH nucleotide leaving group (Steitz and Steitz, 1993; Yang et al., 2006). For XRNs, direct coordination of the scissile phosphate by the second Mg^{2+} would be too large for inner-sphere coordination with phosphate-bound oxygens and are likely to interact through inner-sphere coordinated H_2O molecules with the scissile phosphate (Jinek et al., 2011). Thus, Jinek *et al.* hypothesizes a distinct catalytic mechanism for XRN1 compared to the canonical two-metal-ion catalysis. The processivity of XRN1 is mainly achieved by base stacking residue His41 and 5′- phosphate coordinating Lys93 as mutants thereof show substrate intermediates upon catalysis. Therefore Jinek and colleagues propose a Brownian ratchet-like mechanism by which the substrate translocation is mediated by His41 π – π base stacking in concert with the conserved basic pocket (Jinek et al., 2011). *In vitro* both XRNs show little substrate specificity, but execute specialized functions *in vivo*, pointing to an underlying regulatory network for these enzymes.

2.1.1 The 5′ → 3′ Exoribonuclease 2 is a Complex and Acts on Multiple Substrates

Initially, XRN2 was found to be involved in rRNA maturation, but soon more substrates sensitive to XRN2 were identified (Miki and Großhans, 2013; Nagarajan et al., 2013). Among them are functional RNAs from transcription and translation, such as pre-mRNA and tRNA, respectively as well as small RNAs involved in gene silencing. Moreover functions such as transcription termination and miRNA release off AGO were discovered, which emphasizes its multifunctional character.

As described above, there are many RNA species involved in transcription and translation. Accordingly, XRN2 contributes significantly to their maturation and quality control. A precursor-rRNA (pre-rRNA) molecule is divided in the functional 18S, 5.8S and 25S (in yeast; 28S in mammals) rRNA fragments, two external transcribed spacers (5′ and 3′ ETS) and two internal transcribed spacers (ITS1 and – 2) (Figure 3) (Henras et al., 2008). XRN2 is involved in 5′ trimming of 5.8S and 25S/28S as well as clearance of some spacer fragments (Amberg et al., 1992; Couvillion et al., 2012; Petfalski et al., 1998; Wang and Pestov, 2011; Zakrzewska-Placzek et al., 2010). However prior endonucleolytic cleavage of the pre-rRNA is necessary for substrate access. The MRP endonuclease (evolutionary related to ribonucleoprotein RNase P) generates an XRN2 competent substrate by cleavage within the ITS1 upstream of the 5.8S, which is subsequently trimmed by XRN2 (Shadel et al., 2000). Similarly, XRN2 trims the 5′ extension of a 25S rRNA precursor after endonucleolytic cleavage at ITS2 (Henry et al., 1994; Schmitt and Clayton, 1993). Recruitment of XRN2 to the pre-rRNA is mediated by NOP4 and NOP15 in yeast, as their potential RNA remodeling activity allows for XRN2 substrate access (Granneman et al., 2011). However, 5′-end trimming is not exclusively maintained by XRN2 as recently identified Rrp17 exonuclease redundantly acts on 5′-end rRNA maturation (Oeffinger et al., 2009). Moreover XRN1 can substitute for XRN2 function in rRNA maturation, in case of loss or inactivity (Fang et al., 2005; Henry et al., 1994). Most work elucidating rRNA maturation was done in yeast, but this process seems to be conserved in mammals as XRN2 RNAi in mouse LAP3 cells result in similar accumulation of extended 5.8S and 28S rRNAs (Wang and Pestov, 2011). Due to XRN2's processive activity, questions about termination of this trimming process remain. Apart from rRNA maturation, XRN2 is indicated to support the exosome in clearance of aberrant pre-rRNA species (Fang et al., 2005; Wang and Pestov, 2011). Furthermore XRN2 mediates small nucleolar RNA (snoRNA) maturation in a similar fashion to rRNA maturation, where endoribonuclease Rnt1 renders suitable RNA substrates for 5′ trimming of snR190, U14 and snR72-78 (Chanfreau et al., 1998; Petfalski et al., 1998; Qu et al., 1999). These small ncRNAs bind to pre-rRNAs and support the processing thereof. On the other hand, maturation of tRNAs is driven by RNases, such as RNase Z and RNase P, processing the 3′- and 5′-end, respectively (see above) (Minagawa et al., 2004; Xiao et al., 2001). However, defective tRNAs are rapidly cleared by XRN1 and XRN2, to avoid production of deleterious proteins (Chernyakov et al., 2008). Similarly, XRN2 is involved in surveillance of pre-mRNA. The tight regulation of mRNA quantities correlate with protein production, hence XRN2 and the exosome compete with the splicing machinery for pre-mRNAs as a substrate (Bousquet-Antonelli et al., 2000; Brannan et al., 2012; Das et al., 2003). As defects within pre-mRNAs would lead to erroneous protein products, quality control of aberrant pre-mRNAs and subsequent decay by the exosome and XRN2 are necessary. This task is predominantly executed by the exosome in yeast, but in human cells XRN2 plays a more important role (Davidson et al., 2012; Gudipati et al., 2012).

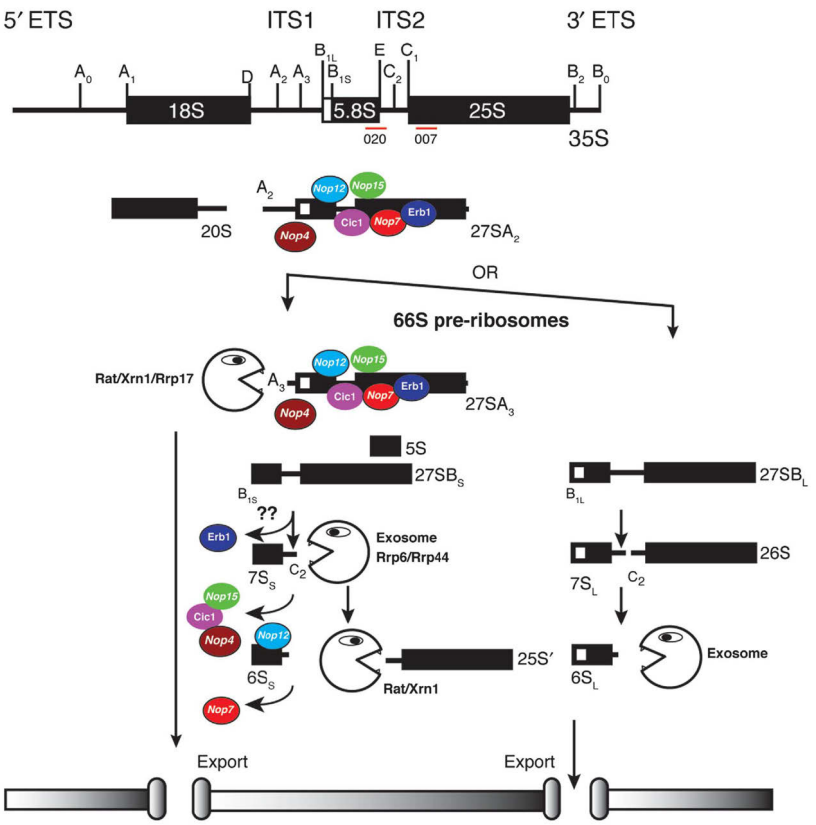

Figure 3: The scheme illustrates the rRNA maturation and RNases involved in this process (adapted from Granneman et al., 2011).

Whereas maturation and decay of RNAs are important for their function and homeostasis/quality control, degradation of RNAs can also influence cell aging and senescence as it was discovered for the TERRA RNA and XRN2. Telomeres are repeat sequences at the end of chromosomes, which are shortened each DNA replication and telomere loss can lead to stop in growth, senescence or apoptosis. Hence the telomerase replenishes and maintains the integrity of telomeres, but it is suggested that its activity is repressed by telomeric repeat-containing RNA (TERRA) (O'Sullivan and Karlseder, 2010). These TERRA molecules bind telomere sequences and XRN2 is implicated in their degradation and thus indirectly regulates telomerase activity (Luke et al., 2008). Likewise, XRN2 catalysis is thought to induce transcription termination. For RNAP II transcription (see details above) to be terminated, there is increasing evidence for XRN2 to play a major role, which is explained by the torpedo model (Kim et al., 2004; West et al., 2004). After cleavage of the nascent pre-mRNA transcript, RNAP II remains bound to the DNA strand and continues transcription. Indeed, the cleavage event yields a 5′ monophosphate and serves as an entry point for XRN2. Thus XRN2 starts degradation and, by colliding, displaces RNAP II from the DNA strand to terminate transcription. However reports in yeast show this mechanism not to be essential and in mammals only a subset of genes are sensitive to XRN2 mediated transcription termination (Banerjee et al., 2009; Brannan et al.,

2012; Luo et al., 2006). Thus, the torpedo model explains a specialized process rather than a general mechanism. Of note, XRN2 is also implicated in premature termination of RNAP II transcription as well as termination of RNAP I pre-rRNA- and intergenic RNAP II pri-miRNA transcription (Ballarino et al., 2009; El Hage et al., 2008; Kawauchi et al., 2008). Taken together XRN2 mediated decay involves maturation and quality control of functional RNAs as well as contributes to processes like cell aging and transcription termination.

So far, all described functions of XRN2 are related to RNA decay, however a recent function with no obvious connection to catalysis was discovered. It was shown that XRN2 depleted worm lysates incubated with immunoprecipitated miRNA-AGO complexes showed elevated miRNA levels remaining on AGO (Chatterjee and Grosshans, 2009). Thus XRN2 depletion leads to reduced release activity, however the underlying mechanism remains elusive.

Small RNAs, such as miRNAs, gained much attention in the last decade and efforts tried to identify specific RNases responsible for their decay. In *C. elegans*, XRN2 has been found to degrade miRNAs, as knock-down of XRN2 rescued let-7 point mutant worms by increasing let-7 levels (Chatterjee and Grosshans, 2009). However, further analysis revealed that only a subset of miRNAs are sensitive to XRN2 degradation, indicating a targeted process for miRNA degradation *in vivo* (Miki et al., 2014a). In contrast, miRNAs might simply be cleared by multiple RNases, depending on their cellular location and accessibility. In a less well-understood mechanism, exogenous non-targeting siRNAs are cleared by XRN2 (Wei et al., 2011). These small RNAs induce NPGPx (non-selenocysteine-containing phospholipid hydroxyperoxide glutathione peroxidase) expression, followed by complex formation through covalent binding of NPGPx to XRN2 and small RNA degradation. Whether this process is relevant under physiological conditions remains unclear.

As just described, XRN2 has many different substrates as well as specific functions, but one wonders how this is achieved by a single molecule? Indeed, during purification of yeast XRN2, a second protein called Rat1p interacting protein (Rai1p) was readily co-purified (Stevens and Poole, 1995; Xiang et al., 2009). Analysis showed, that binding of Rai1p confers stability to XRN2 and enhances/activates nuclease activity (Xiang et al., 2009; Xue et al., 2000). Moreover Rai1p itself was found to harbor pyrophosphatase activity (Xiang et al., 2009). Interestingly, complex formation of XRN2 with Rai1p permits the enzyme complex to access a much broader spectrum of substrate, as XRN2 alone is limited to 5′ monophosphorylated RNA substrates. However, Rai1p homologs Dom3Z/DXO seem not to bind XRN2 (Xiang et al., 2009). Interestingly, we recently identified *C. elegans* XRN2 to form a complex with PAXT-1, but no homology of PAXT-1 and Rai1p is detected (Miki et al., 2014b). Instead PAXT-1 seems to bind XRN2 through its N-terminal segment containing a

domain of unknown functions (DUF3469) also termed XRN2 binding domain (XTBD), which is not detected in Rai1p nor in any other yeast protein (Miki et al., 2014b). Loss of PAXT-1 results in reduced XRN2 protein levels, whereas mRNA levels remain unaffected, suggesting a stabilizing effect of PAXT-1 on XRN2 (Miki et al., 2014b). Other XRN2 interactions with XTBD-containing proteins were identified in *Tetrahymena thermophila* and humans (Brannan et al., 2012; Couvillion et al., 2012; Miki et al., 2014b). *T. thermophila* XRN2 associates in a ternary complex with Ago/Piwi protein Twi12 and XTBD-containing protein Tan1, with both binding to independent XRN2 interfaces. Whereas Twi12 seems to stabilize XRN2, no function is attributed to Tan1 (Couvillion et al., 2012). How these findings relate to reports from *C. elegans,* where XTBD- containing protein PAXT-1 confers stability, remain elusive. Co-immunoprecipitation experiments in humans identified two XTBD- containing proteins NKRF and CDKN2AIP/CARF to interact with XRN2 and Pfam alignments of DUF3469 (XTBD) suggests a third XTBD-containing protein CDKN2AIPNL to exist in an XRN2 complex (Brannan et al., 2012; Close et al., 2012; Miki et al., 2014b). Whereas NF-κ-B-repressing factor (NKRF) acts as a transcriptional repressor, collaborator of ARF (CARF/CDKN2AIP) is a tumor suppressor that acts through p53-activation, but CDKN2AIPNL has no attributed functions (Cheung et al., 2014; Feng et al., 2002; Hasan et al., 2002, 2004). Until now, direct interaction was only shown for the *C. elegans* PAXT-1 – XRN2 complex, but there is evidence for other XTBD-containing proteins to form similar complexes with their XTBD domain (Miki et al., 2014b). Accordingly, XRN2 may exists in multiple complexes that potentially affect or regulate its function. Moreover, studies on transcription termination identified higher order complexes of XRN2. In yeast, a trimeric complex consisting of Rat1p, Rai1p and Rtt103 was identified, which localizes to the 3' end of protein coding genes (Kim et al., 2004). Interestingly, Rtt103 binds to phosphorylated serine2 of the CTD of RNAPII and possibly links the exonuclease complex to the transcription machinery (Kim et al., 2004). In vitro analysis show however, that a this trimeric complex is not enough for transcription termination (Dengl and Cramer, 2009). Similarly, human XRN2 is recruited to RNAPII by the protein complex p54nrb/PSF, which was found to stably interact with the C-terminus of XRN2. p54nrb/PSF itself is a multifunctional protein complex and involved in transcription, splicing and polyadenylation of nascent mRNA transcripts (Gozani et al., 1994; Liang and Lutz, 2006). It is thus suggested, that p54nrb/PSF couples pre-mRNA 3'-end processing and transcription termination (Kaneko et al., 2007).

2.1.2 5' → 3' Exoribonuclease 1

XRN1 is the cytoplasmic paralog of XRN2 and shares high sequence identity with XRN2 in its N-terminal segment (see above). However XRN1 acquired a set of domains absent from XRN2, which possibly provides additional functions to the enzyme (Chang et al., 2011b; Jinek et al., 2011). Both, the SH3- and PAZ/Tudor domain mediate structural stability to XRN1, by interaction with the

nuclease region (Jinek et al., 2011). Whereas the SH3-domain achieves this through non-canonical binding due to the lack of canonical residues involved in proline-rich peptide interactions, Jinek et al. (2011) hypothesize the PAZ/Tudor domain to substitute for Rai1p induced stabilization because of the vast interface formed by this interaction (Jinek et al., 2011). The canonical PAZ and Tudor domains bind RNAs and motifs containing methylated arginine, respectively. In XRN1, however the functional surfaces of the PAZ/Tudor domain are covered by an SH3 protruding loop and thus exclude additional binding capabilities by these domains (Jinek et al., 2011). For the winged-helix domain, which is located above the catalytic center, it is postulated that it supports RNA binding and potential catalytic activity and that it may act as a scaffold for possible protein-protein interaction (Jinek et al., 2011).

XRN1 mainly localizes throughout the cytoplasm, but is sometimes found in distinct foci called P-bodies, co-localizing with enzymes such as decapping factor DCP2 and LSM1-7 complex supporting degradation by coupling deadenylation and decapping events (Bashkirov et al., 1997; Cougot et al., 2004; Heyer et al., 1995; Johnson, 1997; Newbury, 2006). P-bodies are however thought to be storage sites for inactive mRNAs, as mRNAs can either be degraded by XRN1 or released to continue translation (Brengues et al., 2005; Eulalio et al., 2007; Stalder and Mühlemann, 2009). Yet, these foci are no prerequisite for mRNA degradation, but seem to be increased during stress response (Cougot et al., 2004; Kedersha et al., 2005; Sheth and Parker, 2003).

The main task of XRN1 is the clearance of mRNA species. Access to this substrate, however needs preceding mRNA processing to render unpaired 5′ monophosphorylated nucleotides. One way is removal of the 5′ end of the mRNA through decapping enzymes such as DCP2 and its activator DCP1, which usually occurs after deadenylation of the mRNA, however deadenylation is not a prerequisite (Braun et al., 2012; Gazzani et al., 2004; Lejeune et al., 2003; Muhlrad et al., 1994). As previously discussed, endonucleolytic cleavage of mRNAs by siRNA loaded Argonaute also results in XRN1 competent mRNA substrate (Chekulaeva et al., 2011; Sheth and Parker, 2003). Moreover quality control of mRNAs through nonsense-mediated decay (NMD) protects the organism from harmful aberrant mRNAs and triggers XRN1 mediated clearance of these mRNAs (reviewed in Rebbapragada and Lykke-Andersen, 2009). When a premature termination codon (PTC) is detected, NMD triggers its endonucleolytic cleavage through SMG6 endonuclease (which belongs to the FEN1 ribonuclease superfamily) or direct induction of exonucleolytic decay from both ends (Eberle et al., 2009; Glavan et al., 2006; Huntzinger et al., 2008; Yang, 2011). In addition, the exosome, a multi-subunit protein complex with 3′ → 5′ exoribonuclease activity, cooperatively and/or independently degrades deadenylated and endonucleotlytically cleaved mRNAs (see below). Noteworthy, neither XRN1 nor the exosome can substitute for each other in multicellular organisms, suggesting that at least a subset of transcripts are individually regulated and controlled by either enzyme (Jones et al., 2012;

Newbury and Woollard, 2004). Besides its predominant role in mRNA degradation, XRN1 has also been implicated in degradation of some miRNAs, however this evidence seems to support a model, where XRN1 simply clears unprotected miRNAs rather than acting as a specific miRNase (Bail et al., 2010; Chatterjee et al., 2011).

Despite its important role in mRNA surveillance and decay, XRN1 is not essential in unicellular eukaryotes, as its knock-out causes phenotypes such as reduction in growth rate, decreased rates of diploid formation and sporulation, defects in meiotic recombination and reduced transcription of a subset of genes due to XUT (XRN1-sensitive unstable transcripts) accumulation (Amberg et al., 1992; van Dijk et al., 2011; Larimer and Stevens, 1990; Tishkoff et al., 1995). In contrast multicellular organisms depend on XRN1 as null mutations in *D. melanogaster* are lethal and XRN1 mutations cause specific developmental phenotypes, such as reduced fertility and failure in epithelial sheet sealing (Grima et al., 2008; Zabolotskaya et al., 2008). Similar observations were made in *C. elegans*, by XRN1 RNAi, however no XRN1 mutant worm line exist to verify these observations (Newbury and Woollard, 2004). This suggests, that XRN1 is specifically deployed for degradation of certain transcripts involved in development. In line with these observations, studies of patient derived cell samples link XRN1 with osteosarcoma, a common childhood cancer (Zhang et al., 2002). This type of cancer originates from mesenchymal cells, that failed to properly differentiate and XRN1 mRNA levels were reduced, probably due to a mis-sense mutation within the XRN1 gene.

Whereas subunits of XRN2 complexes form strong interactions and mainly act as stabilizers, XRN1 has not been found to exist in such prominent and stable complexes. However XRN1 interacts with proteins such as DCP1, LSM1-7, PAT1 and UPF1, UPF2, UPF3X implicated in mRNA decapping and NMD, respectively (Bouveret et al., 2000; Lejeune et al., 2003; Nissan et al., 2010). Interestingly, in *C. elegans* and yeast, XRN1 was found to interact with DCS1, a scavenger decapping enzyme and DCS1 stimulated XRN1 activity independently of its own catalytic activity *in vitro* and *in vivo* (Bossé et al., 2013; Sinturel et al., 2012).

2.2 The Exosome – Example of a 3' → 5' Exoribonuclease

The eukaryotic exosome is a multi-subunit RNase complex engaged in many RNA decay-, quality control- and processing pathways (see above) and is conserved throughout all kingdoms of life. Whereas ancestral exosomal complexes rely on phosphorolytic catalysis with their 6 RNase PH domains, the eukaryotic exosome switched to a hydrolysis mechanism. Its additional nuclease subunits Rrp44 and Rrp6 supply catalytic activity, whereas all RNase PH domains are catalytically inactive and seem to act solely as scaffolds (Januszyk and Lima, 2014; Schneider and Tollervey, 2013).

The molecular structure of the exosome core (EXO9) is made up of 9 subunits that forms a barrel-like structure, sharing similarities to the proteasome or the bacterial polynucleotide phosphorylase (PNPase) (Liu et al., 2006). In eukaryotes, the barrel is formed by six subunits (Rrp41/42/43/45/46/Mtr3) harboring a phosphorolytic 3′ → 5′ exoribonuclease domain homologous to RNase PH 1 or - 2, which are however catalytically inactive (Liu et al., 2006). Rrp40, Rrp4 and Csl4 subunits form a cap on top of the barrel and contain S1 and/or KH RNA-binding domains. The EXO9 barrel forms a channel with a 8 to 10 Å opening, capable of accommodating only single stranded RNA (Liu et al., 2006). With the lack of active RNase PH domains, the exosome acquired two catalytic competent subunits, Rrp6 and Rrp44, to form the canonical EXO11 complex. Structural analysis revealed Rrp44/Dis3 (human) to bind on the base of the barrel and to contain a processive 3′ → 5′ exoribonuclease domain homologous to RNase II/R as well as an endoribonucleolytic PIN (PilT N terminus) domain (Bonneau et al., 2009; Frazão et al., 2006; Lorentzen et al., 2008). The PIN domain, which is homologous to T4 RNase H, however shows activity only at unphysiological high manganese concentrations of 5 mM (Lebreton et al., 2008). Furthermore Rrp44's catalytic activity depends on the integrity of the EXO9 channel, as the RNA substrate needs to be threaded through the channel to reach the nuclease cleft (Drązkowska et al., 2013; Wasmuth and Lima, 2012). For substrate longer than 35 nt, this seems a prerequisite but if shorter substrates have alternative access paths to Rrp44 remains unclear (Drązkowska et al., 2013; Wasmuth and Lima, 2012). Interestingly, humans have three Rrp44 homologs (DIS3, DIS3L, DIS3L2), which are tied to different subcellular compartments and exosome complexes are found in the cytoplasm and the nucleus associated with DIS3L and DIS3, respectively (Malecki et al., 2013; Tomecki et al., 2010). No interaction of the exosome with DIS3L2 has been described yet. In contrast to Rrp44, Rrp6 locates to the top of the exosome by forming a vast binding interface with EXO9 components and supplies distributive 3′ → 5′ exonucleolytic activity to the exosome (Januszyk et al., 2011; Midtgaard et al., 2006). The catalytic domain is homologous to RNase D, dependent on two Mg^{2+} ions, and substrate pools of Rrp6 and Rrp44 are non-redundant (Gudipati et al., 2012; Kiss and Andrulis, 2010). It has been shown that Rrp6 lacking yeast accumulate nuclear RNA species such as pre-rRNA and snRNA, indicating a specific role for an Rrp6-loaded exosome in nuclear RNA processing (Allmang et al., 1999, 2000; Neil et al., 2009).

Moreover, specialized complex configuration exist to serve its compartmentalization as well as regulation, with a cytoplasmic EXO10 exosome (EXO9 – Rrp44), a nuclear EXO11 and an EXO9 – Rrp6 complex, suggested to exist in the nucleolus (Januszyk and Lima, 2014).

II Results

During the last decade, microRNAs (miRNA) emerged as important regulator of post-transcriptional gene expression, controlling development, cell growth and homeostasis. Accordingly miRNAs are implicated in diseases such as cancer, and they are deregulated in many tumors. Hence dissecting the molecular basis of miRNA biogenesis, mRNA silencing and the active turnover of miRNA marks an important research goal. Previously, we identified the 5'→ 3' exoribonuclease XRN2 as a miRNA nuclease in *C. elegans*. Moreover, we recently identified PAXT-1 as a subunit of an XRN2 complex, which seems to stabilize XRN2. To dissect its function I was expressing XRN2 and PAXT-1 – XRN2 complexes recombinantly to perform in vitro turnover assays, interaction studies and stability assays. Furthermore, I crystallized the XTBD – XRN2 complex and together with Dr. Heinz Gut solved its structure. Dr. Iskra Katic and I then confirmed *in vitro* results concerning the importance of Tyr56 *in vivo* by using MosSCI and CRISPR technology to generate mutant worms.

1 Paper Manuscript: Structural Basis and Function of XRN2-Binding by XTB Domains

Hannes Richter[1, 2], Iskra Katic[1], Heinz Gut[1] and Helge Großhans[1‡]

[1] Friedrich Miescher Institute for Biomedical Research, Maulbeerstrasse 66, CH-4058 Basel, Switzerland

[2] University of Basel, Petersplatz 1, CH-4003 Basel, Switzerland

[‡] Author for correspondence (helge.grosshans@fmi.ch)

Running title: The XTBD is a Generic Binding Adapter for XRN2s

Key words: XRN2, XTBD, DUF3469, crystal structure, protein complex, protein interface, *C. elegans*, CRISPR-Cas9, genome editing, chimeric protein complex, conservation, thermal

stability, thermal shift assay, exoribonuclease, Michaelis-Menten kinetics, RNA turnover, substrate-mediated protein stabilization,

Abstract

The ribonuclease XRN2 is an essential player in RNA metabolism. In *Caenorhabditis elegans*, XRN2 functions in a complex with PAXT-1, which shares a putative XRN2-binding domain (XTBD) with otherwise unrelated mammalian proteins. Here, we characterize structure and function of XTBD in complex with XRN2. Although XTBD stably interconnects two XRN2 domains through numerous interacting residues, we identify a critical residue whose mutation suffices to disrupt XTBD – XRN2 complexes *in vitro*, and recapitulate *paxt-1* null mutant phenotypes *in vivo*. XRN2-binding is highly conserved as vertebrate XTBD-containing proteins form complexes with XRN2 *in vitro*, and human CDKN2AIPNL/C2AIL can substitute for PAXT-1 *in vivo*. With three distinct XTBD-containing proteins existing in vertebrates, stable binding suggests that cellular XRN2 partitions to distinct heterodimeric complexes, likely differing in subcellular localization or function. In *C. elegans*, complex formation with the unique PAXT-1 may serve to preserve the stability of XRN2 when not bound to substrate.

Introduction

Ribonucleases (RNases) are central to both RNA processing and degradation events and hence key enzymes in RNA metabolism. Thus, the nuclear 5' → 3' exoribonuclease XRN2 functions in ribosomal and small RNA processing (Chanfreau *et al.*, 1998; Couvillion *et al.*, 2012; Geerlings *et al.*, 2000; Petfalski *et al.*, 1998; Wang and Pestov, 2011; Zakrzewska-Placzek *et al.*, 2010), transcriptional termination (Kim *et al.*, 2004; West *et al.*, 2004), clearance of aberrant pre-mRNA (Davidson *et al.*, 2012) and hypomodified tRNA (Chernyakov *et al.*, 2008), degradation of miRNAs (Chatterjee and Grosshans, 2009) and other pathways (reviewed in Miki and Großhans, 2013; Nagarajan *et al.*, 2013). Accordingly, XRN2 is conserved from yeast to humans, and encoded by an essential gene in both yeast and worms (Amberg *et al.*, 1992; Miki *et al.*, 2014a). A cytoplasmic paralogue of XRN2, XRN1, plays a central role in mRNA degradation (Parker and Sheth, 2007). The two enzymes share a substrate preference for 5' monophosphorylated, single-stranded RNAs (Jinek et al., 2011; Kenna et al., 1993; Poole and Stevens, 1995; Stevens and Poole, 1995).

In yeast, the XRN2 protein Rat1p occurs in a complex with Rai1p (Rat1 interacting protein; Stevens and Poole, 1995; Xiang et al., 2009), a protein that promotes XRN2 activity through mechanisms that remain to be identified (Xiang et al., 2009; Xue et al., 2000). However, the metazoan Rai1p orthologues Dom3z/DXO do not bind to their respective XRN2s (Xiang et al., 2009). In *C. elegans*, XRN2 forms instead a complex with the novel protein PAXT-1 (Partner of XRN-Two) (Miki et al., 2014b). Loss of PAXT-1 causes a reduction in XRN2 levels, and, when worms are grown at a relatively high temperature of 26°C, embryonic lethality, which can be prevented by increased XRN2 gene levels (Miki *et al.*, 2014b). As *paxt-1* mutations cause reduced XRN2 protein but not mRNA levels, PAXT-1 may stabilize the XRN2 protein (Miki *et al.*, 2014b).

Although PAXT-1 is 375 amino acids (aa) long, its N-terminal 121 amino acids suffice to co-immunoprecipitate XRN2 and restore animal viability and XRN2 levels when expressed as a transgene in *paxt-1* mutant animals (Miki *et al.*, 2014b). This portion of PAXT-1 also comprises a predicted domain of unknown function, DUF3469, and although PAXT-1 is not well conserved outside nematodes, this domain is also found in unrelated vertebrate and ciliate but not yeast proteins (Miki et al., 2014b). Although it is not known whether these proteins also bind XRN2, three of them, mammalian NKRF/NRF and CDKN2AIP/CARF, and ciliate Tan1 were observed in XRN2 complexes (Brannan *et al.*, 2012; Close *et al.*, 2012; Miki *et al.*, 2014b; Couvillion *et al.*, 2012). Hence, DUF3469 may mediate XRN2 binding (Miki *et al.*, 2014b).

Here, we have used biochemical, crystallographic and molecular genetic approaches to test whether DUF3469 is an XRN2-binding domain (XTBD), dissect its structure, and elucidate its function. We identify a core XTBD domain and present its crystal structure in complex with XRN2. We uncover a

conserved interaction interface, on which a single amino acid on XTBD makes crucial contributions to complex formation, such that its mutation disrupts the complex *in vitro* and *in vivo* and renders mutant animals inviable. We demonstrate that XTBDs are generic XRN2 binders, across species, *in vitro*, and that, despite limited sequence similarity, human CDKN2AIPNL/C2AIL can substitute for *C. elegans* PAXT-1 *in vivo.* Although XRN2 has low thermal stability, which PAXT-1 binding greatly increases, it retains activity at elevated temperature in vitro. This appears to be a consequence of a stabilizing effect of substrate binding, in turn suggesting that a function of PAXT-1 is to preserve stability of 'empty' XRN2 to buffer cellular RNase activity.

Results

The Crystal Structure of the XTBD – XRN2 Complex Reveals a Conserved Binding Interface

Our previous work examined the function of the N-terminal amino acids 1 - 121 of *C. elegans* PAXT-1, which contains the DUF3469 domain, and showed that this truncated PAXT-1 sufficed for both binding to XRN2 *in vivo* and restoration of viability in *paxt-1(0)* worms (Miki *et al.*, 2014b). However, Pfam annotates the boundaries of this domain as residues 7 – 93 (http://pfam.xfam.org/family/DUF3469). Hence, we sought to redefine the XTBD core element. Based on HHPred secondary structure predictions (Söding *et al.*, 2005) and disorder analysis by PSIPRED Protein Analysis Workbench (Buchan *et al.*, 2013) and DisEMBL (Linding *et al.*, 2003), we decided to test recombinant proteins comprising residues 1 – 121, 1 – 96, and 1 – 75, respectively, for binding to XRN2. We found that the binding properties of all three polypeptides were comparable to that of the full-length protein (Fig. S1A). Thus, at 75 amino acids the functional XTBD is substantially smaller than previously annotated.

To obtain structural information on XTBD, we sought to express and purify an XRN2 – PAXT-1_1-75 complex for crystallographic analysis. Extensive protein engineering on XRN2 was necessary to yield high-quality diffracting protein crystals. We deleted a zinc-finger containing loop (residues 258 – 294), a predicted disordered region in the middle of the protein (residues 417 – 532), and the glycine-rich C-terminus (residues 788 – 975). This protein construct is referred to as XRN2Δ^{ZLC}. Following co-expression of XRN2Δ^{ZLC} and PAXT-1_1-75 in bacterial cells, purification and crystallization, we determined the crystal structure of the 83 kDa complex at 2.85 Å resolution. The macromolecular complex crystallized in space group $P2_12_12_1$ with six XTBD – XRN2Δ^{ZLC} heterodimers in the crystallographic asymmetric unit and a solvent content of ~64%. The structure was determined by molecular replacement and model building was carried out with the help of phased anomalous difference Fourier electron density maps obtained from seleno-methionine derivative crystals. Data collection and refinement statistics are summarized in Table 1. The final XTBD – XRN2Δ^{ZLC} structure consists of residues 4 – 25, 35 – 149, 153 – 413, and 534 – 787 for XRN2Δ^{ZLC} (chain A) and 1 – 73 for XTBD (chain B), which show clear electron density.

A previous domain assignment of XRN2 was based on sequence conservation and annotated two domains, CR1 (conserved region 1; corresponding to residues 1 – 409) and CR2 (residues 543 – 713), connected by an non-conserved disordered region and a poorly conserved C-terminus (Xiang *et al.*, 2009). Based on our structural data, and taking into account previous structures of Rat1p (Xiang et al., 2009) and XRN1 (Jinek et al., 2011), we further refine the XRN2 domain classification. We now define the nuclease core domain 1 (NCD1, residues 1 – 310), the nuclease core domain 2 (NCD2, 311 – 612),

the PAXT-1 binding domain (PBD, 613 – 705), the C-terminal domain 1 (CTD1, 706 – 787) and the C-terminal domain 2 (CTD2, 788 – 975) (Fig. 1A and 1B). The structure of XRN2Δ^{ZLC} is highly similar to *S. pombe* Rat1 (PDB 3FQD) (Xiang *et al.*, 2009) with a root-mean-square deviation (r.m.s.d.) of 1.46 Å over 580 aligned Cα atoms (53% sequence identity). It also superimposes very well onto the exonuclease cores of *D. melanogaster* and *K. lactis* XRN1s with r.m.s.d. values of 1.51 Å (503 aligned Cα atoms, 44% sequence identity, PDB 2Y35) (Jinek *et al.*, 2011) and 1.36 Å (475 atoms, 42% identity, PDB 3PIE) (Chang *et al.*, 2011), respectively.

Consistent with the PAXT-1 truncation analysis above, the crystal structure confirms PAXT-1_1-75 as the core XRN2-binding domain. It binds to a large groove on XRN2, which is formed by NCD1 and PBD. XRN2 residues 645 – 681 form a long loop protruding from the globular core of the PBD and fold around the base of a large α-helix, known as the tower domain (residues 108-139; Xiang et al., 2009) (Fig. 1B and S1B). XTBD folds into a globular four-helix bundle (H1 – H4) connected by three loops (L1 – L3) (Figure 1C). H1 – H3 form an antiparallel helical array and H4 folds back on top of H2/H3 at a 90° angle. H1 is short, comprising only six residues, whereas helices H2 – H4 are much longer (10-15 residues). The four-helical bundle is mainly stabilized by hydrophobic helix – helix interactions together with additional polar interactions between side chains located on neighboring helices. A peculiarity is L3, connecting H3 and H4, which is in a completely linear conformation (Fig. S1C). Although a DALI (Holm and Rosenström, 2010) search against the Protein Data Bank (PDB) identified many structures with a topologically similar arrangement of three to four α- helices, either as single units or as part of a larger helical array, these differed substantially in their helix to helix angles and therefore represent only distant hits with low Z-scores (Z < 4.5) and rather large r.m.s.d. values (> 3.0 Å). Hence, it seems that the four-helical bundle of XTBD represents a structurally unique arrangement for XRN2 binding with no closely related protein structure present in the PDB.

XTBD Tyrosine 56 is Critical for Complex Formation *in vitro* and *in vivo*

Crystal packing analysis suggests that the XTBD – XRN2Δ^{ZLC} complex exists as a single heterodimer and SEC MALS (size exclusion coupled to multi-angle light scattering) experiments confirm this. The XTBD – XRN2Δ^{ZLC} complex elutes as monodisperse heterodimer with a measured mass of 80.9 kDa (calculated mass: 83.0 kDa) (Fig. S2A). Analysis of the protein – protein interface by PISA (Krissinel and Henrick, 2007) and EPPIC (Duarte et al., 2012) reveals a rather small buried solvent-accessible area on either protein of ~1000 Å^2 upon complex formation. 24 residues of XTBD interact with 36 residues of XRN2Δ^{ZLC} in a hydrophobic and polar manner, and these interface residues are highly conserved as shown by ConSurf analysis of both proteins (Ashkenazy *et al.*, 2010; Celniker *et al.*, 2013) (Fig. 2A). The

hydrophobic character of the interface is mainly formed by XTBD residues on L1, H3, and L3 (Trp14, Ile37, Cys41, Leu52, Cys54, Tyr56, Leu60) and contributes to interaction with XRN2Δ^{ZLC} residues Val553, Phe560, Pro591, Pro650, Ile652, Asp653, Pro656, Pro677, and Phe678 (Fig. 2B and S2B). Additional binding energy is provided by the formation of 13 hydrogen bonds and three salt bridges upon complex formation (Fig. 2C, 2D and S2C). Although the XTBD - XRN2 interface is relatively small at ~1000 Å^2, the complex is very stable and resists disruption by high salt washes (data not shown) and high dilution (Fig. S2A).

To further dissect the XTBD – XRN2Δ^{ZLC} interaction, we generated PAXT-1 interface point mutant proteins based on the structural information. To test their binding capacities we co-expressed them with XRN2 and purified the PAXT-1 mutant proteins through their His_6-tags by Immobilized Metal Affinity Chromatography (IMAC) (Fig. 2E). While XRN2 co-purification through PAXT-1 pull-down was unaffected by the PAXT-1 point mutations Trp14-to-Ala and Cys41-to-Gly, respectively, less XRN2 was seen with the Cys54-to-Gly mutation. However, this mutation also decreased PAXT-1 levels, leaving it unclear whether decreased XRN2 purification truly reflects decreased binding capacity. By contrast, the Tyr56-to-Ala mutation completely abrogated interaction of XTBD with XRN2 without destabilizing PAXT-1, highlighting Tyr56 as a key interface residue.

The fact that a single point mutation, Tyr56-to-Ala, abrogates binding although numerous side chains contribute to the total binding energy of the interface, appears surprising. However, it is explained by its crucial role in shaping the unique linear conformation of the loop L3. With all seven residues, XTBD_51-57 engaged in XRN2 binding (Fig. S2C), L3 contributes 33% (338 Å^2) buried surface area (BSA) and four hydrogen bonds to the XTBD – XRN2 interface, whereas the other 17 interacting residues together contribute the remaining 698 Å^2 BSA and nine hydrogen bonds. Mutation of Tyr56 to alanine lacks the key constraint for the 51 – 57 conformation due to the missing phenol ring, which is normally sandwiched between Leu45 (XTBD, H3) and Pro656 (XRN2Δ^{ZLC}), forming a CH – π – interaction with Pro656 (XRN2Δ^{ZLC}) (Fig. 2C). Through its hydroxyl group, Tyr56 also forms hydrogen bonds (2.8 Å) with the backbone carbonyl of Asp653 (XRN2Δ^{ZLC}) (Fig. 2C). A second constraining residue, XTBD Cys54, is found in hydrophobic interaction with Pro656 (XRN2Δ^{ZLC}) and additionally forms a hydrogen bond with the backbone carbonyl of Leu675 (XRN2Δ^{ZLC}) (Fig. S2C). Together, Cys54 and Tyr56 promote formation of an isolated β-bridge between backbone atoms of XTBD_Glu55 and XRN2_Asp658 (Fig. 2D). Mutation of Tyr56 to alanine and Cys54 to glycine removes the constraining side chains for this stretch and induces backbone flexibility, thus compromising/disrupting all interactions between 51 – 57 XTBD residues and XRN2. The resulting loss of one third of BSA explains the severe consequences of these mutations. By contrast Trp14-to-Ala or Cys41-to-Gly have only limited effects on the BSA and thus no major effect on complex formation *in vitro*.

To validate the importance of XTBD Tyr56 for XRN2 binding under physiological conditions, we sought to test whether mutating it would similarly translate into a loss of interaction *in vivo*. We utilized genome editing through CRISPR/Cas9 and homology-directed DNA repair (Arribere et al., 2014; Dickinson et al., 2013) to create the Tyr56-to-Ala point mutation in endogenous PAXT-1. Strikingly, when we grew the resulting *paxt-1(xe29)* worms at 26°C, they arrested as L1 larvae, just like *paxt1(0)* animals (Fig. 2F). Also, just like in *paxt-1(0)* animals, (Miki *et al.*, 2014b), accumulation of XRN2 was reduced and PAXT-1 not detectable as revealed by western blotting (Fig. 2G). Altogether, our data thus identify Tyr56 as a critical residue for interaction with XRN2 *in vitro* and *in vivo*, and explain the structural basis of this importance, as well as the high degree of conservation of this XTBD residue: In XTBDs, this position is always held by residues with aromatic side chains (Tyr, Phe, Trp, Fig. 1A), which can occupy the XRN2 Pro656 pocket *via* a stacking interaction.

XTBD Is a Generic XRN2 Adapter

Although different XTBD/DUF3469-containing proteins occur in complexes with XRN2 (Brannan *et al.*, 2012; Close *et al.*, 2012; Couvillion *et al.*, 2012; Miki *et al.*, 2014b), these interactions were generally examined through co-immunoprecipitation, leaving it unclear whether the interaction is indeed direct and mediated by this specific domain. The fact that the interaction surfaces of both XRN2 and XTBD are highly conserved (Fig. 2A), supported a conserved and direct interaction. To test this notion experimentally, we produced recombinant XRN2 and the XTBD-containing proteins CDKN2AIP and CDKN2AIPNL/C2AIL (for brevity we use C2AIL in the following) from *Danio rerio* (zebrafish) in *E. coli* and determined their interactions. Whereas CDKN2AIP is a tumor suppressor that can activate p53, C2AIL is as yet uncharacterized. When purifying the N-terminally-His_6-tagged XTBD-proteins, XRN2 co-purification was readily detectable in both cases (Fig. 3A). Similarly, human XRN2 co-purified with human His_6-C2AIL (data not shown). To confirm that the mode of interaction between XTBD and XRN2 was also conserved, we sought to disrupt it in the human C2AIL – XRN2 complex by mutating C2AIL Tyr82, which corresponds to PAXT-1 Tyr56 (Fig. S3B). Thus, we transfected human HEK293T cells with either wild-type or Tyr82-to-Ala mutant human FLAG-HA-C2AIL and immunoprecipitated the respective protein by use of an anti-FLAG antibody. Western blotting confirmed robust co-immunoprecipitation of endogenous XRN2 with wild-type but not mutant FLAG-HA-C2AIL (Fig. 3B). This result confirms the specificity of this interaction and the importance of this residue for XRN2-binding by XTBD. Finally, we showed by SEC that *D. rerio* XRN2 formed a stable, chimeric complex with human C2AIL (Fig. 3C). We conclude that XTBD constitutes a generic XRN2-binding domain whose function is conserved across animal phylogeny.

Human C2AIL can substitute for *C. elegans* PAXT-1 *in vivo*

To validate our insights on XTBD conservation that the *in vitro* and cell-based studies had generated, we sought to test them *in vivo* by expressing a codon-optimized and *flag*-tagged human *c2ail* single-copy transgene in *C. elegans paxt-1* null mutant animals. Strikingly, immunoprecipitation of FLAG-Hs_C2AIL from *paxt-1(0); hs_c2ail* worm lysates co-immunoprecipitated endogenous *C. elegans* XRN2 as confirmed by western blot (Fig. 3D) and mass spectrometry (data not shown). This validates the formation of a chimeric complex *in vivo*.

Although PAXT-1 is dispensable at lower temperatures, *paxt-1(0)* animals arrest as L1-stage larvae when grown at 26°C, a phenotype that can be rescued by expression of PAXT-1_1 – 121 (Miki *et al.*, 2014b). Strikingly, the *hs_c2ail* transgenic worms similarly continue development into adulthood and go on to produce F2 progeny (Fig. 3E). Hence, not only the molecular but also the developmental function of PAXT-1 can be taken over by human C2AIL, despite the fact that these two proteins share only ~35% sequence identity in their XTBDs, but consistent with the good correlation of the C2AIL homology model with the XTBD structure (Fig. S3A, S3B).

XRN2 Stability Depends on the Structural Integrity of the PBD

We recently reported that loss of PAXT-1 in *C. elegans* causes a reduction of XRN2 protein but not mRNA levels *in vivo*, consistent with destabilization of the nuclease (Miki *et al.*, 2014b). To test a stabilizing function of PAXT-1 towards XRN2 directly, we examined the thermal stability of recombinant XRN2 and its complex. For this we monitored the unfolding of the PAXT-1 – XRN2 complex versus XRN2 alone. Whereas XRN2 alone has an experimentally determined melting temperature T_m of ~31°C, the T_m of the PAXT-1 – XRN2 complex is ~55°C (Fig. 4A). This striking shift of melting temperatures by a ΔT_m of 24°C reveals that PAXT-1 indeed has a pronounced stabilizing activity towards XRN2. Moreover, PAXT-1 – XRN2, PAXT-1 – XRN2Δ^{ZLC} and XTBD – XRN2Δ^{ZLC} complexes have measured T_m values of 55°C, 54°C, and 53°C, respectively. Hence, the major stabilizing activity of PAXT-1 resides in the XTBD. Finally, the fact that the T_m of 31°C for XRN2 alone is close to the temperature at which larval arrest phenotypes in *C. elegans paxt-1(0)* mutants are observed (26°C) suggests the possibility that XRN2 destabilization *in vivo* occur through its unfolding and subsequent degradation.

Previously we examined the influence of PAXT-1 on the enzymatic activity of XRN2 (Miki et al., 2014b) and found the PAXT-1 – XRN2 complex more active than XRN2 alone over extended periods of time. However, initial velocities remained unchanged in the presence or absence of PAXT-1, implying a

stabilizing rather than a stimulatory effect. Indeed, although closer inspection of the XTBD – XRN2 structure suggested the possibility of a modulatory function of PAXT-1 on XRN2 activity (see below), examination of Michaelis-Menten enzyme kinetics failed to provide any evidence for such a function (Fig. S4A). To test the consequences of destabilization by temperature increase, we compared the activity of XRN2 *in vitro* at two temperatures, 25°C (default temperature of previous activity assays) and 30°C. We chose these two temperatures because they are within, or close to, the physiological range of *C. elegans*. [*C. elegans* can survive at 30°C for at least several hours, but does not procreate.] From the melt curve, we estimate that 45% of XRN2 would be unfolded at 30°C. Nonetheless, and contrary to our expectation, we found that XRN2 activity was consistently, and over extended times, higher at 30°C than 25°C (Fig. 4B).

Although an increase in temperature accelerates enzymatic reaction, according to Arrhenius' equation, we would expect at most a modest effect with the narrow temperature window that we used. Hence, we considered the possibility that XRN2 might indeed be unexpectedly stable under the conditions of the assay, stabilized by substrate binding. To test this, we examined XRN2 thermal stability in the absence and presence of the 30mer RNA substrate used for catalytic assays. This revealed a stabilizing effect of the substrate, which increased the T_m by 2°C to ~33°C (Fig. 4C). Although the effect was small relative to that seen for PAXT-1, it is above the 1°C threshold previously proposed to be significant (Querol et al., 1996), and it occurred reproducibly at two different substrate concentrations (data not shown). Moreover, it was highly specific, as inclusion of tRNA, which is not a good XRN2 substrate due to high secondary structure and paired 5' terminal nucleotides (Jinek et al., 2011; Stevens and Poole, 1995), did not increase thermal stability of XRN2. Hence, we conclude that substrate binding can stabilize XRN2.

To understand the interaction of XRN2 with substrate, we superimposed the XRN1 – substrate complex (Jinek et al., 2011; PDB 2Y35) onto the XTBD – XRN2 structure. This revealed a crucial role of the PBD-protruding loop in substrate binding, as its Trp670 base-stacks with three unpaired 5'- terminal nucleotides and His60 of α-helix 2 (Fig. 4D). Moreover, Trp670 in XRN2, as Trp540 in XRN1 (Jinek et al., 2011), forms a steric barrier in concert with N-terminal α-helix 1 to restrict access to the active site for single stranded RNA. That the mode of substrate binding is indeed conserved between the two RNases is confirmed by the identification of a sulfate ion from the crystallization buffer of the XTBD – XRN2 complex occupying the precise position of the 5' phosphate of the XRN1 – RNA substrate complex (Fig. 4D).

From the structures of the two complexes it is thus evident that both substrate and PAXT-1 bind to the PBD. To determine whether this might affect PBD structure, we compared the PBDs from these two complexes to that of *K. lactis* XRN1, which was crystallized in the absence of both substrate and

additional proteins (Chang et al., 2011; PDB 3PIF). Strikingly, whereas the PBD is fully structured in XRN2 – XTBD and *Drosophila* XRN1, it is heavily disordered in the structure of *K. lactis* XRN1 and the domain could not be entirely built in the crystallographic model (Fig. 4E). Hence, although not a proof, these structures are consistent with the notion that stabilization of XRN2 is achieved through maintenance of the integrity of the PBD, which both XTBD- and substrate-binding can accomplish (Fig. 4E).

Discussion

Based on the recurring identification of DUF3469 domain-containing proteins in complexes that also contain XRN2 (Brannan et al., 2012; Couvillion et al., 2012; Miki et al., 2014b), we previously hypothesized that it mediates XRN2-binding. Here, we have tested this notion and demonstrate that a core DUF3469/XTBD domain, substantially smaller than initially predicted, mediates direct and specific binding to XRN2. Chimeric interactions between XTBD-containing proteins and XRN2 from different species *in vivo* and *in vitro* confirm the generality of this finding. Moreover, although the XRN2 paralogue XRN1 is highly similar in sequence to XRN2, including in the PAXT-1 binding groove formed by the NCD2 and the PBD (Fig. S1D, S1E), binding of PAXT-1 to XRN1 is disfavored: the NCD2 of XRN1 extends further into the groove than that of XRN2, suggesting a steric clash between this domain and XTBD (Fig. S1E). This is consistent with co-immunoprecipitation (co-IP) experiments, which revealed a specific interaction of PAXT-1 with XRN2, but not XRN1 (Miki *et al.*, 2014b). We conclude that XTBD is a generic and specific XRN2 binding domain.

Although PAXT-1 is the only XTBD-containing protein in *C. elegans*, many vertebrates have three such predicted XTBD proteins, CDKN2AIP, C2AIL, and NKRF (Miki *et al.*, 2014b). Outside their XTBDs, these proteins exhibit little sequence homology, and their cellular functions, although not well characterized, appear distinct: Mammalian NKRF was identified as a transcriptional repressor, CDKN2AIP appears to function as an activator of p53 (Cheung *et al.*, 2014; Feng *et al.*, 2002; Hasan *et al.*, 2002, 2004), and C2AIL has currently no known function. However, the strong interaction that we observe between XTBDs and XRN2, resistant to high salt levels and high dilution, implies that all of these proteins will exert at least part of their functions with or through XRN2. The ability to uncouple these proteins from XRN2 through a single point mutation now provides the tool to test, in future work, whether and to what extent this holds true for each of these proteins.

A second implication of the stable and heterodimeric binding between XRN2 and XTBD is that vertebrate XRN2 can be assumed to exist in multiple complexes that occur in separate, non-interchangeable pools, thus potentially diversifying XRN2 functions. Different binding partners may endow XRN2 with distinct catalytic activities, facilitate differential regulation of XRN2 through distinct subunits, or recruit XRN2 to distinct cellular locations. Results from immunofluorescence experiments on human U-2 OS osteosarcoma cell lines indeed provide circumstantial evidence for the latter, as XRN2 staining is observed in both nucleus and nucleoplasms, whereas NKRF locates to the nucleolus, from which the nucleoplasmic CDKN2AIP appears excluded (Uhlén et al., 2015).

According to such a model of functional specialization of XRN2 complexes, XTBD serves a bridging function between XRN2 and specific protein domains that provide additional functionalities. As a complex of XRN2 with full-length PAXT-1 did not crystallize, we do not know what such functions could

be in the case of the PAXT-1 C-terminal sequence, which is conserved across nematodes. However, we may speculate that it could serve to modulate XRN2 activity or to block access of specific substrates to the XRN2 active site. This is because the structure of the XRN2 – XTBD complex implies that the PAXT-1 C-terminus would be located right in front of the XRN2 nuclease cleft, and because analysis by PSIPRED (Buchan et al., 2013) and DisEMBL (Linding et al., 2003) suggests it to be structured (data not shown). However, since we have thus far been unable to observe regulation of XRN2 activity by PAXT-1 *in vitro*, it seems possible that such functions would only occur on specific substrates or under specific conditions that remain to be identified.

In agreement with a more specialized role of the PAXT-1 C-terminus, it is dispensable for *C. elegans* viability (Miki et al., 2014b). Together with the fact that the heterologous human C2AIL can substitute for PAXT-1 *in vivo*, this then implies functions of XTBD beyond that of a passive XRN2 adapter. Our data support this function to be stabilization of XRN2 by promoting the folding of its PBD domain. The T_m is a measure of a protein's thermal stability and depends on numerous molecular parameters such as the amino acid composition, surface hydrophobicity, number of hydrogen bonds and labile secondary structures such as loops (reviewed in Vieille and Zeikus, 2001). Upon XTBD-binding, 13 hydrogen bonds are formed, a hydrophobic patch covered and the flexibility of the PBD loop reduced. Decreased thermal stability of XRN2 in the absence of XTBD *in vitro* may then reflect decreased half-life *in vivo* (Ghaemmaghami and Oas, 2001; McLendon and Radany, 1978; Parsell and Sauer, 1989), as even partially unfolded proteins exhibit increased susceptibility to proteolysis (Kumar et al., 2000; Parsell and Sauer, 1989). This then explains how PAXT-1/XTBD binding increases XRN2 levels *in vivo*.

Although PAXT-1 is expressed throughout *C. elegans* development (Miki et al., 2014b), its loss causes defects only at specific stages: when *paxt-1(0)* mutant animals are shifted to the restrictive temperature of 26°C during the L4 stage, they will continue development through adulthood and produce F1 progeny, which, however, will arrest at the first larval (L1) stage (Miki et al., 2014b). This delayed effect does not appear to simply reflect the time it takes to deplete XRN2, as L1 stage arrest of F1s also occurs if parental animals were already shifted to 26°C during their L1 stage (Miki et al., 2014b). Moreover, although animals may conceivably be more dependent on XRN2 activity during some developmental stages than others, developmental arrest can be induced in virtually any stage upon direct inactivation of XRN2 (Miki et al., 2014a). Hence, we speculate that it is the stability of XRN2 that varies with development stage. Specifically, with substrate binding conferring some stability to XRN2, the stabilizing activity of PAXT-1 may be more important when substrate levels are low. Thus, a key function of XTBD may be to preserve, rather than promote XRN2 activity, guarding enzyme not bound by substrate against decay to retain a constant pool of active protein.

Material & Methods

Protein Expression and Purification

Constructs were expressed in *E. coli* BL21(DE3) using a modified bis-cistronic vector from Novagen where XTBD-containing proteins carried an N-terminal His_6-tag whereas XRN2 proteins were untagged. Cleared lysate was obtained by sonication and centrifugation. Target protein was purified using IMAC, TEV-cleavage, ion-exchange and size-exclusion chromatography. Protein fractions were subsequently concentrated as desired and used for crystallography or aliquoted and flash-frozen for storage. See Supplementary Methods for details.

Crystallization, Data Collection and Structure Solution

Protein crystallization was carried out at 20°C using the sitting-drop vapor diffusion method with a Phoenix robot (Art Robbins) dispensing 300 nl drops (100 nl crystallization buffer and 200 nl protein solution). XRN2Δ^{ZLC} – XTBD crystals, obtained in 2 M ammonium sulfate, 0.1 M Bis-TRIS pH 6.5 or 0.1 M TRIS pH 8.5 were harvested and flash-cooled in liquid nitrogen after cryoprotection with 3.2 M ammonium sulfate, 0.1 M Bis-TRIS pH 6.5 or 0.1 M TRIS pH 8.5. Highest resolution data was obtained with a seleno-methionine derivative crystal, which diffracted to 2.85 Å at the SLS PX-II beamline (Villigen, Switzerland) and belonged to space group $P2_12_12_1$ with six XRN2Δ^{ZLC} – XTBD heterodimers in the asymmetric unit. Diffraction data was integrated and scaled using the XDS program package (Kabsch, 2010) and the structure was solved by the molecular replacement method with PHASER (McCoy *et al.*, 2007) using an XRN2 homology model consisting of the exonuclease core as search model. Phases from this solution were calculated and used for automatic model building with BUCCANEER (Cowtan, 2006). The XRN2Δ^{ZLC} – XTBD structure was further improved by the crystallographic simulated annealing routine followed by grouped B-factor refinement in PHENIX (Afonine *et al.*, 2012), several rounds of manual rebuilding in COOT (Emsley *et al.*, 2010), and refinement in PHENIX and BUSTER (Bricogne et al., 2011). Non-crystallographic symmetry restraints were used throughout the structure solution and refinement process. Model building and validation was carried out with the help of anomalous difference Fourier electron density maps to locate seleno-methionine positions. The final structure was validated using COOT. Structural images for figures were prepared with PyMOL (Schrödinger, 2010).

Thermal Shift Assay

A Protein Thermal Shift™ Dye Kit (Applied Biosystems) was used according to the manufacturer's instruction. Two µg total protein (1 µg when mixed with substrate) was assayed in triplicates using the melt-curve program of a StepOnePlus™ real-time PCR system. The sigmoidal part of the melt curve was fitted to the Boltzman equation with the non-linear regression analysis using Microsoft Excel. These functions were normalized to 1, scaled for concise representation and plotted along with the corresponding raw-data.

Real-time Exonuclease Activity Assay and Kinetic Analysis

The kinetic assay was performed as described in Sinturel *et al.*, (2009) with the following modifications: A substrate mix of RNA – DNA duplex, where the RNA is FAM-labeled whereas the DNA carries a quencher, and unlabeled *let-7* was used at a ratio of 1:4 to increase the dynamic range of the assay. Enzymes were assayed with an excess of total substrate of 5 to 200 fold. Data was subsequently fitted to the Michaelis – Menten-model by the least square method.

Strains

Standard procedures were used to culture the Bristol N2 wild-type, mutant and transgenic strains (Brenner, 1974). HW1091: *paxt1-(xe5)* is the null mutation described by Miki *et al.* (2014b). Generation of HW 1641: *paxt-1(xe5) I; xeSi203[Ppaxt-1::C.elegans_co_human_C2AIL_FLAG_ operon_GFP_tbb-2-3'UTR, unc-119(+)] II* and HW 1644: *paxt-1(xe29[I:8597012-8597014 = TAT -> GCT, I:8597041 A -> T]* (expressing PAXT-1_Y56A and containing a silent mutation to facilitate screening for genome editing events) are described in detail below.

Genome Editing of *C. elegans* Using CRISPR-Cas9

A suitable site for 20 nt long sgRNA was identified by considering availability of a PAM site to create a double strand break on the *paxt-1* gene. Two complementary nucleotides were hybridized and cloned by Gibson assembly (Gibson *et al.*, 2009) into pIK111, a derivative of the PU6::sgRNA backbone (Friedland *et al.*, 2013; Katic et al., 2015). Furthermore, a 100 nt DNA single stranded repair oligo was designed with the desired point mutation and a silent mutation at the sgRNA binding site. A CRISPR co-conversion mix, also containing *Peft-3::Cas9::tbb-2 3' UTR* (Dickinson et al., 2013), the sgRNA and oligonucleotide to recreate the *sqt-1(sc1)* mutation (analogous to (Arribere *et al.*, 2014)) was injected

into N2 animals (Katic et al., 2015). Roller progeny were cloned and their progeny were analyzed for desired mutations by PCR.

Rescue Experiments Using MosSCI

The *paxt-1* promoter, *H. sapiens C2AIL* (codon-optimized + two artificial introns) coding sequence and *tbb-2* 3' UTR sequences were cloned into pCFJ150 by Gateway cloning. An operon_GFP sequence between *C2AIL* and the *tbb*-2 3'UTR was included to permit visualization of transgene expression without altering the sequence of the encoded protein. The resulting plasmid was inserted into the *ttTi5605* site by MosSCI (Frøkjaer-Jensen *et al.*, 2008; Frøkjær-Jensen *et al.*, 2012), yielding *xeIs203[Ppaxt-1::C.elegans_co_human_C2AIL_FLAG_operon_GFP_tbb-2-3'UTR,unc-119(+)] II* animals. The integrants were outcrossed to wild-type N2 and crossed into the *paxt-1(xe5*) mutant. Rescue of the *paxt-1(0)* mutant phenotype was examined as reported (Miki *et al.*, 2014b).

Cell Culture and Transient Transfection of HEK293T Cells

Transfection and culturing of HEK293T cells were done as described in de la Mata et al. (2015). pIRESneo (Addgene plasmid #10822) harboring either wild type or Tyr82-to-Ala mutated Hs_C2AIL and pSD44 (modified Addgene plasmid #12252) expressing GFP were used for transfection.

Antibodies, Co-Immunoprecipitation and Western Blot Experiments

Antibodies, immunoprecipitation and western blotting are described in detail in the supplementary methods.

Microscopy

Stereoscopic images were taken with a M205 A stereo microscope (Leica, Solms, Germany).

Acknowledgements

We thank Jeremy Keusch for technical support and Daniel Hess for mass spectrometry analysis; Manuel de la Mata for help with cell transfections; Jeffrey A. Chao and Nicolas Thomä for critical comments on the manuscript. We are grateful to the staff of the Swiss Light Source, Paul Scherrer Institute, Villingen, where parts of the experiments were performed.

References

Afonine, P. V, Grosse-Kunstleve, R.W., Echols, N., Headd, J.J., Moriarty, N.W., Mustyakimov, M., Terwilliger, T.C., Urzhumtsev, A., Zwart, P.H., and Adams, P.D. (2012). Towards automated crystallographic structure refinement with phenix.refine. Acta Crystallogr. D. Biol. Crystallogr. *68*, 352–367.

Amberg, D.C., Goldstein, A.L., and Cole, C.N. (1992). Isolation and characterization of RAT1: An essential gene of Saccharomyces cerevisiae required for the efficient nucleocytoplasmic trafficking of mRNA. Genes Dev. *6*, 1173–1189.

Arribere, J. a, Bell, R.T., Fu, B.X., Artiles, K.L., Hartman, P.S., and Fire, A.Z. (2014). Efficient Marker-Free Recovery of Custom Genetic Modifications with CRISPR/Cas9 in Caenorhabditis elegans. Genetics *198*, 837–846.

Ashkenazy, H., Erez, E., Martz, E., Pupko, T., and Ben-Tal, N. (2010). ConSurf 2010: Calculating evolutionary conservation in sequence and structure of proteins and nucleic acids. Nucleic Acids Res. *38*, 529–533.

Brannan, K., Kim, H., Erickson, B., Glover-Cutter, K., Kim, S., Fong, N., Kiemele, L., Hansen, K., Davis, R., Lykke-Andersen, J., et al. (2012). mRNA Decapping Factors and the Exonuclease Xrn2 Function in Widespread Premature Termination of RNA Polymerase II Transcription. Mol. Cell 1–14.

Brenner, S. (1974). The genetics of Caenorhabditis elegans. Genetics *77*, 71–94.

Bricogne, G., Blanc, E., Brandl, M., Flensburg, C., Keller, P., Paciorek, W., Roversi, P., Sharff, A., Smart, O.S., and Vonrhein, C. (2011). BUSTER 2.11.4.

Buchan, D.W. a, Minneci, F., Nugent, T.C.O., Bryson, K., and Jones, D.T. (2013). Scalable web services for the PSIPRED Protein Analysis Workbench. Nucleic Acids Res. *41*, 349–357.

Celniker, G., Nimrod, G., Ashkenazy, H., Glaser, F., Martz, E., Mayrose, I., Pupko, T., and Ben-Tal, N. (2013). ConSurf: Using evolutionary data to raise testable hypotheses about protein function. Isr. J. Chem. *53*, 199–206.

Chanfreau, G., Rotondo, G., Legrain, P., and Jacquier, A. (1998). Processing of a dicistronic small nucleolar RNA precursor by the RNA endonuclease Rnt1. EMBO J. *17*, 3726–3737.

Chang, J.H., Xiang, S., Xiang, K., Manley, J.L., and Tong, L. (2011). Structural and biochemical studies of the 5’→3' exoribonuclease Xrn1. Nat. Struct. Mol. Biol. *18*, 270–276.

Chatterjee, S., and Grosshans, H. (2009). Active turnover modulates mature microRNA activity in Caenorhabditis elegans. Nature *461*, 546–549.

Chernyakov, I., Whipple, J.M., Kotelawala, L., Grayhack, E.J., and Phizicky, E.M. (2008). Degradation of several hypomodified mature tRNA species in Saccharomyces cerevisiae is mediated by Met22 and the 5’-3' exonucleases Rat1 and Xrn1. Genes Dev. *22*, 1369–1380.

Cheung, C.T., Singh, R., Kalra, R.S., Kaul, S.C., and Wadhwa, R. (2014). Collaborator of ARF (CARF) regulates proliferative fate of human cells by dose-dependent regulation of DNA damage signaling. J. Biol. Chem. *289*, 18258–18269.

Close, P., East, P., Dirac-Svejstrup, a. B., Hartmann, H., Heron, M., Maslen, S., Chariot, A., Söding, J., Skehel, M., and Svejstrup, J.Q. (2012). DBIRD complex integrates alternative mRNA splicing with RNA polymerase II transcript elongation. Nature *484*, 386–389.

Couvillion, M.T., Bounova, G., Purdom, E., Speed, T.P., and Collins, K. (2012). A Tetrahymena Piwi bound to mature tRNA 3' fragments activates the exonuclease Xrn2 for RNA processing in the nucleus. Mol. Cell *48*, 509–520.

Cowtan, K. (2006). The Buccaneer software for automated model building. 1. Tracing protein chains. Acta Crystallogr. D. Biol. Crystallogr. *62*, 1002–1011.

Davidson, L., Kerr, A., and West, S. (2012). Co-transcriptional degradation of aberrant pre-mRNA by Xrn2. EMBO J. *31*, 2566–2578.

Dickinson, D.J., Ward, J.D., Reiner, D.J., and Goldstein, B. (2013). Engineering the Caenorhabditis elegans genome using Cas9-triggered homologous recombination. Nat. Methods *10*, 1028–1034.

Duarte, J.M., Srebniak, A., Schärer, M. a, and Capitani, G. (2012). Protein interface classification by evolutionary analysis. BMC Bioinformatics *13*, 334.

Emsley, P., Lohkamp, B., Scott, W.G., and Cowtan, K. (2010). Features and development of Coot. Acta Crystallogr. D. Biol. Crystallogr. *66*, 486–501.

Feng, X., Guo, Z., Nourbakhsh, M., Hauser, H., Ganster, R., Shao, L., and Geller, D. a (2002). Identification of a negative response element in the human inducible nitric-oxide synthase (hiNOS) promoter: The role of NF-kappa B-repressing factor (NRF) in basal repression of the hiNOS gene. Proc. Natl. Acad. Sci. U. S. A. *99*, 14212–14217.

Friedland, A.E., Tzur, Y.B., Esvelt, K.M., Colaiácovo, M.P., Church, G.M., and Calarco, J. a (2013). Heritable genome editing in C. elegans via a CRISPR-Cas9 system. Nat. Methods *10*, 741–743.

Frøkjaer-Jensen, C., Davis, M.W., Hopkins, C.E., Newman, B.J., Thummel, J.M., Olesen, S., Grunnet, M., and Jorgensen, E.M. (2008). Single-copy insertion of transgenes in Caenorhabditis elegans. Nat. Genet. *40*, 1375–1383.

Frøkjær-Jensen, C., Davis, M.W., Ailion, M., and Jorgensen, E.M. (2012). Improved Mos1-mediated transgenesis in C. elegans. Nat. Methods *9*, 117–118.

Geerlings, T.H., Vos, J.C., and Raué, H. a (2000). The final step in the formation of 25S rRNA in Saccharomyces cerevisiae is performed by 5'-->3' exonucleases. RNA *6*, 1698–1703.

Ghaemmaghami, S., and Oas, T.G. (2001). Quantitative protein stability measurement in vivo. Nat. Struct. Biol. *8*, 879–882.

Gibson, D.G., Young, L., Chuang, R.-Y., Venter, J.C., Hutchison, C. a, and Smith, H.O. (2009). Enzymatic assembly of DNA molecules up to several hundred kilobases. Nat. Methods *6*, 343–345.

Hasan, M.K., Yaguchi, T., Sugihara, T., Kumar, P.K.R., Taira, K., Reddel, R.R., Kaul, S.C., and Wadhwa, R. (2002). CARF is a novel protein that cooperates with mouse p19ARF (human p14ARF) in activating p53. J. Biol. Chem. *277*, 37765–37770.

Hasan, M.K., Yaguchi, T., Minoda, Y., Hirano, T., Taira, K., Wadhwa, R., and Kaul, S.C. (2004). Alternative reading frame protein (ARF)-independent function of CARF (collaborator of ARF) involves its interactions with p53: evidence for a novel p53-activation pathway and its negative feedback control. Biochem. J. *380*, 605–610.

Holm, L., and Rosenström, P. (2010). Dali server: conservation mapping in 3D. Nucleic Acids Res. *38*, W545–W549.

Jinek, M., Coyle, S.M., and Doudna, J. a (2011). Coupled 5' nucleotide recognition and processivity in Xrn1-mediated mRNA decay. Mol. Cell *41*, 600–608.

Kabsch, W. (2010). XDS. Acta Crystallogr. D. Biol. Crystallogr. *66*, 125–132.

Katic, I., Xu, L., and Ciosk, R. (2015). CRISPR/Cas9 Genome Editing in Caenorhabditis elegans: Evaluation of Templates for Homology-Mediated Repair and Knock-Ins by Homology-Independent DNA Repair. G3 *3*, 2305–2312.

Kenna, M., Stevens, A., McCammon, M., and Douglas, M.G. (1993). An essential yeast gene with homology to the exonuclease-encoding XRN1/KEM1 gene also encodes a protein with exoribonuclease activity. Mol. Cell. Biol. *13*, 341–350.

Kim, M., Krogan, N.J., Vasiljeva, L., Rando, O.J., Nedea, E., Greenblatt, J.F., and Buratowski, S. (2004). The yeast Rat1 exonuclease promotes transcription termination by RNA polymerase II. Nature *432*, 517–522.

Krissinel, E., and Henrick, K. (2007). Inference of macromolecular assemblies from crystalline state. J. Mol. Biol. *372*, 774–797.

Kumar, S., Tsai, C.J., and Nussinov, R. (2000). Factors enhancing protein thermostability. Protein Eng. *13*, 179–191.

De la Mata, M., Gaidatzis, D., Vitanescu, M., Stadler, M.B., Wentzel, C., Scheiffele, P., Filipowicz, W., and Großhans, H. (2015). Potent degradation of neuronal miRNAs induced by highly complementary targets. EMBO Rep. *16*, 500–511.

Linding, R., Jensen, L.J., Diella, F., Bork, P., Gibson, T.J., and Russell, R.B. (2003). Protein disorder prediction: Implications for structural proteomics. Structure *11*, 1453–1459.

McCoy, A.J., Grosse-Kunstleve, R.W., Adams, P.D., Winn, M.D., Storoni, L.C., and Read, R.J. (2007). Phaser crystallographic software. J. Appl. Crystallogr. *40*, 658–674.

McLendon, G., and Radany, E. (1978). Is protein turnover thermodynamically controlled? J. Biol. Chem. *253*, 6335–6337.

Miki, T.S., and Großhans, H. (2013). The multifunctional RNase XRN2. Biochem. Soc. Trans. *41*, 825–830.

Miki, T.S., Rüegger, S., Gaidatzis, D., Stadler, M.B., and Großhans, H. (2014a). Engineering of a conditional allele reveals multiple roles of XRN2 in Caenorhabditis elegans development and substrate specificity in microRNA turnover. Nucleic Acids Res. 1–12.

Miki, T.S., Richter, H., Rüegger, S., and Großhans, H. (2014b). PAXT-1 promotes XRN2 activity by stabilizing it through a conserved domain. Mol. Cell *53*, 351–360.

Nagarajan, V.K., Jones, C.I., Newbury, S.F., and Green, P.J. (2013). XRN 5'→3' exoribonucleases: Structure, mechanisms and functions. Biochim. Biophys. Acta - Gene Regul. Mech. *1829*, 590–603.

Parker, R., and Sheth, U. (2007). P Bodies and the Control of mRNA Translation and Degradation. Mol. Cell *25*, 635–646.

Parsell, D.A., and Sauer, R.T. (1989). The structural stability of a protein is an important determinant of its proteolytic susceptibility in Escherichia coli. J. Biol. Chem. *264*, 7590–7595.

Petfalski, E., Dandekar, T., Henry, Y., and Tollervey, D. (1998). Processing of the precursors to small nucleolar RNAs and rRNAs requires common components. Mol. Cell. Biol. *18*, 1181–1189.

Poole, T.L., and Stevens, A. (1995). Comparison of features of the RNase activity of 5'-exonuclease-1 and 5'-exonuclease-2 of Saccharomyces cerevisiae. Nucleic Acids Symp. Ser. 79–81.

Querol, E., Perez-Pons, J. a, and Mozo-Villarias, a (1996). Analysis of protein conformational characteristics related to thermostability. Protein Eng. *9*, 265–271.

Schrödinger, L. (2010). The PyMOL Molecular Graphics System, Version 1.3r1.

Sinturel, F., Pellegrini, O., Xiang, S., Tong, L., Condon, C., and Bénard, L. (2009). Real-time fluorescence detection of exoribonucleases. RNA *15*, 2057–2062.

Söding, J., Biegert, A., and Lupas, A.N. (2005). The HHpred interactive server for protein homology detection and structure prediction. Nucleic Acids Res. *33*, W244–W248.

Stevens, A., and Poole, T.L. (1995). 5'-exonuclease-2 of Saccharomyces cerevisiae. Purification and features of ribonuclease activity with comparison to 5'-exonuclease-1. J. Biol. Chem. *270*, 16063–16069.

Uhlén, M., Fagerberg, L., Hallström, B.M., Lindskog, C., Oksvold, P., Mardinoglu, A., Sivertsson, Å., Kampf, C., Sjöstedt, E., Asplund, A., et al. (2015). Tissue-based map of the human proteome. Science *347*, 1260419–1260419.

Vieille, C., and Zeikus, G.J. (2001). Hyperthermophilic enzymes: sources, uses, and molecular mechanisms for thermostability. Microbiol. Mol. Biol. Rev. *65*, 1–43.

Wang, M., and Pestov, D.G. (2011). 5'-end surveillance by Xrn2 acts as a shared mechanism for mammalian pre-rRNA maturation and decay. Nucleic Acids Res. *39*, 1811–1822.

West, S., Gromak, N., and Proudfoot, N.J. (2004). Human 5' --> 3' exonuclease Xrn2 promotes transcription termination at co-transcriptional cleavage sites. Nature *432*, 522–525.

Wheeler, T.J., Clements, J., and Finn, R.D. (2014). Skylign: a tool for creating informative, interactive logos representing sequence alignments and profile hidden Markov models. BMC Bioinformatics *15*, 7.

Xiang, S., Cooper-Morgan, A., Jiao, X., Kiledjian, M., Manley, J.L., and Tong, L. (2009). Structure and function of the 5'-->3' exoribonuclease Rat1 and its activating partner Rai1. Nature *458*, 784–788.

Xue, Y., Bai, X., Lee, I., Kallstrom, G., Ho, J., Brown, J., Stevens, A., and Johnson, a W. (2000). Saccharomyces cerevisiae RAI1 (YGL246c) is homologous to human DOM3Z and encodes a protein that binds the nuclear exoribonuclease Rat1p. Mol. Cell. Biol. *20*, 4006–4015.

Zakrzewska-Placzek, M., Souret, F.F., Sobczyk, G.J., Green, P.J., and Kufel, J. (2010). Arabidopsis thaliana XRN2 is required for primary cleavage in the pre-ribosomal RNA. Nucleic Acids Res. *38*, 4487–4502.

Figure Legends

Figure 1: Overall Structure and Domain Architecture of the XTBD – XRN2Δ^{ZLC} Complex

(A) Schematic of the domain architecture of PAXT-1 and XRN2 and protein constructs used in this study. Hatched and dotted areas within NCD1 and NCD2 mark the zinc-finger and disordered loop, respectively. The blow-up shows a sequence logo (Wheeler et al., 2014) of XTBD. (B) Overall structure of the XTBD – XRN2Δ^{ZLC} complex as cartoon model with transparent surface for XRN2Δ^{ZLC}. Colors for XRN2Δ^{ZLC} and for XTBD correspond to colors in (A). (C) Cartoon representation of XRN2 (red, green and cyan) in complex with the XTBD (yellow). Seleno-Methionine residues are shown as sticks with corresponding anomalous difference Fourier peaks in magenta (5 σ).

Figure 2: Tyr56 Is Critical for Stability of the Highly Conserved XTBD – XRN2Δ^{ZLC} Interface

(A) Surface representation of XRN2Δ^{ZLC} and XTBD structures highlighting the high degree of conservation of the protein – protein interface (XTBD rotated 180 ° with respect to XRN2Δ^{ZLC}). Position-specific conservation scores computed by Consurf (Ashkenazy et al., 2010; Celniker et al., 2013) are displayed from white (weak to average conservation, Consurf levels 1-6) to red (most conserved, level 9). The dashed-dotted line on XRN2Δ^{ZLC} represents the projection of bound XTBD. (B) XTBD residues Cys54 and Tyr56 and their interaction with XRN2Δ^{ZLC} residues. (C) Zoom-in on Tyr56, which is locked by Leu45 and forms a CH – π interaction with Pro656 and a hydrogen bond with the backbone carbonyl of Asp653. (D) Zoom-in on the Tyr56/Cys54 side chain arrangement, which allows formation of the isolated β-bridge between backbone atoms of Glu55 (XTBD) and Asp658 (XRN2Δ^{ZLC}). Hydrogen bonds are indicated by gray dotted lines. (E) Ni-NTA pull-down experiment of His_6-PAXT-1 (arrow) and its point mutants co-expressed with XRN2 (arrowhead). XRN2 is not co-purified with His_6-PAXT-1 Tyr56-to-Ala (lane 6) and Cys54-to-Gly (lane 5) mutant proteins, where Cys54-to-Gly but not Tyr56-to-Ala destabilizes PAXT-1. (F) Stereoscopic images of nematodes at a magnification of 25x. *C. elegans* were grown as indicated by the scheme (above pictures). *paxt-1(xe29)* Tyr56-to-Ala point mutant animals arrest at L1 larval stage similar to *paxt-1(0)*, whereas wild type worms continue to develop. (G) Western blot of 100 µg lysate from worms grown at 26°C. XRN2 levels are reduced in *paxt-1(0)* and *paxt-1(xe29)* mutant relative to wild-type animals.

Figure 3: XTBD is a Generic Binding Adapter for XRN2

(A) *D. rerio* XRN2 (arrowhead; aa 1-803), co-purifies with *D. rerio* His_6-C2AIL (black arrow) and *D. rerio* His_6-CDKN2AIP (blue arrow), respectively. The proteins were co-expressed in *E. coli* and the XTBD-containing proteins pulled down by Ni-NTA. (B) Endogenous XRN2 co-immunoprecipitates from HEK293T cells with wild-type transgenic human FLAG-HA-tagged C2AIL (FH-C2AIL) but not a Tyr82-to-Ala mutant variant thereof. Immunoprecipitation occurred by anti-FLAG antibody; transfection of a GFP-expressing vector was used as mock control (-). Anti-XRN2 and anti-HA antibodies, respectively were used to detect the proteins. (C) SEC elution profiles of *C. elegans* XRN2 alone (blue line), and complexes of PAXT-1 – XRN2 (orange), XTBD – XRN2Δ^{ZLC} (yellow) and *H. sapiens* C2AIL – *D. rerio* XRN2 (aa 1-803, purple line). (D) Human FLAG-tagged C2AIL (FLAG-Hs_C2AIL) was expressed in *paxt-1(0)* mutant *C. elegans* from an integrated single-copy integrated transgene and precipitated by anti-FLAG antibody. Western blotting of 3% lysate (Input) and 50% eluate reveals co-immunoprecipitation of endogenous XRN2, detected by an anti-XRN2 antibody. Non-transgenic wild-type animals were used as negative control. (E) *paxt-1(0)* mutant animals carrying the FLAG-Hs_C2AIL encoding transgenes or no transgene were grown as indicated by the scheme (above pictures) and imaged under a stereomicroscope. In the absence of the transgene, animals arrest at L1 larval stage, whereas expression of Hs_C2AIL permits their progression to adulthood.

Figure 4: The Structural Integrity of the PBD can be Maintained by XTBD or RNA Substrate

(A), (C) XTBD and substrate binding promote XRN2 thermal stability. Protein unfolding was recorded for (A) XRN2 alone (blue line), a PAXT-1 – XRN2 complex (orange line), a PAXT-1 – XRN2Δ^{ZLC} complex (green line), an XTBD – XRN2Δ^{ZLC} complex (yellow line), and (C) XRN2 alone or in the presence of a single-stranded, 5' phosphorylated substrate (purple line) or tRNA (gray line) respectively. The sigmoidal part of each melt curve was fitted to the Boltzman equation, normalized to 1 and scaled for concise representation, and plotted along with the corresponding raw-data. A right shift in the curve signals stabilization. Melting points (T_m), calculated as the inflection point of each curve are indicated by squares. The same curve for XRN2 alone is shown in (A) and (C). (B) Enzymatic activity of XRN2 at a substrate excess of 50x over time. Despite thermal instability, consistently higher activity is recorded at 30°C (dashed blue line) than at 25°C. The negative control (no enzyme) at 30°C is shown as a gray line. (D) XRN2 substrate binding is inferred by superposition of XTBD (yellow) in complex with XRN2Δ^{ZLC} (gray/red/cyan) and *D. melanogaster* XRN1 in complex with substrate (PDB 2Y35). Only substrate is shown, in stick model, for the latter, and a mF_o-DF_c map of the XTBD – XRN2Δ^{ZLC} complex is overlaid and displayed at the SO_4^{2-} position only (5.5 σ). XRN2 employs the identical substrate binding mechanism as XRN1 by base-stacking a tri-nucleotide with its His60 and Trp670. (E) *Left:* Comparison of the PBDs of *C. elegans* XRN2 (cyan) in complex with XTBD (yellow, surface representation), *D.*

melanogaster XRN1 (purple; PDB 2Y35, Jinek et al., 2011) in complex with a tri-nucleotide substrate and *K. lactis* XRN1 (orange; PDB 3PIF Chang et al., 2011). Disordered regions within the *K. lactis* PBD are marked in orange dashed lines. *Right:* A superposition of all three PBDs including XTBD (yellow) and tri-nucleotide (stick-model).

Table I. Crystallographic Data Collection and Refinement Statistics

	XTBD-XRN2Δ^{ZLC} (Se-Met)
Data collection	
Space group	$P2_12_12_1$
Unit cell dimensions	
a, *b*, *c* (Å)	170.2, 200.8, 203.0
α, β, γ (°)	90.0, 90.0, 90.0
Resolution range (Å)[a]	50.0 – 2.84 (2.91-2.84)
Wavelength (Å)	0.97796
Completeness (%)[a]	94.6 (84.5)
Redundancy[a]	3.2 (3.1)
R_{sym}[a]	0.126 (1.261)
$I/\sigma(I)$[a]	7.1 (0.75)
CC (1/2) (%)[a]	99.3 (36.5)
Unique reflections	155519
Refinement	
R_{work}	0.197
R_{free}	0.221
Resolution range (Å)	41.6 – 2.84
Reflections (all)	155439
Reflections (test set)	3899 (2.5%)
Number of atoms	34653
RMS Deviations	
Bond lengths (Å)	0.008
Bond angles (°)	0.97
Ramachandran plot	
Allowed (%)	99.6
Outliers (%)	0.4

[a] Values in parentheses refer to the highest resolution shell

Figure 1

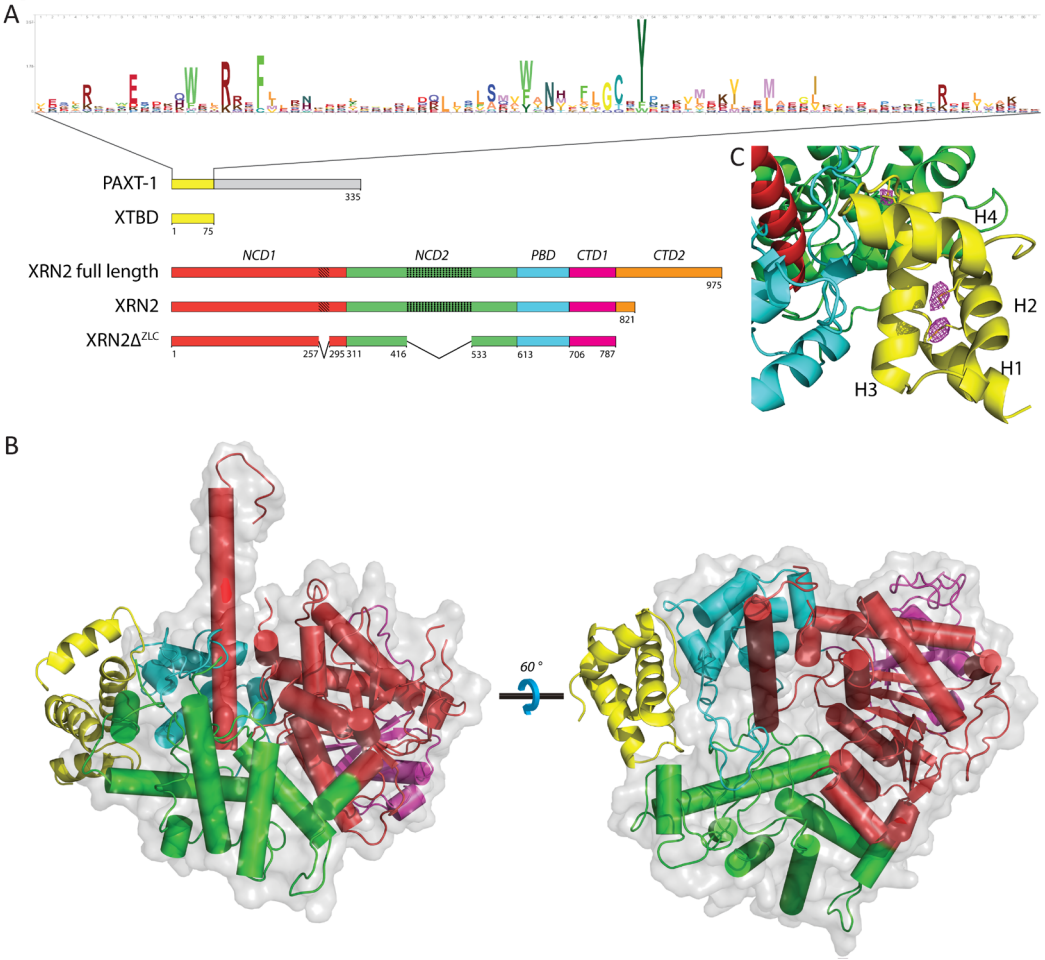
A
PAXT-1
335
XTBD
1
75
NCD1
NCD2
PBD
CTD1
CTD2
XRN2 full length
975
XRN2
821
XRN2Δ^ZLC
1
257
295
311
416
533
613
706
787
C
H4
H2
H1
H3
B
60 °

Figure 2

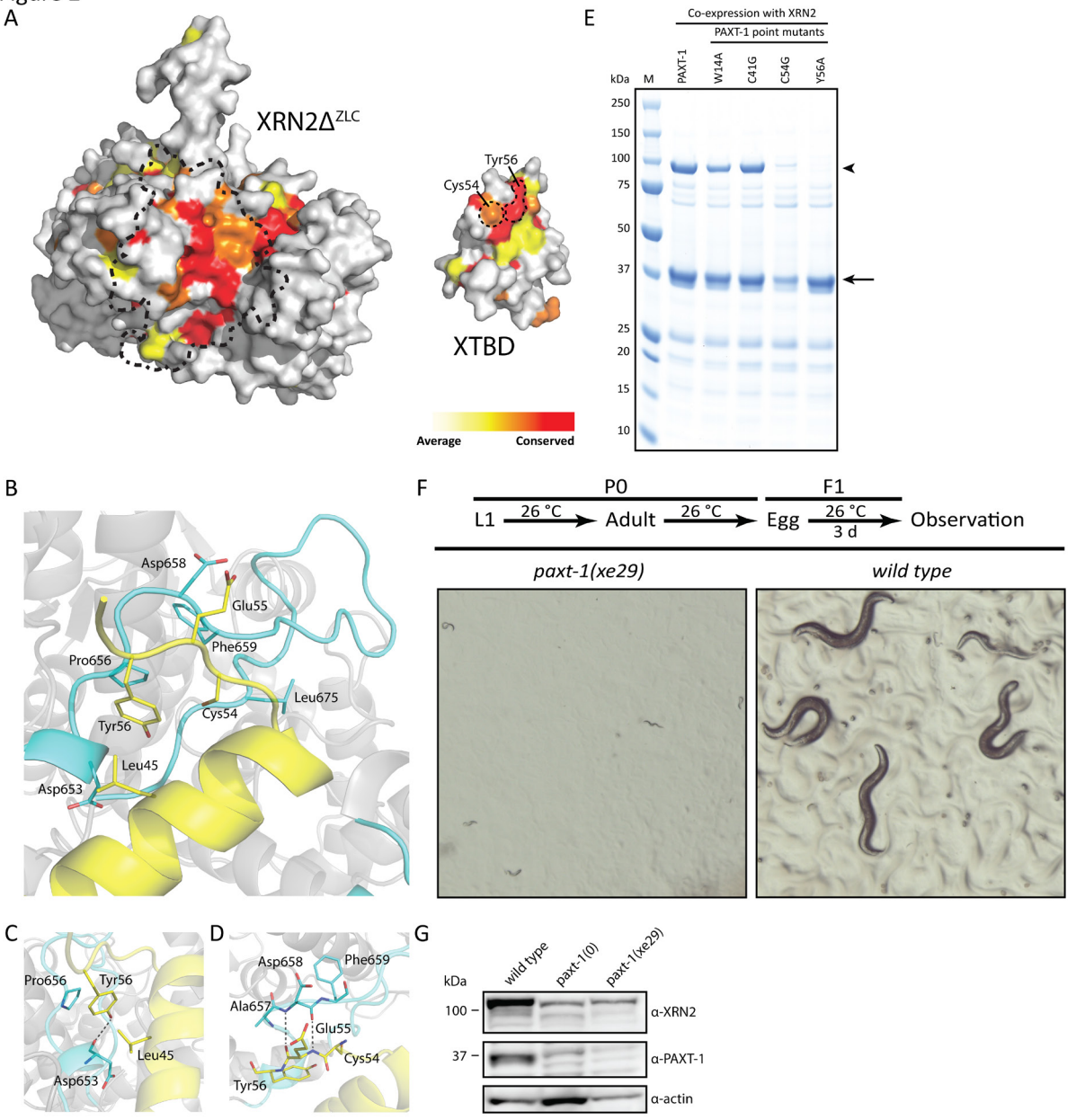
A
XRN2Δ^ZLC
Tyr56
Cys54
XTBD
Average
Conserved
E
Co-expression with XRN2
PAXT-1 point mutants
PAXT-1
W144A
C41G
C54G
Y56A
kDa
M
250
150
100
75
50
37
25
20
15
10
B
Asp658
Glu55
Phe659
Pro656
Leu675
Cys54
Tyr56
Leu45
Asp653
F
P0
F1
L1
26 °C
Adult
26 °C
Egg
26 °C
3 d
Observation
paxt-1(xe29)
wild type
C
Pro656
Tyr56
Leu45
Asp653
D
Asp658
Phe659
Ala657
Glu55
Cys54
Tyr56
G
kDa
wild type
paxt-1(0)
paxt-1(xe29)
100
37
α-XRN2
α-PAXT-1
α-actin

Figure 3

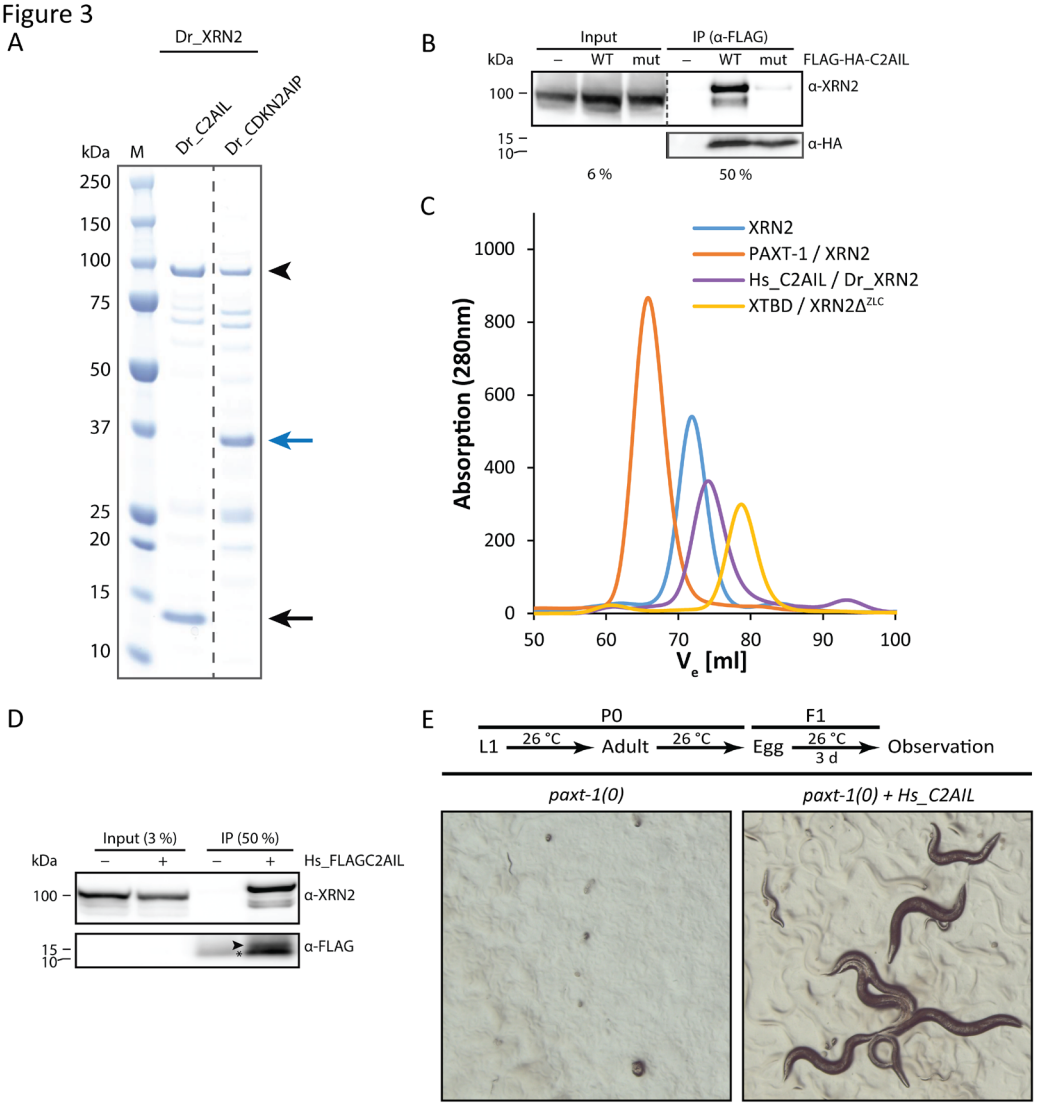
A
Dr_XRN2
kDa
M
Dr_C2AIL
Dr_CDKN2AIP
250
150
100
75
50
37
25
20
15
10
B
Input
IP (α-FLAG)
kDa
–
WT
mut
–
WT
mut
FLAG-HA-C2AIL
100
α-XRN2
15
10
α-HA
6 %
50 %
C
XRN2
PAXT-1 / XRN2
Hs_C2AIL / Dr_XRN2
XTBD / XRN2Δ^ZLC
Absorption (280nm)
1000
800
600
400
200
0
50
60
70
80
90
100
V_e [ml]
D
Input (3 %)
IP (50 %)
kDa
–
+
–
+
Hs_FLAGC2AIL
100
α-XRN2
15
10
α-FLAG
E
P0
F1
L1
26 °C
Adult
26 °C
Egg
26 °C
3 d
Observation
paxt-1(0)
paxt-1(0) + Hs_C2AIL

Figure 4

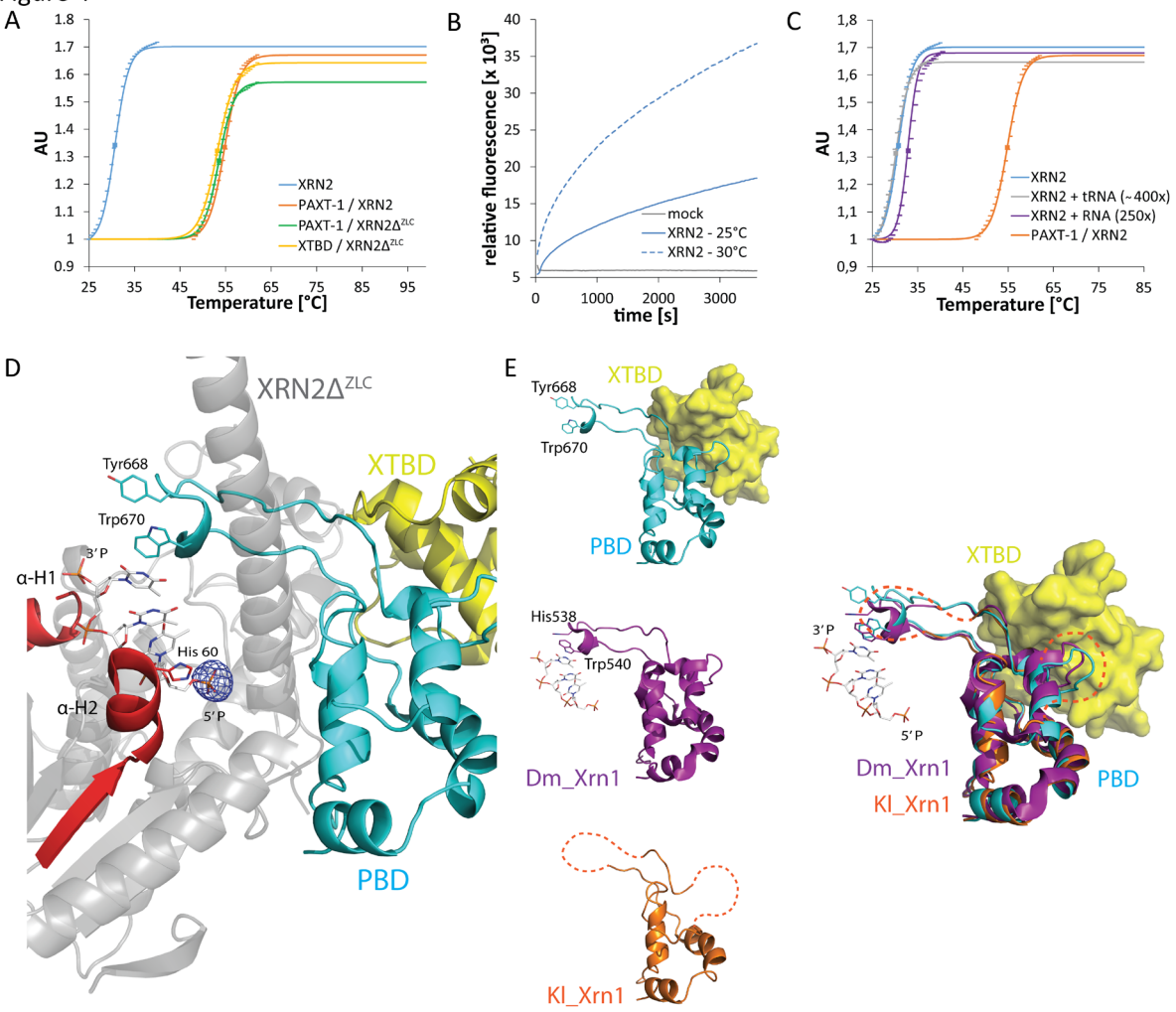
A
AU
Temperature [°C]
XRN2
PAXT-1 / XRN2
PAXT-1 / XRN2Δ^ZLC
XTBD / XRN2Δ^ZLC
B
relative fluorescence [x 10³]
time [s]
mock
XRN2 - 25°C
XRN2 - 30°C
C
AU
Temperature [°C]
XRN2
XRN2 + tRNA (~400x)
XRN2 + RNA (250x)
PAXT-1 / XRN2
D
XRN2Δ^ZLC
XTBD
Tyr668
Trp670
3′P
α-H1
His 60
α-H2
5′P
PBD
E
XTBD
Tyr668
Trp670
PBD
His538
Trp540
Dm_Xrn1
Kl_Xrn1
XTBD
3′P
5′P
Dm_Xrn1
Kl_Xrn1
PBD

Figure S1.

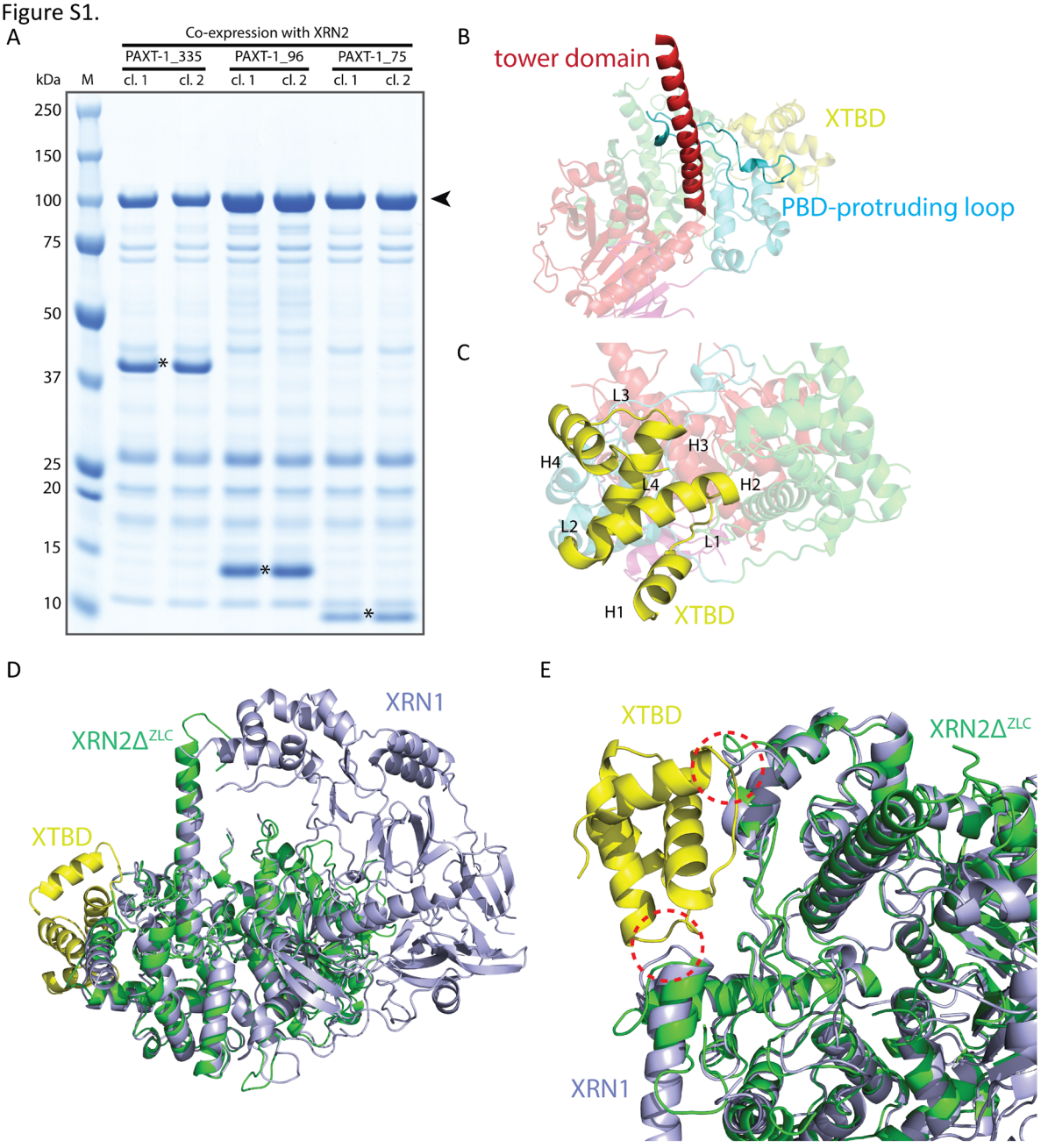

Figure S1, related to Figure 1. The XTBD in Context of XRN2 and XRN1
(A) A Coomassie stained SDS-PAGE gel of PAXT-1 truncation mutants (asterisks) co-expressed with XRN2 (arrowhead). All mutants are capable of binding XRN2 in similar amounts. For each PAXT-1 mutant, two clones were expressed and pulled on their His_6-tag to co-elute XRN2. (B) The tower domain and the PBD-protruding loop are highlighted in red and cyan, respectively. The remaining parts of XRN2 are in light colors. (C) XTBD bound to XRN2, indicating all four helices and loops, respectively. (D), (E) Superposition of *C. elegans* XTBD (yellow) - XRN2 (green) complex and *D. melanogaster* XRN1 (light blue), reveals potential structural clashes of XRN1 with XTBD (dashed red circles).

Figure S2.

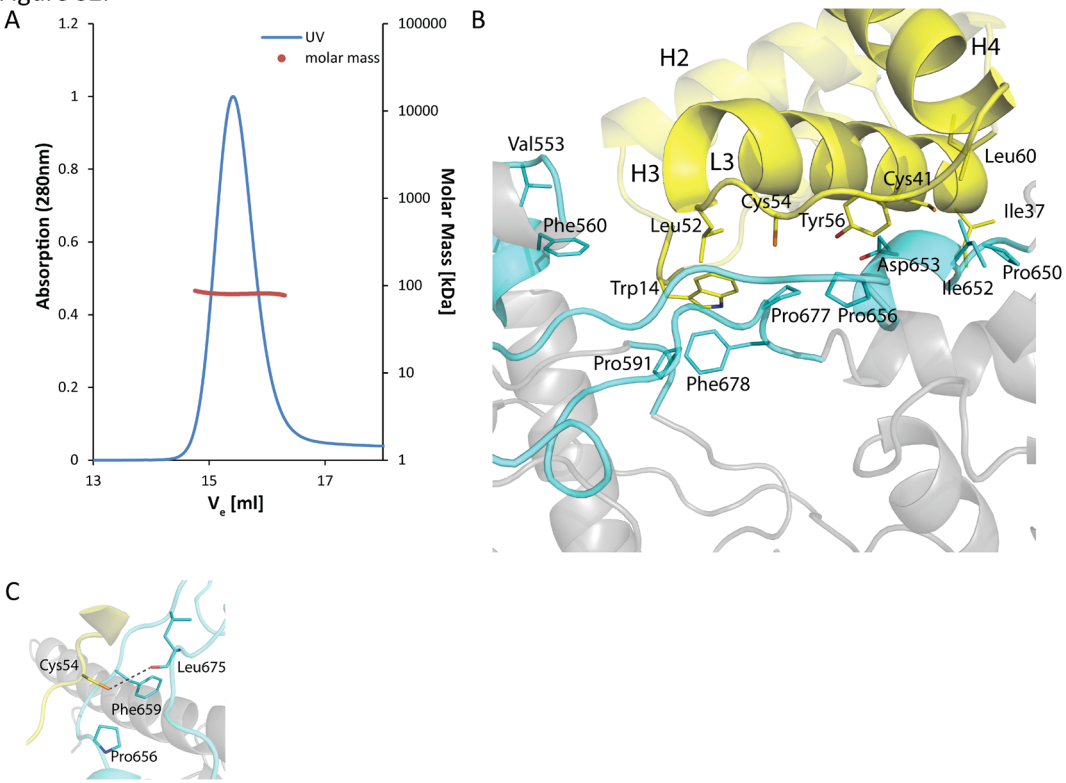

Figure S2, related to Figure 2. The Stable Heterodimeric Complex is formed By Key Interface Residues
(A) SEC-MALS analysis of the XTBD – XRN2Δ^{ZLC} complex. The gel filtration elution profile monitoring UV absorption at 280 nm is displayed in blue. Molar mass values under the peak are shown as red dots. The measured molar mass for the complex (80.9 kDa) was calculated over peak fractions covering the elution volume 14.8 ml – 16.3 ml representing a completely monodisperse sample (polydispersity = 1.000). (B) Close-up of the binding interface of XTBD (yellow) and XRN2Δ^{ZLC} (cyan/gray). Key residues mediating interaction are represented as sticks with oxygens and nitrogens colored in red and blue (atom colors), respectively. (C) Zoom-in on residue Cys54, which forms hydrophobic interactions with Pro656 and Cα / Cβ of Phe659 as well as a weak hydrogen bond with Leu675.

Figure S3.

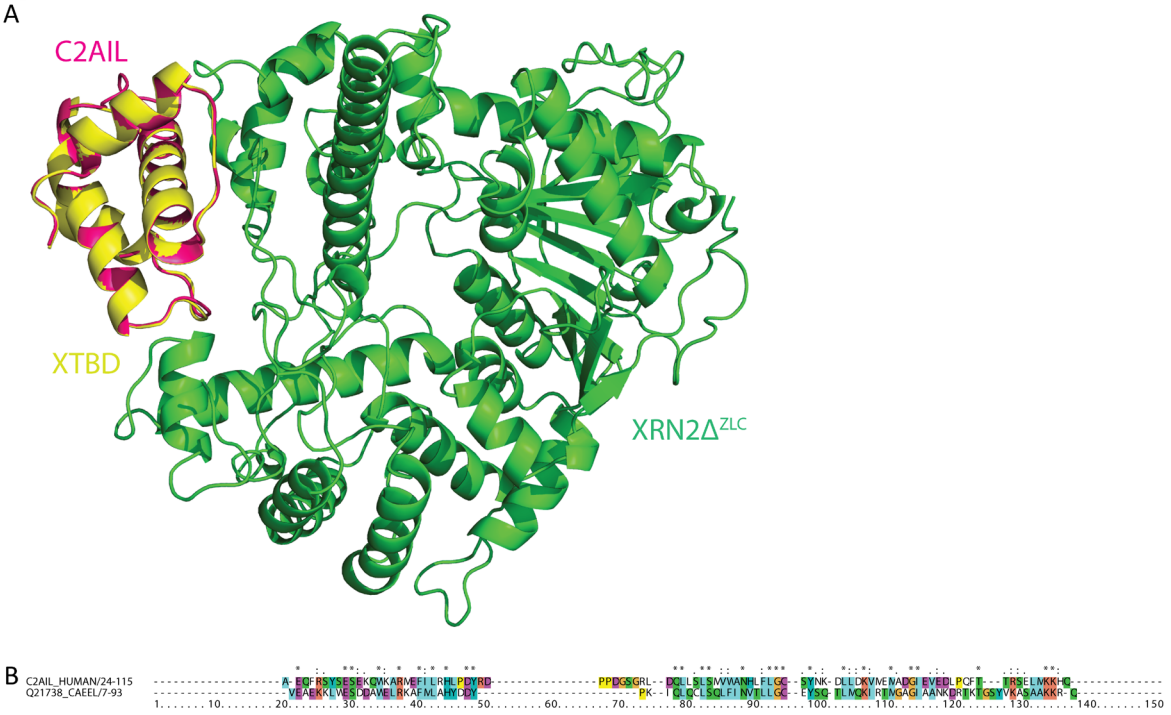

Figure S3, related to Figure 3. The Human C2AIL Homology Model is Based on Pfam DUF3469 Alignment
(A) A human C2AIL homology model (magenta) superimposed onto the XTBD - XRN2 complex (yellow and green, respectively). (B) Pfam alignment of DUF3469 of human C2AIL and *C. elegans* PAXT-1, on which the homology model is based.

Figure S4.

A

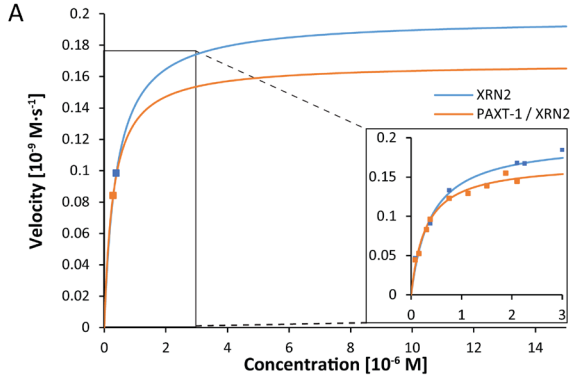

Enzyme	V_{max} [10^{-9} M·s^{-1}]	K_M [10^{-9} M^{-1}]	k_{cat} [s^{-1}]
XRN2	0.197	391.3	0.013
XRN2 / PAXT1	0.168	287.0	0.011

Figure S4, related to Figure 4. Kinetic Analysis of XRN2 Alone Versus the XTBD – XRN2 Complex

(A) Michaelis-Menten kinetic curves of XRN2 and PAXT-1 – XRN2 complex in blue and orange lines, respectively. XRN2's catalytic activity was determined on a broad range of substrate concentrations using an assay based on a FAM fluorophore-coupled RNA substrate and a quencher-coupled DNA primer (Sinturel et al., 2009). As the substrate range accessible by this assay is limited by the dynamic range of measurable FAM fluorescence by the qPCR machine, we extended it by adding a four-fold excess of unlabeled 22 nt let-7 miRNA to the 30 nt RNA – DNA duplex. The curves are extrapolations from measurements shown in the inset. The corresponding K_M values are marked as colored squares. PAXT-1 does not alter catalytic activity, as k_{cat} of XRN2 alone is 0.013 s^{-1} and k_{cat} of the PAXT-1 – XRN2 complex is 0.011 s^{-1} (table). Moreover, at substrate concentrations up to $0.5 \cdot 10^{-6}$ M, turnover rates are identical (inset). The Michaelis-Menten constant K_M for XRN2 alone is 391.3 nM compared to 287.0 nM for the PAXT-1 – XRN2 complex, suggesting a subtle increase in affinity of PAXT-1-bound XRN2 to its substrate. We conclude that PAXT-1 has little or no stimulatory activity on XRN2, at least under the conditions of this assay.

Supplementary Methods

Protein Expression and Purification

Expression constructs were cloned into a modified bis-cistronic pCOLADuet™ vector from Novagen. XTBD-containing constructs were cloned into the first multi-cloning site (MSC), and thus N-terminally extended by a Hexahistidine (His_6) tag followed by a tobacco etch virus protease (TEV) cleavage site, whereas the XRN2 constructs in the second MSC remain untagged. All constructs were expressed in *E. coli* BL21 (DE3). Cells were lysed by sonication and the lysate cleared by centrifugation. Immobilized metal affinity chromatography (IMAC) slurry (Qiagen) was used to bind the His_6-tag of the target protein. Next, protein was eluted through cleavage by TEV (home made (Blommel and Fox, 2007). IMAC was repeated and the unbound fraction collected, diluted, and subjected to a Mono Q™ 5/50 GL (GE Healthcare) anion exchange column. Positive fractions were pooled, filtered with a Millex-GV 0.22 µm filter and loaded onto a Superdex™ 200 HiLoad™ 16/600 (GE Healthcare) column. Finally the target fractions were collected and concentrated using Millipore® Amicon® Ultra Centifugal Filter Concentrators with suitable pore size.

Incorporation of seleno-methionine was done as described by Molecular Dimensions' SelenoMethionine media kit, using *E.coli* B834 (DE3).

Crystallization, Data Collection, and Structure Solution

Protein crystallization was carried out at 20°C using the sitting-drop vapor diffusion method with a Phoenix robot (Art Robbins) dispensing 300 nl drops (100 nl crystallization buffer and 200 nl protein solution). XRN2Δ^{ZLC} – XTBD crystals, obtained in 2 M ammonium sulfate, 0.1 M Bis-TRIS pH 6.5 or 0.1 M TRIS pH 8.5 were harvested and flash-cooled in liquid nitrogen after cryoprotection with 3.2 M ammonium sulfate, 0.1 M Bis-TRIS pH 6.5 or 0.1 M TRIS pH 8.5. Highest resolution data was obtained with a seleno-methionine derivative crystal diffracting to 2.85 Å at the SLS PX-II beamline (Villigen, Switzerland) and belonged to space group $P2_12_12_1$ with six XRN2Δ^{ZLC} – XTBD heterodimers in the asymmetric unit. Diffraction data was integrated and scaled using the XDS program package (Kabsch, 2010) and the structure was solved by the molecular replacement method with PHASER (McCoy *et al.*, 2007) using an XRN2 homology model consisting of the exonuclease core as search model. Phases from this solution were calculated and used for automatic model building with BUCCANEER (Cowtan, 2006). The XRN2Δ^{ZLC} – XTBD structure was further improved by the crystallographic simulated annealing routine followed by grouped B-factor refinement in PHENIX (Afonine *et al.*, 2012) and several rounds

of manual rebuilding in COOT (Emsley *et al.*, 2010) and refinement in PHENIX and BUSTER (Bricogne et al., 2011). Non-crystallographic symmetry restraints were used throughout the structure solution and refinement process. Model building and validation was carried out with the help of anomalous difference Fourier electron density maps to locate seleno-methionine positions. The final structure was validated using COOT. Structural images for figures were prepared with PyMOL (Schrödinger, 2010).

Sequence Logo

The profile hidden Markov model (HMM) of DUF3469 from Pfam was exported and uploaded to Skylign.org (Wheeler et al., 2014). For concise representation, the following parameters were set: a) Alignment Processing to "Create HMM - remove mostly-empty columns", b) Fragment Handling to "Alignment sequences are full length" and c) Letter Height to "Information Content - Above Background". The resulting logo was exported without showing the gap parameters.

Thermal Shift Assay

In a 20 µl reaction, 2 µg of assayed protein was mixed with Protein Thermal Shift™ Dye and – Buffer from Applied Biosystems to a final concentration of 1x. In the presence of RNA substrate however, 1 µg of protein was used instead to reduce the otherwise high concentrations of RNA. Purified yeast tRNA (Ambion™) or a 30mer XRN2 substrate, identical to that used in the kinetic assays (see below) were used when examining the effect of substrate binding. The reaction was prepared in a 96 well MicroAmp® optical microplate at 4°C and sealed with MicroAmp® Optical Adhesive Film. After centrifugation for 25 s at 1,000 g the plate was read in a StepOnePlus™ real-time PCR system using a melt curve program from 25 – 99°C. No normalizing quencher was used and reactions were run in triplicates. Raw data was exported and plotted using Microsoft Excel. The sigmoidal part of the curve was fitted to the Boltzman equation to calculate the melting point T_m using non-linear regression by maximizing R^2 and varying T_m and C. The resulting function was normalized to 1 and plotted (see below). Raw-data was also normalized to 1 and plotted as dashed lines. In addition, XRN2, XRN2 + tRNA and XRN2 + RNA curves and values were re-scaled by a factor of 1.9, 1.3, and 1.8, respectively for concise representation.

$F(T) = F_{pre} + \frac{F_{post} - F_{pre}}{1 + e^{\frac{T_m - T}{C}}}$, where F_{pre} is baseline fluorescence, F_{post} is maximal fluorescence, T is temperature in °C, T_m is melting temperature in °C and C is entalphy.

Real-time Exonuclease Activity Assay and Kinetic Analysis

The kinetic assay was performed as described in (Sinturel *et al.*, 2009) with the following modifications: The RNA-DNA duplex substrate, where the RNA is FAM-labeled whereas the DNA carries a quencher, was diluted with fourfold excess of unlabeled 5' phosphorylated *let-7*, which increased the dynamic range of the qPCR system. 300 fmol enzyme was assayed with varying concentrations of total substrate (sum of RNA-DNA duplex and let-7) in an excess from 5 to 200 fold. Each kinetic reaction was run in triplicates and gave 1 data point. After each data point was normalized to its baseline, the initial linear phase from 0 to 180 s was fitted by linear regression. The slope of this function equals the velocity at the corresponding substrate concentration [S]. Furthermore the average of three velocities was plotted over [S] and fitted to the Michaelis – Menten-model (see below) with the least-square method.

$v = \frac{V_{max} \cdot [S]}{K_M + [S]}$, where V is velocity, V_{max} is maximal velocity, [S] is substrate concentration and K_M is the Michaelis-Menten- constant.

Cell Culture and Transient Transfection of HEK293T Cells

HEK293T cells were available in our lab, checked for mycoplasma contamination and grown in DMEM-F12 (Gibco™) supplemented with 10% (v/v) FCS and 25 U/ml Penicillin-Streptomycin (Gibco™) at 37°C. Prior to transfection (described in de la Mata et al., 2015) using the PEI method, $2 \cdot 10^6$ cells were plated on a 6 cm dish per construct and grown for one day. Each transfection was run in 2 technical duplicates with plasmids derived from pIRESneo (Addgene plasmid #10822) to encode N-terminally FLAG-HA-tagged wild-type or Tyr82-to-Ala mutated hsa_C2AIL. pSD44 harboring GFP was used as mock control. It is modified from the pRRLSIN.cPPT.PGK-GFP.WPRE (Addgene plasmid #12252) backbone, containing the SV40 enhancer/early promoter driving expression of a puromycin selectable marker. Cells were harvested 72 h after transfection.

Western Blot and Co-Immunoprecipitation Experiments

Worm lysates were prepared by douncing harvested worms with 150 pestle strokes in extraction buffer (50 mM HEPES, pH 7.4, 50 mM KCl, 5 mM $MgCl_2$, 0.1% w/v Triton X-100, 10% w/v Glycerol) finalized with 7 mg protease inhibitor (Roche complete EDTA-free), 2 µl 1 M DTT and 10 µl 100 mM PMSF per ml extraction buffer. The lysate was cleared by centrifugation at 16,000 g for 20 min and protein concentrations of the lysates were measured using Bradford reagent (Bio-Rad Protein Assay).

Subsequently, 100 µg of lysate were loaded and separated by a Bis-TRIS SDS-PAGE 4 – 12% gradient gel (NuPAGE® Life Technologies). Proteins were then blotted on a PVDF membrane using standard procedures. Antibodies against XRN2, PAXT-1 (Miki et al., 2014) and FLAG-tag (Monoclonal ANTI-FLAG® M2-Peroxidase, Sigma) were used in a 1:500, 1:500 and 1:2000 dilution, respectively. Horseradish peroxidase-conjugated antibodies (GE Healthcare, Little Chalfont, UK) were used for detection, except for FLAG (see above). For IP experiments, 3 mg lysate was incubated with 40 µl magnetic anti-FLAG bead slurry (Sigma. Cat # M8823) in 1 ml finalized extraction buffer for 2 h on the rotating wheel at 4°C. Then beads were washed 4 times with 600 µl extraction buffer followed by 1 h elution on a vertical shaker (4°C) with 40 µl of 1 µg / µl FLAG peptide.

Immunoprecipitation of FLAG-HA-tagged Hs_C2AIL was performed using Anti-FLAG M2 Magnetic Beads (Sigma. Cat # M8823) as described in de la Mata et al. (2015). For this, $2 \cdot 10^6$ transfected HEK293T cells per IP and construct were washed with 4 ml cold PBS, harvested and lysed in 500 µl lysis buffer (50 mM TRIS pH 7.5, 150 mM NaCl, 1% v/v TritonX-100, 1 mM EDTA, 1x EDTA-free Roche cOmplete Protease Inhibitor Cocktail) and incubated for 30 min on ice. Subsequently, the lysate was cleared by centrifugation at 16,000 g for 10 min. Per IP, 40 µl of bead slurry (see above) was washed twice with cold TBS (50 mM TRIS pH7.4, 150 mM NaCl), added to the lysate and filled to 1 ml final volume with TBS. After 2 h of incubation on the rotating wheel, beads were washed three times with 400 µl TBS and boiled at 70°C for 10 min in 40 µl SDS loading buffer for western blot analysis detecting the transgene with anti-HA antibody (1:1000 dilution; clone 3F10, Roche). Human XRN2 was detected as described in Miki et al. (2014).

References

Afonine, P. V, Grosse-Kunstleve, R.W., Echols, N., Headd, J.J., Moriarty, N.W., Mustyakimov, M., Terwilliger, T.C., Urzhumtsev, A., Zwart, P.H., and Adams, P.D. (2012). Towards automated crystallographic structure refinement with phenix.refine. Acta Crystallogr. D. Biol. Crystallogr. *68*, 352–367.

Blommel, P.G., and Fox, B.G. (2007). A combined approach to improving large-scale production of tobacco etch virus protease. Protein Expr. Purif. *55*, 53–68.

Bricogne, G., Blanc, E., Brandl, M., Flensburg, C., Keller, P., Paciorek, W., Roversi, P., Sharff, A., Smart, O.S., and Vonrhein, C. (2011). BUSTER 2.11.4.

Cowtan, K. (2006). The Buccaneer software for automated model building. 1. Tracing protein chains. Acta Crystallogr. D. Biol. Crystallogr. *62*, 1002–1011.

Emsley, P., Lohkamp, B., Scott, W.G., and Cowtan, K. (2010). Features and development of Coot. Acta Crystallogr. D. Biol. Crystallogr. *66*, 486–501.

Kabsch, W. (2010). XDS. Acta Crystallogr. D. Biol. Crystallogr. *66*, 125–132.

De la Mata, M., Gaidatzis, D., Vitanescu, M., Stadler, M.B., Wentzel, C., Scheiffele, P., Filipowicz, W., and Großhans, H. (2015). Potent degradation of neuronal miRNAs induced by highly complementary targets. EMBO Rep. *16*, 500–511.

McCoy, A.J., Grosse-Kunstleve, R.W., Adams, P.D., Winn, M.D., Storoni, L.C., and Read, R.J. (2007). Phaser crystallographic software. J. Appl. Crystallogr. *40*, 658–674.

Miki, T.S., Richter, H., Rüegger, S., and Großhans, H. (2014). PAXT-1 promotes XRN2 activity by stabilizing it through a conserved domain. Mol. Cell *53*, 351–360.

Schrödinger, L. (2010). The PyMOL Molecular Graphics System, Version 1.3r1.

Sinturel, F., Pellegrini, O., Xiang, S., Tong, L., Condon, C., and Bénard, L. (2009). Real-time fluorescence detection of exoribonucleases. RNA *15*, 2057–2062.

Wheeler, T.J., Clements, J., and Finn, R.D. (2014). Skylign: a tool for creating informative, interactive logos representing sequence alignments and profile hidden Markov models. BMC Bioinformatics *15*, 7.

2 XRN2 Processively Degrades miRNAs Under Single Turnover Conditions

The XRN2 paralog *D. melanogaster* XRN1 was shown to processively degrade 5′ monophosphorylated RNA molecules under single turnover conditions (Jinek et al., 2011). In contrast, Rat1p (yeast XRN2) seems to processively degrade RNA molecules only in complex with its interaction partner Rai1p, despite extensive sequence and structural similarities to XRN1 (Jinek et al., 2011; Kenna et al., 1993; Stevens and Poole, 1995; Xiang et al., 2009). On the other hand, XRN2s from other species have not been investigated in respect to their mode of catalysis. Thus, questions of how *C. elegans* XRN2 executes processive substrate decay remains to be analyzed. Hence, we checked for processive catalysis of recombinant *C. elegans* XRN2 under single turnover conditions. For this, 50 pmol synthetic 5′-monophosphorylated let-7 were labeled on the 3′-end with equimolar amounts of pCp using T4 RNA ligase. Subsequently, the substrate was spin-column purified and adjusted to 0.5 nM radiolabeled substrate using the scintillation counter. For each reaction, 1 µl labeled substrate was used, corresponding to 0.5 fmol, and incubated with 90 fmol of recombinant enzyme at 25 °C. Of note, 3′-end labeling depends on an inefficient enzymatic ligation reaction and therefore a considerable amount of unlabeled substrate is present in each reaction. Finally, the reaction mix was resolved with an 8 M urea PAGE-gel and the RNA detected by autoradiography. Remarkably, for XRN2, without being complexed by PAXT-1, processivity similar to XRN1 was observed for let-7 decay in time course experiments (Figure 4). No intermediates are detected, as degradation bands for full length XRN2 (XRN2_fl) and XRN2 lanes represent pCp (determined in other experiments, data not shown). In contrast, previous results show, that Rat1p needs to be in complex with Rai1 to achieve similar results (Xiang et al., 2009). However earlier experiments with Rat1 were performed with much longer substrates and potential secondary structure elements might have inhibited processivity.

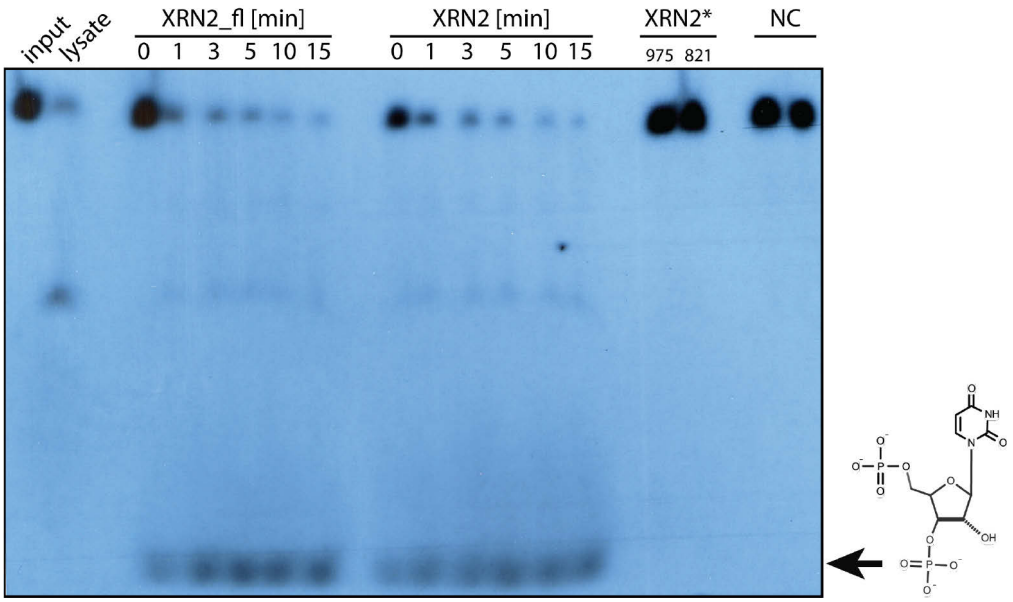

Figure 4: Shown is an autoradiography of the turnover of 0.5 fmol 3'- labeled let-7 miRNA comparing full length XRN2 (XRN2_fl, residues 1 – 975) and XRN2 (residues 1 – 821) over a period of 15 minutes at indicated times. Moreover catalytic dead XRN2 (XRN2*) of both constructs, buffer components (NC, negative control) and a *C. elegans* worm lysate were tested for activity and incubated for 15 min. The final reaction product for XRN2_fl and XRN2 corresponds to pCp (arrow/schematic).

While activity and processivity is maintained by *C. elegans* XRN2 alone under single turnover conditions, we were wondering if PAXT-1 could influence the enzymatic activity of XRN2 under multiple turnover conditions. For this we followed its enzymatic activity in real-time in presence or absence of PAXT-1 as described by Sinturel and colleagues (Sinturel et al., 2009). In short, a 30 nt RNA, coupled to a fluorophore (FAM) at its 3'-end, is hybridized with a 17 nt DNA primer harboring a quencher (TAMRA) at its 5'-end. Upon catalysis, the DNA primer is dislodged and fluorescence of released single nucleotide-fluorophore conjugates are measured over time (Figure 5A). Of note, it cannot be excluded that the RNA – DNA duplex substrate affects the kinetic behavior of the enzyme as it relies on primer dissociation and therefore deviates from a true single stranded RNA catalysis. In a multiple-turnover setup with 50 fold excess of RNA substrate (DNA primer hybridized in two-fold excess in respect to RNA), we followed RNA decay over 1 h in presence or absence of PAXT-1 (Figure 5B). Whereas the PAXT-1 – XRN2 complex degrades approx. 58% (+/- 0.3%) of the substrate after 3600 s, XRN2 alone degrades approx. 43% (+/- 1%) in the same time, so that both reactions are in multiple-turnover conditions for the entire measurement (published in Miki et al., 2014b). Interestingly, PAXT-1 – XRN2 complexes seem more active after approx. 1000 s (Figure 5B). However initial velocities (initial 150 s) of XRN2 and PAXT-1 – XRN2 complex are equal, indicated by equal slopes (Figure 5B, inset). Thus, higher activity of the PAXT-1 – XRN2 complex is not due to stimulation of enzymatic activity of XRN2 by PAXT-1, but rather through the stabilizing effect of PAXT-1 on XRN2. Yet, the assayed RNA substrate is only 30 nt of length and we cannot rule out influences of PAXT-1 on XRN2 catalysis on larger substrates.

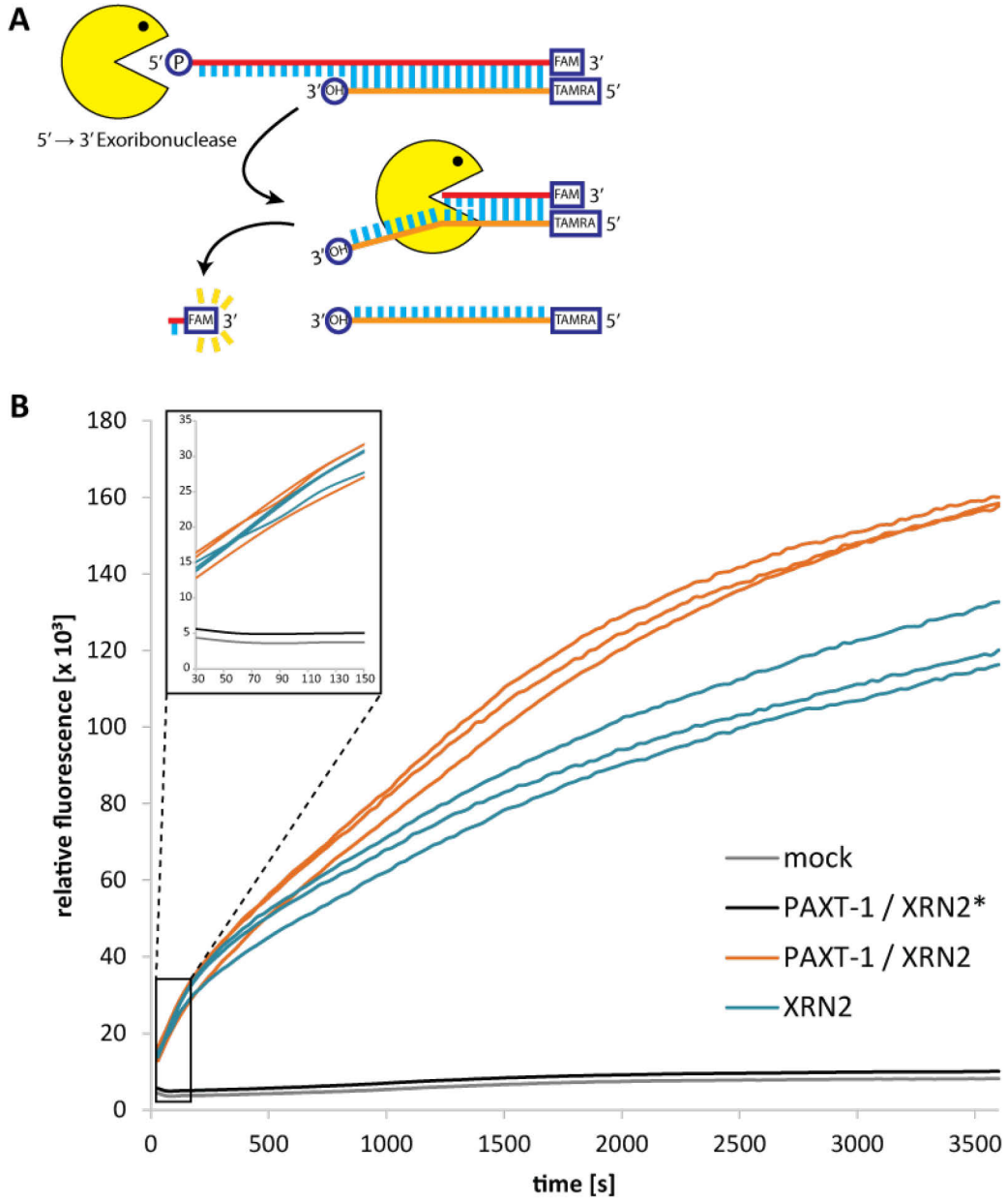

Figure 5: **A**, Schematic shows the principle of the real time degradation assay for 5′ → 3′ exoribonucleases. **B**, Shows the kinetic behavior of PAXT-1 – XRN2 complex (orange line) in comparison with XRN2 alone (blue line), nuclease dead complex (black line) and mock control (gray line) using 10 nM protein and 500 nM substrate in multiple turnover condition over 3600 seconds. The inset magnifies the initial velocity of the reaction.

3 No Detection of MiRNA Release Off AGO with Recombinant XRN2 *in vitro*

Previously, Chatterjee et al. (2009) showed that *C. elegans* lysates are capable of releasing the miRNA let-7 off immunoprecipitated ALG-1/2 complexes and upon depletion of XRN2 by RNAi, release activity of these lysates was reduced (see above). So we were curious to see if XRN2 and its complex with PAXT-1 has releasing capabilities *in vitro*. For this we incubated co-immunoprecipitated

miRNA – ALG-1/2 complexes from *C. elegans* lysates with recombinant XRN2 or PAXT-1 – XRN2 complex and measured let-7 retained on ALG-1/2 by qPCR. To account for potential losses of miRNAs during RNA extraction, 3 fmol of an unrelated rat miRNA, miR-132, was spiked-in and used to normalize for let-7 levels using a standard curve. Release of let-7 could be detected on ALG-1/2 complexes incubated with worm lysates (Figure 6A), whereas signals similar to input were detected when incubated with full length XRN2 (XRN2_fl), XRN2 (residues 1 – 821), PAXT-1 – XRN2 and XTBD – XRN2 complexes (Figure 6A and C). To confirm qPCR results, 50% of the release reaction mix was analyzed using northern blot optimized for small RNA detection (Pall and Hamilton, 2008). There, extracted RNAs are separated by an 8 M urea PAGE-gel, transferred (blotted) and cross-linked to a membrane, followed by hybridization with a complementary ^{32}P labeled nucleic acid probe. This signal is then detected using autoradiography. Similar to the qPCR assay, loss of RNA, due to extraction and handling procedures, was controlled for by spike-in of 3 ng yeast leucine tRNA ($tRNA^{Leu}$). When probing release reactions of lysate and full length XRN2 (XRN2_fl) with an α-let-7 probe by northern blot, observations made by qPCR (Figure 6A) were confirmed (Figure 6B). Taken together, no release activity could be detected for recombinant XRN2 nor in complex with PAXT-1. Thus, other factors within the worm lysate seem to mediate release activity but could potentially be linked with XRN2. This could explain partial loss of release activity upon XRN2 RNAi.

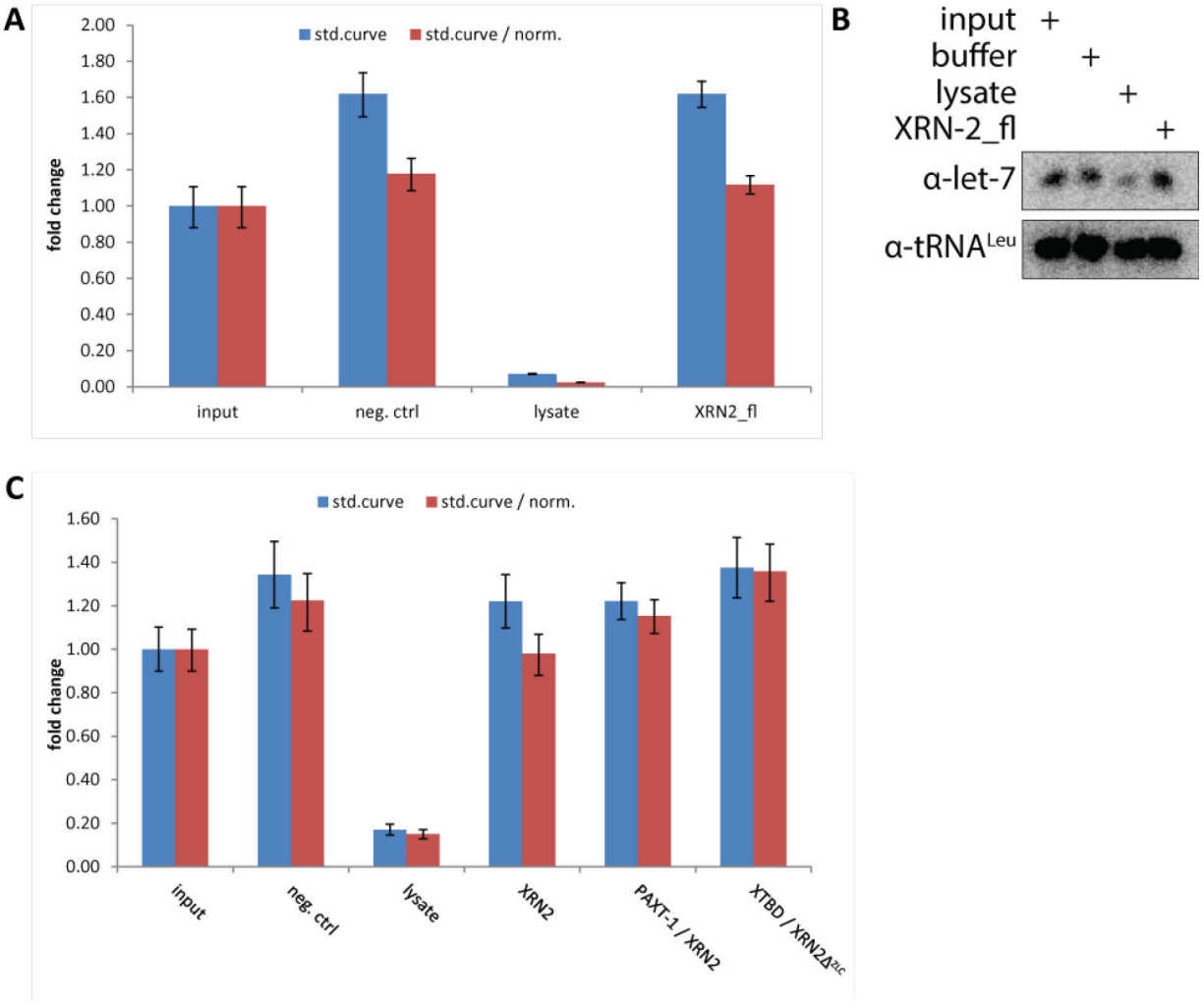

Figure 6: **A and B**, Shown is the fold change and northern blot of co-immunoprecipitated ALG-1 and -2 bound let-7 incubated with buffer (neg. ctrl), *C. elegans* N2 worm lysate or full length XRN2 (XRN2_fl) for 15 min at 25 °C compared to input. Samples were quantified using a standard curve (blue bars) and normalized to spiked-in mir-132 (red bars) to correct for losses during RNA purification. Plotted values represent the mean ± standard deviations from three technical replicates (n = 3). **C**, Repitition of the assay from A, at which also PAXT-1 – XRN2 and XTBD – XRN2Δ^{ZLC} (deletion of the zinc-finger, loop and C-terminal tail) complexes were tested for release activity.

III Discussion

With the rapid discoveries of new RNA species and their respective functions, scientists became increasingly interested in RNA nucleases as these are capable to process, decay or mediate function to RNAs. Thus, a growing number of new nucleases or proteins harboring conserved RNase folds are discovered, such as AGO or Dicer. Although new multiple sequence alignment algorithms based on probabilistic models, such as the Hidden Markov model, can help such discoveries (Finn et al., 2011, 2014), conservation of the primary amino acid sequence is lower than its three dimensional fold. Thus X-ray crystallography of proteins involved in the RNA metabolism made important contributions in identifying new RNases or RNase domains, such as AGO, spliceosome component Prp8 or NMD factor SMG6, and their molecular mode of action (Glavan et al., 2006; Pena et al., 2008; Song et al., 2004).

Functional Implications Based on XRN Structures

Up to now, structures of yeast and *C. elegans* XRN2 as well as *K. lactis* and *D. melanogaster* XRN1 are solved and elucidated the substrate binding mode as well as the structural elements mediating processivity for this class of enzymes. However, there are observed discrepancies of RNA decay between XRN1 and XRN2, which cannot simply be explained by their respective structures.

Structural analysis of the XRN1 – substrate complex revealed a $\pi - \pi$ base stacking mode for substrate binding formed by residues His41 and Trp540 as well as the Brownian ratchet-like mode for processive degradation, which relies on α-helix 1 and a conserved loop harboring Trp540 (Jinek et al., 2011). In line with our structural data and comparison to Rat1p, XRN2 seems to use the same substrate binding mechanism as key residues and structural features are conserved and electron densities from sulfate ions (component within the crystallization buffer) are detected at the substrate 5' phosphate position. Upon degradation of structured substrates, such as stem-loop containing RNAs, however, stalling of XRN2 was observed (Xiang et al., 2009). In contrast, such substrates are efficiently degraded by XRN1, with only G-quartet tracts harboring RNAs and some viral RNA being capable of inducing stalling (Chapman et al., 2014; Poole and Stevens, 1997). Thus an unwinding mechanism for XRN1 is proposed, by which the conserved loop and α-helix 1 form a small entrance allowing for single stranded substrate only and thus acting as a steric barrier. Either unwinding is conveyed actively by substrate translocation or simply by thermal breathing of the substrate, as it is threaded through the steric barrier to access the nuclease cleft. It thus is an extended mechanism of the Brownian ratchet model and processive substrate degradation (Jinek et al., 2011). It is puzzling, however that studies from yeast show XRN2 degradation to be limited by RNA secondary structure

elements, but all structural features responsible for processivity and duplex unwinding are present in XRN2 as well. It is worth mentioning, that XRN turnover studies do not use identical substrates consistently, nor turnover conditions. Studies on XRN1 from Jinek et al. were performed under single turnover conditions, with a large excess in enzyme concentration and so did Xiang et al. for yeast XRN2 with yet longer substrates. Our studies suggest a processive activity for XRN2 in multiple turnover conditions for small sized substrates such as miRNAs, even without being in complex with PAXT-1. Thus it remains to be seen, if there are indeed differences in substrate degradation on the molecular level between XRN1 and XRN2, and if, it would be interesting to pin point these differences on a structural level.

Strikingly, the XTBD – XRN2 interface is mainly formed by the conserved loop, which would suggest an influence on XRN2's catalytic activity. Yet, we do not observe any alterations in XRN2's kinetic behavior in presence or absence of PAXT-1, but support of RNA binding and/or degradation of structured/longer substrates by PAXT-1 cannot be excluded. Conversely, PAXT-1 might as well regulate XRN2's activity by restricting for certain substrate types. Unfortunately, thorough biochemical analysis of XRN2 substrate degradation is sparse, which might be due to the fact, that production of larger and structured high quality RNA molecules harboring desired modifications still pose a huge problem. However those studies are needed and could help to gain insights of how this molecular machinery works. A less appealing hypothesis would suggest XRN2 to be an ordinary degradation machine, which has to be kept in check by supporting cellular factors. Then XRN2 would possibly acquire specificity by localizing and limiting it to certain substrates.

Compared to XRN1, XRN2 acts on a diverse spectrum of substrate classes and takes part in processes like transcription termination and miRNA release off AGO. Thus, it could well be, that such specialized functions are reflected on the structural level. One of the most prominent structural feature of XRN2 is its tower domain. It is a long α-helix spanning from the bottom through the molecule and well above the globular surface, thus mainly contributing to the unique shape of XRN2 (Xiang et al., 2009). The tower domain makes important contributions to substrate binding/access and stability (Jinek et al., 2011; Xiang et al., 2009). However it is unlikely that either of these contributions require the tower domain's extended length. Remarkably, the tower domain of XRN1 is smaller and the XRN1 molecule adapts a more globular shape through its additional domains than XRN2 does. Hence it seems unlikely, that such a prominent shape is evolutionary conserved without any functions attributed to it. As XRN2 is involved in transcription termination in a model by which RNAPII is sterically displaced by XRN2, it is tempting to link this function to the tower domain. While approaching RNAPII, which is significantly bigger than XRN2, through substrate degradation, the tower domain could function as a battering ram for displacement of RNAP II. Hence the extended length of the tower domain coupled with XRN2's catalytic activity would increase the "power"

available for this process. But maybe XRN2 doesn't displace RNAP II directly, as suggested by the torpedo model, but uses the tower domain as an extension to kick off certain subunits bound to RNAP II's tail. This idea is especially interesting, as RNAP II could be loaded with specific sets of factors regulating the transcription of specific genes and XRN2 might reach only subunits bound to specific interfaces of RNAP II due to the length of its tower domain. As a consequence, termination of transcription by XRN2 could be controlled by such factors and add another layer of regulation.

The Subunits of the XRN2 Nuclease: What, Where, Why?

In the past, XRN2 has been studied thoroughly in yeast, elucidating many substrates and functions, but just recently it became apparent, that XRN2 exists in a tight complex with a single additional subunit. Surprisingly, its paralogue XRN1, despite interacting with many proteins, was not found to form a similar nuclease complex. Two crystal structures of an XRN2 complex, from yeast and *C. elegans*, are available to date (Xiang et al., 2009; this study). Strikingly, both subunits, Rai1p and PAXT-1 from yeast and *C. elegans*, respectively, bind to different XRN2 interfaces and share no similarities. In contrast they do share their function in stabilization of XRN2 through binding. Moreover Rai1 was shown to enhance nuclease activity of XRN2, whereas no such effect could be attributed to PAXT-1 (Xiang et al., 2009; Xue et al., 2000). It is however unclear, how Rai1p stimulates XRN2, since it binds to the bottom of XRN2, far away from the nuclease cleft. One explanation could be that previous observations of increased activity of Rai1 – XRN2 complexes are merely mediated by an increased stability of the complex rather than increased catalytic activity. This notion is supported by observations of *C. elegans* XRN2 complexes, where real-time turnover analysis revealed increased activity over time for PAXT-1 – XRN2 complexes compared to XRN2 alone, but Michaelis-Menten kinetics analysis thereof revealed no change in catalytic activity. Therefore it was concluded, that increased activity mediated by PAXT-1 was due to its stabilizing function towards XRN2. Moreover, questions, of how XRN2 stabilization through binding to two different interfaces is mediated, remain. PAXT-1 forms a tight complex with XRN2 through a yet small interface of approx. 1000 $Å^2$ close to the substrate binding site, but makes significant contributions to complex formation (PISA score = 1) (Krissinel and Henrick, 2007). Rai1p's interface however, scatters around the bottom of the nuclease, totaling to approx. 800 $Å^2$ and PISA interface analysis scores the Rai1 – XRN2 interface to be insignificant (Krissinel and Henrick, 2007; Xiang et al., 2009). Curiously, biochemical data from yeast, XRN2 purifications readily detect Rai1p bound to XRN2 and the complex is regarded stable (Kenna et al., 1993; Stevens and Poole, 1995; Xiang et al., 2009). Hence, direct comparison of the stability of PAXT-1 – XRN2 and Rai1p – Rat1p complexes as well as their stabilizing function could shed light on these discrepancies.

The crystal structure of the *C. elegans* XRN2 nuclease complex was solved using a construct containing only the N-terminal XTBD of PAXT-1, whereas the remaining C-terminus is missing. Bioinformatics analysis predicts a structurally well-ordered PAXT-1 C-terminus, however sequence alignments do not identify any known domains. It is tempting to imply RNA-related functions for this C-terminus, such as RNA-binding or substrate specificity, especially since structural data suggests its location just in front of the nuclease cleft. Therefore structural determination of the PAXT-1 C-terminus alone could give further insights to PAXT-1 function and how this relates to XRN2.

As PAXT-1 was recently identified as a subunit in the XRN2 nuclease complex, available data is concerned with its function related to XRN2. Nevertheless it might well be, that PAXT-1 has additional functions independently of XRN2, which are yet to be discovered. However, recent results show a direct relationship on protein stability for PAXT-1 and XRN2 as knock-down of either subunit of the PAXT-1 – XRN2 complex results in loss of the other, with mRNA levels being unaffected. Therefore dissecting any independent function of PAXT-1 seems difficult. Moreover production of recombinant PAXT-1 failed, as it seems unstable in high dilution *in vitro*.

From an evolutionary perspective, PAXT-1 homologs are only found in nematodes, whereas the XTB domain is readily detected in proteins from metazoans and ciliates (Pfam DUF3469). It is puzzling though, that yeast lack proteins with an XTBD completely. Whether yeast XRN2 is intrinsically more stable than its metazoan counterpart or Rai1 has indeed similar stabilizing capabilities as PAXT-1 (discussed above) remains to be tested. Also, it could very well be, that the XTBD evolved besides the existing Rai1 and gradually replaced it, as it turned out to be more stable and more suitable as an adapter. Conversely, the Rai1 – XRN2 interaction also couples two enzymatic activities plus stabilization. In certain situations this enzymatic coupling is maybe undesirable, as potential protection of an RNA by a 5'- trisphosphate would be a substrate for the Rai1 – XRN2 complex. Moreover, it could be that other functions than pyrophosphatase activity became increasingly important, such as substrate specificity, and displaced Rai1 with XTBD interaction/stabilization.

Interestingly, alignment algorithms predict three different XTBD-containing proteins in mammals, in contrast to only one found in nematodes (PAXT-1). An enticing model could be, that XRN2 is capable of acquiring additional functionality by complex formation with different XTBD-proteins. Especially NKRF and CARF are not well characterized, functionally nor structurally, and their domain architecture is largely undetermined, apart from their predicted XTBD and RNA binding domain. Moreover, biochemical studies show PAXT-1 and XRN2 to form a strong complex, as this complex resists disruption in high salt environments and high dilutions. Hence, it is hard to imagine how XRN2 subunits will be interchanged within the cellular environment. Either different XRN2 complexes are formed co-transcriptionally/co-translationally or there is an active exchange mechanism facilitating

loading/unloading of different XTBD-containing subunits. The first hypothesis is particularly interesting, as it permits the cell to use the regulatory machineries during gene expression to time and setup XRN2 complexes with different functionalities. Yet, it is possible that other proteins interact with XRN2 independently of an XTB domain. Conversely, XTBD-proteins may also recruit and bind additional subunits in an XRN2 complex. Considering all these possibilities, XRN2 possibly gains many of its specialized functions directly or indirectly by complex formation with XTBD- proteins. As now the XTBD key interface residue Tyr56 was identified, mutations will thus allow further dissections of XRN2's complex functions and potential regulation. Also elucidating the interactome of the XTBD-proteins could shed more light on potential functions, substrates and subcellular localization related to XRN2

XRN2 and the Mysterious Release Factor

Previously, Chatterjee and colleagues observed an unusual function of XRN2 with no obvious link to catalysis. When co-immunoprecipitated miRNA – AGO complexes were incubated with XRN2 depleted *C. elegans* lysates more miRNAs remained bound to AGO compared to wild type lysates. This led to the hypothesis, that XRN2 is involved in mediating miRNA release off AGO. However testing for potential release activity *in vitro* using recombinant XRN2 and PAXT-1 – XRN2 complex, no such activity was observed. This suggests, that XRN2 guides releasing factors to AGO complexes rather than exhibiting release activity itself. As pointed out earlier, XTBD-proteins could serve as protein scaffolds, recruiting more subunits to XRN2, hence also serving as a release factor binding platform. Thus it would be interesting to create PAXT-1 C-terminus deletion worm lines and check if similar release defects occur as observed for XRN2 knock-downs. However, off-target effects of XRN2 RNAi or secondary effects thereof, such as reduced stability of yet unknown proteins, could have led to wrong assumption of an XRN2 mediated miRNA unloading off AGO and this mechanism might be completely unrelated to XRN2.

Implication for XRN2 in Human Diseases

XRN2 and its important functions are well studied in various model organisms, such as yeast and *C. elegans*. It plays crucial roles in the RNA metabolism as described earlier, however studies investigating its physiological role in humans lack behind. Interestingly, it could recently be shown, how hepatitis virus C (HCV) uses endogenous miRNAs to prevent degradation of its RNA genome by XRN2 as well as XRN1 (Li et al., 2015; Sedano and Sarnow, 2014). HCV's RNA genome harbors binding sites at its 5'-end for liver miRNA miR-122, which forms a duplex protecting for potential degradation.

It is however not well understood, how a predominantly nuclear nuclease like XRN2 acts on HCV's cytoplasmic genome, especially since its 5'-end harbors a triphosphate group.

Moreover, XRN2 is found to be amplified in breast cancer coinciding with amplifications of CDKN2AIP (Cerami et al., 2012; Eirew et al., 2014; Gao et al., 2013). Also, mutations of cis-acting regulatory elements in spontaneous lung cancer of nonsmokers lead to increased XRN2 mRNA levels. Accordingly, XRN2 is implicated in proliferation and differentiation of lung epithelial cells (Lu et al., 2010). Remarkably, staining of CDKN2AIP and NKRF in human U-2 OS osteosarcoma cells reveal specific localization to the nucleus and the nucleolus, respectively (Uhlén et al., 2015). This underlines the hypothesis, of XRN2 forming multiple complexes to execute its diverse functions at different subcellular compartments.

IV References

Akoulitchev, S., Mäkelä, T.P., Weinberg, R.A., and Reinberg, D. (1995). Requirement for TFIIH kinase activity in transcription by RNA polymerase II. Nature *377*, 557–560.

Allmang, C., Kufel, J., Chanfreau, G., Mitchell, P., Petfalski, E., and Tollervey, D. (1999). Functions of the exosome in rRNA, snoRNA and snRNA synthesis. EMBO J. *18*, 5399–5410.

Allmang, C., Mitchell, P., Petfalski, E., and Tollervey, D. (2000). Degradation of ribosomal RNA precursors by the exosome. Nucleic Acids Res. *28*, 1684–1691.

Amberg, D.C., Goldstein, A.L., and Cole, C.N. (1992). Isolation and characterization of RAT1: An essential gene of Saccharomyces cerevisiae required for the efficient nucleocytoplasmic trafficking of mRNA. Genes Dev. *6*, 1173–1189.

Aza-Blanc, P., Cooper, C.L., Wagner, K., Batalov, S., Deveraux, Q.L., and Cooke, M.P. (2003). Identification of modulators of TRAIL-induced apoptosis via RNAi-based phenotypic screening. Mol. Cell *12*, 627–637.

Bail, S., Swerdel, M., Liu, H., Jiao, X., Goff, L.A., Hart, R.P., and Kiledjian, M. (2010). Differential regulation of microRNA stability. RNA *16*, 1032–1039.

Balbo, P.B., and Bohm, A. (2007). Mechanism of Poly(A) Polymerase: Structure of the Enzyme-MgATP-RNA Ternary Complex and Kinetic Analysis. Structure *15*, 1117–1131.

Ballarino, M., Pagano, F., Girardi, E., Morlando, M., Cacchiarelli, D., Marchioni, M., Proudfoot, N.J., and Bozzoni, I. (2009). Coupled RNA processing and transcription of intergenic primary microRNAs. Mol. Cell. Biol. *29*, 5632–5638.

Banerjee, A., Sammarco, M.C., Ditch, S., Wang, J., and Grabczyk, E. (2009). A novel tandem reporter quantifies RNA polymerase II termination in mammalian cells. PLoS One *4*.

Bashkirov, V.I., Scherthan, H., Solinger, J. a., Buerstedde, J.M., and Heyer, W.D. (1997). A mouse cytoplasmic exoribonuclease (mXRN1p) with preference for G4 tetraplex substrates. J. Cell Biol. *136*, 761–773.

Behm-Ansmant, I., Rehwinkel, J., Doerks, T., Stark, A., Bork, P., and Izaurralde, E. (2006). mRNA degradation by miRNAs and GW182 requires both CCR4:NOT deadenylase and DCP1:DCP2 decapping complexes. Genes Dev. *20*, 1885–1898.

Ben-Shem, A., Garreau de Loubresse, N., Melnikov, S., Jenner, L., Yusupova, G., and Yusupov, M. (2011). The Structure of the Eukaryotic Ribosome at 3.0 A Resolution. Science (80-.). *334*, 1524–1529.

Bentley, D. (1999). Coupling RNA polymerase II transcription with pre-mRNA processing. Curr. Opin. Cell Biol. *11*, 347–351.

Bernstein, E., Caudy, a a, Hammond, S.M., and Hannon, G.J. (2001). Role for a bidentate ribonuclease in the initiation step of RNA interference. Nature *409*, 363–366.

Bernstein, P., Peltz, S.W., and Ross, J. (1989). The poly(A)-poly(A)-binding protein complex is a major determinant of mRNA stability in vitro. Mol. Cell. Biol. *9*, 659–670.

Bohnsack, M.T., Czaplinski, K., and Gorlich, D. (2004). Exportin 5 is a RanGTP-dependent dsRNA-binding protein that mediates nuclear export of pre-miRNAs. RNA *10*, 185–191.

Bonneau, F., Basquin, J., Ebert, J., Lorentzen, E., and Conti, E. (2009). The Yeast Exosome Functions as a Macromolecular Cage to Channel RNA Substrates for Degradation. Cell *139*, 547–559.

Bossé, G.D., Rüegger, S., Ow, M.C., Vasquez-Rifo, A., Rondeau, E.L., Ambros, V.R., Großhans, H., and Simard, M.J. (2013). The Decapping Scavenger Enzyme DCS-1 Controls MicroRNA Levels in Caenorhabditis elegans. Mol. Cell *2*, 1–7.

Bousquet-Antonelli, C., Presutti, C., and Tollervey, D. (2000). Identification of a regulated pathway for nuclear pre-mRNA turnover. Cell *102*, 765–775.

Bouveret, E., Rigaut, G., Shevchenko, A., Wilm, M., and Séraphin, B. (2000). A Sm-like protein complex that participates in mRNA degradation. EMBO J. *19*, 1661–1671.

Brannan, K., Kim, H., Erickson, B., Glover-Cutter, K., Kim, S., Fong, N., Kiemele, L., Hansen, K., Davis, R., Lykke-Andersen, J., et al. (2012). mRNA Decapping Factors and the Exonuclease Xrn2 Function in Widespread Premature Termination of RNA Polymerase II Transcription. Mol. Cell 1–14.

Braun, J.E., Huntzinger, E., Fauser, M., and Izaurralde, E. (2011). GW182 proteins directly recruit cytoplasmic deadenylase complexes to miRNA targets. Mol. Cell *44*, 120–133.

Braun, J.E., Truffault, V., Boland, A., Huntzinger, E., Chang, C.-T., Haas, G., Weichenrieder, O., Coles, M., and Izaurralde, E. (2012). A direct interaction between DCP1 and XRN1 couples mRNA decapping to 5′ exonucleolytic degradation. Nat. Struct. Mol. Biol. *19*, 1324–1331.

Brengues, M., Teixeira, D., and Parker, R. (2005). Movement of eukaryotic mRNAs between polysomes and cytoplasmic processing bodies. Science *310*, 486–489.

Brosius, J., and Tiedge, H. (2004). RNomenclature. RNA Biol. *1*, 81–83.

Bushati, N., and Cohen, S.M. (2007). microRNA functions. Annu. Rev. Cell Dev. Biol. *23*, 175–205.

Carmody, S.R., and Wente, S.R. (2009). mRNA nuclear export at a glance. J. Cell Sci. *122*, 1933–1937.

Cerami, E., Gao, J., Dogrusoz, U., Gross, B.E., Sumer, S.O., Aksoy, B.A., Jacobsen, A., Byrne, C.J., Heuer, M.L., Larsson, E., et al. (2012). The cBio Cancer Genomics Portal: An open platform for exploring multidimensional cancer genomics data. Cancer Discov. *2*, 401–404.

Chanfreau, G., Rotondo, G., Legrain, P., and Jacquier, A. (1998). Processing of a dicistronic small nucleolar RNA precursor by the RNA endonuclease Rnt1. EMBO J. *17*, 3726–3737.

Chang, J.H., Xiang, S., and Tong, L. (2011a). Ribonucleases. 167–192.

Chang, J.H., Xiang, S., Xiang, K., Manley, J.L., and Tong, L. (2011b). Structural and biochemical studies of the 5′ *18*, 270–276. nuclease Xrn1. Nat. Struct. Mol. Biol.

Chapman, E.G., Moon, S.L., Wilusz, J., and Kieft, J.S. (2014). RNA structures that resist degradation by Xrn1 produce a pathogenic dengue virus RNA. Elife *2014*, 1–25.

Chatterjee, S., and Grosshans, H. (2009). Active turnover modulates mature microRNA activity in Caenorhabditis elegans. Nature *461*, 546–549.

Chatterjee, S., Fasler, M., Büssing, I., and Großhans, H. (2011). Target-Mediated Protection of Endogenous MicroRNAs in C. elegans. Dev. Cell *20*, 388–396.

Chekulaeva, M., Mathys, H., Zipprich, J.T., Attig, J., Colic, M., Parker, R., and Filipowicz, W. (2011). miRNA repression involves GW182-mediated recruitment of CCR4–NOT through conserved W-containing motifs. Nat. Struct. Mol. Biol. *18*, 1218–1226.

Chen, C.-Y. a, Zheng, D., Xia, Z., and Shyu, A.-B. (2009). Ago-TNRC6 triggers microRNA-mediated decay by promoting two deadenylation steps. Nat. Struct. Mol. Biol. *16*, 1160–1166.

Chernyakov, I., Whipple, J.M., Kotelawala, L., Grayhack, E.J., and Phizicky, E.M. (2008). Degradation of several hypomodified mature tRNA species in Saccharomyces cerevisiae is mediated by Met22 and the 5′-3' exonucleases Rat1 and Xrn1. Genes Dev. *22*, 1369–1380.

Cheung, C.T., Singh, R., Kalra, R.S., Kaul, S.C., and Wadhwa, R. (2014). Collaborator of ARF (CARF) regulates proliferative fate of human cells by dose-dependent regulation of DNA damage signaling. J. Biol. Chem. *289*, 18258–18269.

Close, P., East, P., Dirac-Svejstrup, a. B., Hartmann, H., Heron, M., Maslen, S., Chariot, A., Söding, J., Skehel, M., and Svejstrup, J.Q. (2012). DBIRD complex integrates alternative mRNA splicing with RNA polymerase II transcript elongation. Nature *484*, 386–389.

Cougot, N., Babajko, S., and Séraphin, B. (2004). Cytoplasmic foci are sites of mRNA decay in human cells. J. Cell Biol. *165*, 31–40.

Couvillion, M.T., Bounova, G., Purdom, E., Speed, T.P., and Collins, K. (2012). A Tetrahymena Piwi bound to mature tRNA 3′ fragments activates the exonuclease Xrn2 for RNA processing in the nucleus. Mol. Cell *48*, 509–520.

Das, B., Butler, J.S., and Sherman, F. (2003). Degradation of normal mRNA in the nucleus of Saccharomyces cerevisiae. Mol. Cell. Biol. *23*, 5502–5515.

Davidson, L., Kerr, A., and West, S. (2012). Co-transcriptional degradation of aberrant pre-mRNA by Xrn2. EMBO J. *31*, 2566–2578.

Dayie, K.T., and Padgett, R. a (2008). A glimpse into the active site of a group II intron and maybe the spliceosome, too. RNA *14*, 1697–1703.

Dengl, S., and Cramer, P. (2009). Torpedo nuclease Rat1 is insufficient to terminate RNA polymerase II in Vitro. J. Biol. Chem. *284*, 21270–21279.

Denli, A.M., Tops, B.B.J., Plasterk, R.H. a, Ketting, R.F., and Hannon, G.J. (2004). Processing of primary microRNAs by the Microprocessor complex. Nature *432*, 231–235.

Van Dijk, E.L., Chen, C.L., D'Aubenton-Carafa, Y., Gourvennec, S., Kwapisz, M., Roche, V., Bertrand, C., Silvain, M., Legoix-Né, P., Loeillet, S., et al. (2011). XUTs are a class of Xrn1-sensitive antisense regulatory non-coding RNA in yeast. Nature *475*, 114–117.

Drązkowska, K., Tomecki, R., Stoduś, K., Kowalska, K., Czarnocki-Cieciura, M., and Dziembowski, A. (2013). The RNA exosome complex central channel controls both exonuclease and endonuclease Dis3 activities in vivo and in vitro. Nucleic Acids Res. *41*, 3845–3858.

Eberle, A.B., Lykke-Andersen, S., Mühlemann, O., and Jensen, T.H. (2009). SMG6 promotes endonucleolytic cleavage of nonsense mRNA in human cells. Nat. Struct. Mol. Biol. *16*, 49–55.

Ecker, J.R., and Davis, R.W. (1986). Inhibition of gene expression in plant cells by expression of antisense RNA. Proc. Natl. Acad. Sci. U. S. A. *83*, 5372–5376.

Eirew, P., Steif, A., Khattra, J., Ha, G., Yap, D., Farahani, H., Gelmon, K., Chia, S., Mar, C., Wan, A., et al. (2014). Dynamics of genomic clones in breast cancer patient xenografts at single-cell resolution. Nature *518*, 422–426.

Elkayam, E., Kuhn, C.-D., Tocilj, A., Haase, A.D.D., Greene, E.M.M., Hannon, G.J.J., and Joshua-Tor, L. (2012). The Structure of Human Argonaute-2 in Complex with miR-20a. Cell 1–11.

Ender, C., and Meister, G. (2010). Argonaute proteins at a glance. J. Cell Sci. *123*, 1819–1823.

Eulalio, A., Behm-Ansmant, I., Schweizer, D., and Izaurralde, E. (2007). P-body formation is a consequence, not the cause, of RNA-mediated gene silencing. Mol. Cell. Biol. *27*, 3970–3981.

Fabian, M.R., and Sonenberg, N. (2012). The mechanics of miRNA-mediated gene silencing: a look under the hood of miRISC. Nat. Struct. Mol. Biol. *19*, 586–593.

Fabian, M.R., Cieplak, M.K., Frank, F., Morita, M., Green, J., Srikumar, T., Nagar, B., Yamamoto, T., Raught, B., Duchaine, T.F., et al. (2012). miRNA-mediated deadenylation is orchestrated by GW182 through two conserved motifs that interact with CCR4–NOT. Nat. Struct. Mol. Biol. *19*, 364–364.

Faehnle, C.R., Elkayam, E., Haase, A.D., Hannon, G.J., and Joshua-Tor, L. (2013). The Making of a Slicer: Activation of Human Argonaute-1. Cell Rep. 1–9.

Fang, F., Phillips, S., and Butler, J.S. (2005). Rat1p and Rai1p function with the nuclear exosome in the processing and degradation of rRNA precursors. RNA *11*, 1571–1578.

Feaver, W.J., Gileadi, O., Li, Y., and Kornberg, R.D. (1991). CTD kinase associated with yeast RNA polymerase II initiation factor b. Cell *67*, 1223–1230.

Feng, X., Guo, Z., Nourbakhsh, M., Hauser, H., Ganster, R., Shao, L., and Geller, D. a (2002). Identification of a negative response element in the human inducible nitric-oxide synthase (hiNOS) promoter: The role of NF-kappa B-repressing factor (NRF) in basal repression of the hiNOS gene. Proc. Natl. Acad. Sci. U. S. A. *99*, 14212–14217.

Finn, R.D., Clements, J., and Eddy, S.R. (2011). HMMER web server: Interactive sequence similarity searching. Nucleic Acids Res. *39*, 29–37.

Finn, R.D., Bateman, A., Clements, J., Coggill, P., Eberhardt, R.Y., Eddy, S.R., Heger, A., Hetherington, K., Holm, L., Mistry, J., et al. (2014). Pfam: The protein families database. Nucleic Acids Res. *42*, 222–230.

Fire, A., Xu, S., Montgomery, M.K., Kostas, S.A., Driver, S.E., and Mello, C.C. (1998). Potent and specific genetic interference by double-stranded RNA in Caenorhabditis elegans. Nature *391*, 806–811.

Ford, L.P., Bagga, P.S., and Wilusz, J. (1997). The poly(A) tail inhibits the assembly of a 3'-to-5' exonuclease in an in vitro RNA stability system. Mol. Cell. Biol. *17*, 398–406.

Förstemann, K., Horwich, M.D., Wee, L., Tomari, Y., and Zamore, P.D. (2007). Drosophila microRNAs Are Sorted into Functionally Distinct Argonaute Complexes after Production by Dicer-1. Cell *130*, 287–297.

Frand, A.R., Russel, S., and Ruvkun, G. (2005). Functional genomic analysis of C. elegans molting. PLoS Biol. *3*, e312.

Frazão, C., McVey, C.E., Amblar, M., Barbas, A., Vonrhein, C., Arraiano, C.M., and Carrondo, M. a (2006). Unravelling the dynamics of RNA degradation by ribonuclease II and its RNA-bound complex. Nature *443*, 110–114.

Frith, M.C., Pheasant, M., and Mattick, J.S. (2005). The amazing complexity of the human transcriptome. Eur. J. Hum. Genet. *13*, 894–897.

Gan, J., Tropea, J.E., Austin, B.P., Court, D.L., Waugh, D.S., and Ji, X. (2006). Structural insight into the mechanism of double-stranded RNA processing by ribonuclease III. Cell *124*, 355–366.

Gao, J., Aksoy, B.A., Dogrusoz, U., Dresdner, G., Gross, B., Sumer, S.O., Sun, Y., Jacobsen, A., Sinha, R., Larsson, E., et al. (2013). Integrative analysis of complex cancer genomics and clinical profiles using the cBioPortal. Sci. Signal. *6*, pl1.

Garneau, N.L., Wilusz, J., and Wilusz, C.J. (2007). The highways and byways of mRNA decay. Nat. Rev. Mol. Cell Biol. *8*, 113–126.

Gazzani, S., Lawrenson, T., Woodward, C., Headon, D., and Sablowski, R. (2004). A link between mRNA turnover and RNA interference in Arabidopsis. Science *306*, 1046–1048.

Gerbi, S. a., Borovjagin, a. V., Ezrokhi, M., and Lange, T.S. (2001). Ribosome biogenesis: Role of small nucleolar RNA in maturation of eukaryotic rRNA. In Cold Spring Harbor Symposia on Quantitative Biology, pp. 575–590.

Girard, A., Sachidanandam, R., Hannon, G.J., and Carmell, M. a (2006). A germline-specific class of small RNAs binds mammalian Piwi proteins. Nature *442*, 199–202.

Glavan, F., Behm-Ansmant, I., Izaurralde, E., and Conti, E. (2006). Structures of the PIN domains of SMG6 and SMG5 reveal a nuclease within the mRNA surveillance complex. EMBO J. *25*, 5117–5125.

Gnatt, A.L., Cramer, P., Fu, J., Bushnell, D.A., and Kornberg, R.D. (2001). Structural basis of transcription: an RNA polymerase II elongation complex at 3.3 A resolution. Science *292*, 1876–1882.

Gozani, O., Patton, J.G., and Reed, R. (1994). A novel set of spliceosome-associated proteins and the essential splicing factor PSF bind stably to pre-mRNA prior to catalytic step II of the splicing reaction. EMBO J. *13*, 3356–3367.

Granneman, S., Petfalski, E., and Tollervey, D. (2011). A cluster of ribosome synthesis factors regulate pre-rRNA folding and 5.8S rRNA maturation by the Rat1 exonuclease. EMBO J. *30*, 4006–4019.

Gray, N.K., Coller, J.M., Dickson, K.S., and Wickens, M. (2000). Multiple portions of poly(A)-binding protein stimulate translation in vivo. EMBO J. *19*, 4723–4733.

Gregory, R.I., Yan, K.-P., Amuthan, G., Chendrimada, T., Doratotaj, B., Cooch, N., and Shiekhattar, R. (2004). The Microprocessor complex mediates the genesis of microRNAs. Nature *432*, 235–240.

Grima, D.P., Sullivan, M., Zabolotskaya, M. V, Browne, C., Seago, J., Wan, K.C., Okada, Y., and Newbury, S.F. (2008). The 5'-3' exoribonuclease pacman is required for epithelial sheet sealing in Drosophila and genetically interacts with the phosphatase puckered. Biol. Cell *100*, 687–701.

Grishok, A., Pasquinelli, A.E., Conte, D., Li, N., Parrish, S., Ha, I., Baillie, D.L., Fire, A., Ruvkun, G., and Mello, C.C. (2001). Genes and mechanisms related to RNA interference regulate expression of the small temporal RNAs that control C. elegans developmental timing. Cell *106*, 23–34.

Gudipati, R.K., Xu, Z., Lebreton, A., Séraphin, B., Steinmetz, L.M., Jacquier, A., and Libri, D. (2012). Extensive Degradation of RNA Precursors by the Exosome in Wild-Type Cells. Mol. Cell *48*, 409–421.

Guttman, M., and Rinn, J.L. (2012). Modular regulatory principles of large non-coding RNAs. Nature *482*, 339–346.

El Hage, A., Koper, M., Kufel, J., and Tollervey, D. (2008). Efficient termination of transcription by RNA polymerase I requires the 5' exonuclease Rat1 in yeast. Genes Dev. *22*, 1069–1081.

Hamilton, a J., and Baulcombe, D.C. (1999). A species of small antisense RNA in posttranscriptional gene silencing in plants. Science *286*, 950–952.

Hammond, S.M., Bernstein, E., Beach, D., and Hannon, G.J. (2000). An RNA-directed nuclease mediates post-transcriptional gene silencing in Drosophila cells. Nature *404*, 293–296.

Hasan, M.K., Yaguchi, T., Sugihara, T., Kumar, P.K.R., Taira, K., Reddel, R.R., Kaul, S.C., and Wadhwa, R. (2002). CARF is a novel protein that cooperates with mouse p19ARF (human p14ARF) in activating p53. J. Biol. Chem. *277*, 37765–37770.

Hasan, M.K., Yaguchi, T., Minoda, Y., Hirano, T., Taira, K., Wadhwa, R., and Kaul, S.C. (2004). Alternative reading frame protein (ARF)-independent function of CARF (collaborator of ARF) involves its interactions with p53: evidence for a novel p53-activation pathway and its negative feedback control. Biochem. J. *380*, 605–610.

Hauptmann, J., Dueck, A., Harlander, S., Pfaff, J., Merkl, R., and Meister, G. (2013). Turning catalytically inactive human Argonaute proteins into active slicer enzymes. Nat. Struct. Mol. Biol. *20*, 814–817.

Henras, a. K., Soudet, J., Gérus, M., Lebaron, S., Caizergues-Ferrer, M., Mougin, A., and Henry, Y. (2008). The post-transcriptional steps of eukaryotic ribosome biogenesis. Cell. Mol. Life Sci. *65*, 2334–2359.

Henry, Y., Wood, H., Morrissey, J.P., Petfalski, E., Kearsey, S., and Tollervey, D. (1994). The 5′ end of yeast 5.8S rRNA is generated by exonucleases from an upstream cleavage site. EMBO J. *13*, 2452–2463.

Heyer, W.D., Johnson, a W., Reinhart, U., and Kolodner, R.D. (1995). Regulation and intracellular localization of Saccharomyces cerevisiae strand exchange protein 1 (Sep1/Xrn1/Kem1), a multifunctional exonuclease. Mol. Cell. Biol. *15*, 2728–2736.

Hilliker, A.K., and Staley, J.P. (2004). Multiple functions for the invariant AGC triad of U6 snRNA. RNA *10*, 921–928.

Holley, R.W., Apgar, J., Everett, G.A., Madison, J.T., Marquisee, M., Merrill, S.H., Penswick, J.R., and Zamir, A. (1965). Structure of a Ribonucleic Acid. Science *147*, 1462–1465.

Holstege, F.C., Fiedler, U., and Timmers, H.T. (1997). Three transitions in the RNA polymerase II transcription complex during initiation. EMBO J. *16*, 7468–7480.

Houseley, J., and Tollervey, D. (2009). The Many Pathways of RNA Degradation. Cell *136*, 763–776.

Hsin, J., and Manley, J.L. (2012). The RNA polymerase II CTD coordinates transcription and RNA processing. Genes Dev. *26*, 2119–2137.

Huntzinger, E., Kashima, I., Fauser, M., Saulière, J., and Izaurralde, E. (2008). SMG6 is the catalytic endonuclease that cleaves mRNAs containing nonsense codons in metazoan. RNA *14*, 2609–2617.

Hutvágner, G., McLachlan, J., Pasquinelli, a E., Bálint, E., Tuschl, T., and Zamore, P.D. (2001). A cellular function for the RNA-interference enzyme Dicer in the maturation of the let-7 small temporal RNA. Science *293*, 834–838.

Imataka, H., Gradi, A., and Sonenberg, N. (1998). A newly identified N-terminal amino acid sequence of human eIF4G binds poly(A)-binding protein and functions in poly(A)-dependent translation. EMBO J. *17*, 7480–7489.

Jannot, G., Boisvert, M.-E.L., Banville, I.H., and Simard, M.J. (2008). Two molecular features contribute to the Argonaute specificity for the microRNA and RNAi pathways in C. elegans. RNA *14*, 829–835.

Januszyk, K., and Lima, C.D. (2014). The eukaryotic RNA exosome. Curr. Opin. Struct. Biol. *24*, 132–140.

Januszyk, K., Liu, Q., and Lima, C.D. (2011). Activities of human RRP6 and structure of the human RRP6 catalytic domain. RNA *17*, 1566–1577.

Jinek, M., Coyle, S.M., and Doudna, J. a (2011). Coupled 5′ nucleotide recognition and processivity in Xrn1-mediated mRNA decay. Mol. Cell *41*, 600–608.

Johnson, a W. (1997). Rat1p and Xrn1p are functionally interchangeable exoribonucleases that are restricted to and required in the nucleus and cytoplasm, respectively. Mol. Cell. Biol. *17*, 6122–6130.

Jones, C.I., Zabolotskaya, M.V., and Newbury, S.F. (2012). The 5′ - 3' exoribonuclease XRN1/Pacman and its functions in cellular processes and development. Wiley Interdiscip. Rev. RNA *3*, 455–468.

Kaneko, S., Rozenblatt-Rosen, O., Meyerson, M., and Manley, J.L. (2007). The multifunctional protein p54nrb/PSF recruits the exonuclease XRN2 to facilitate pre-mRNA 3′ processing and transcription termination. Genes Dev. *21*, 1779–1789.

Kapranov, P., St Laurent, G., Raz, T., Ozsolak, F., Reynolds, C.P., Sorensen, P.H.B., Reaman, G., Milos, P., Arceci, R.J., Thompson, J.F., et al. (2010). The majority of total nuclear-encoded non-ribosomal RNA in a human cell is "dark matter" un-annotated RNA. BMC Biol. *8*, 149.

Kastenmayer, J.P., and Green, P.J. (2000). Novel features of the XRN-family in Arabidopsis: evidence that AtXRN4, one of several orthologs of nuclear Xrn2p/Rat1p, functions in the cytoplasm. Proc. Natl. Acad. Sci. U. S. A. *97*, 13985–13990.

Kawauchi, J., Mischo, H., Braglia, P., Rondon, A., and Proudfoot, N.J. (2008). Budding yeast RNA polymerases I and II employ parallel mechanisms of transcriptional termination. Genes Dev. *22*, 1082–1092.

Kedersha, N., Stoecklin, G., Ayodele, M., Yacono, P., Lykke-Andersen, J., Fitzler, M.J., Scheuner, D., Kaufman, R.J., Golan, D.E., and Anderson, P. (2005). Stress granules and processing bodies are dynamically linked sites of mRNP remodeling. J. Cell Biol. *169*, 871–884.

Kenna, M., Stevens, A., McCammon, M., and Douglas, M.G. (1993). An essential yeast gene with homology to the exonuclease-encoding XRN1/KEM1 gene also encodes a protein with exoribonuclease activity. Mol. Cell. Biol. *13*, 341–350.

Kershnar, E., Wu, S.Y., and Chiang, C.M. (1998). Immunoaffinity purification and functional characterization of human transcription factor IIH and RNA polymerase II from clonal cell lines that conditionally express epitope-tagged subunits of the multiprotein complexes. J. Biol. Chem. *273*, 34444–34453.

Kerwitz, Y., Kühn, U., Lilie, H., Knoth, A., Scheuermann, T., Friedrich, H., Schwarz, E., and Wahle, E. (2003). Stimulation of poly(A) polymerase through a direct interaction with the nuclear poly(A) binding protein allosterically regulated by RNA. EMBO J. *22*, 3705–3714.

Khorana, H.G., Büchi, H., Ghosh, H., Gupta, N., Jacob, T.M., Kössel, H., Morgan, R., Narang, S.A., Ohtsuka, E., and Wells, R.D. (1966). Polynucleotide synthesis and the genetic code. Cold Spring Harb. Symp. Quant. Biol. *31*, 39–49.

Khvorova, A., Reynolds, A., and Jayasena, S.D. (2003). Functional siRNAs and miRNAs exhibit strand bias. Cell *115*, 209–216.

Kim, M., Krogan, N.J., Vasiljeva, L., Rando, O.J., Nedea, E., Greenblatt, J.F., and Buratowski, S. (2004). The yeast Rat1 exonuclease promotes transcription termination by RNA polymerase II. Nature *432*, 517–522.

Kim, T.K., Lagrange, T., Wang, Y.H., Griffith, J.D., Reinberg, D., and Ebright, R.H. (1997). Trajectory of DNA in the RNA polymerase II transcription preinitiation complex. Proc. Natl. Acad. Sci. U. S. A. *94*, 12268–12273.

Kim, T.K., Ebright, R.H., and Reinberg, D. (2000). Mechanism of ATP-dependent promoter melting by transcription factor IIH. Science *288*, 1418–1422.

Kim, V.N., Han, J., and Siomi, M.C. (2009). Biogenesis of small RNAs in animals. Nat. Rev. Mol. Cell Biol. *10*, 126–139.

Kirsebom, L.A. (2007). RNase P RNA mediated cleavage: Substrate recognition and catalysis. Biochimie *89*, 1183–1194.

Kiss, D.L., and Andrulis, E.D. (2010). Genome-wide analysis reveals distinct substrate specificities of Rrp6, Dis3, and core exosome subunits. RNA *16*, 781–791.

Klinge, S., Voigts-Hoffmann, F., Leibundgut, M., Arpagaus, S., and Ban, N. (2011). Crystal Structure of the Eukaryotic 60S Ribosomal Subunit in Complex with Initiation Factor 6. Science (80-.). *334*, 941–948.

Knight, S.W., and Bass, B.L. (2001). A role for the RNase III enzyme DCR-1 in RNA interference and germ line development in Caenorhabditis elegans. Science *293*, 2269–2271.

Körner, C.G., and Wahle, E. (1997). Poly(A) tail shortening by a mammalian poly(A)-specific 3'-exoribonuclease. J. Biol. Chem. *272*, 10448–10456.

Krissinel, E., and Henrick, K. (2007). Inference of macromolecular assemblies from crystalline state. J. Mol. Biol. *372*, 774–797.

Krol, J., Loedige, I., and Filipowicz, W. (2010). The widespread regulation of microRNA biogenesis, function and decay. Nat. Rev. Genet.

Kruger, K., Grabowski, P.J., Zaug, A.J., Sands, J., Gottschling, D.E., and Cech, T.R. (1982). Self-splicing RNA: autoexcision and autocyclization of the ribosomal RNA intervening sequence of Tetrahymena. Cell *31*, 147–157.

Kühn, U., Gündel, M., Knoth, A., Kerwitz, Y., Rüdel, S., and Wahle, E. (2009). Poly(A) tail length is controlled by the nuclear Poly(A)-binding protein regulating the interaction between Poly(A) polymerase and the cleavage and polyadenylation specificity factor. J. Biol. Chem. *284*, 22803–22814.

De la Sierra-Gallay, I.L., Pellegrini, O., and Condon, C. (2005). Structural basis for substrate binding, cleavage and allostery in the tRNA maturase RNase Z. Nature *433*, 657–661.

Lai, E.C. (2002). Micro RNAs are complementary to 3' UTR sequence motifs that mediate negative post-transcriptional regulation. Nat. Genet. *30*, 363–364.

Larimer, F.W., and Stevens, A. (1990). Disruption of the gene XRN1, coding for a 5' --> 3' exoribonuclease, restricts yeast cell growth. Gene *95*, 85–90.

Lebreton, A., Tomecki, R., Dziembowski, A., and Séraphin, B. (2008). Endonucleolytic RNA cleavage by a eukaryotic exosome. Nature *456*, 993–996.

Lee, R.C., Feinbaum, R.L., and Ambros, V. (1993). The C. elegans heterochronic gene lin-4 encodes small RNAs with antisense complementarity to lin-14. Cell *75*, 843–854.

Lee, Y., Jeon, K., Lee, J.T., Kim, S., and Kim, V.N. (2002). MicroRNA maturation: Stepwise processing and subcellular localization. EMBO J. *21*, 4663–4670.

Lee, Y., Ahn, C., Han, J., Choi, H., Kim, J., Yim, J., Lee, J., Provost, P., Rådmark, O., Kim, S., et al. (2003). The nuclear RNase III Drosha initiates microRNA processing. Nature *425*, 415–419.

Lejeune, F., Li, X., and Maquat, L.E. (2003). Nonsense-mediated mRNA decay in mammalian cells involves decapping, deadenylating, and exonucleolytic activities. Mol. Cell *12*, 675–687.

Lesser, C.F., and Guthrie, C. (1993). Mutations in U6 snRNA that alter splice site specificity: implications for the active site. Science *262*, 1982–1988.

Lewis, B.P., Shih, I.H., Jones-Rhoades, M.W., Bartel, D.P., and Burge, C.B. (2003). Prediction of Mammalian MicroRNA Targets. Cell *115*, 787–798.

Li, S., Lian, S.L., Moser, J.J., Fritzler, M.L., Fritzler, M.J., Satoh, M., and Chan, E.K.L. (2008). Identification of GW182 and its novel isoform TNGW1 as translational repressors in Ago2-mediated silencing. J. Cell Sci. *121*, 4134–4144.

Li, Y., Yamane, D., and Lemon, S.M. (2015). Dissecting the roles of the 5′ exoribonucleases Xrn1 and Xrn2 in restricting hepatitis C virus replication. J. Virol. JVI.03692–14.

Liang, S., and Lutz, C.S. (2006). p54nrb is a component of the snRNP-free U1A (SF-A) complex that promotes pre-mRNA cleavage during polyadenylation. RNA *12*, 111–121.

Lim, L.P., Lau, N.C., Garrett-Engele, P., Grimson, A., Schelter, J.M., Castle, J., Bartel, D.P., Linsley, P.S., and Johnson, J.M. (2005). Microarray analysis shows that some microRNAs downregulate large numbers of target mRNAs. Nature *433*, 769–773.

Lingel, A., Simon, B., Izaurralde, E., and Sattler, M. (2003). Structure and nucleic-acid binding of the Drosophila Argonaute 2 PAZ domain. Nature *426*, 465–469.

Liu, Q., Greimann, J.C., and Lima, C.D. (2006). Reconstitution, Activities, and Structure of the Eukaryotic RNA Exosome. Cell *127*, 1223–1237.

Lorentzen, E., Basquin, J., Tomecki, R., Dziembowski, A., and Conti, E. (2008). Structure of the Active Subunit of the Yeast Exosome Core, Rrp44: Diverse Modes of Substrate Recruitment in the RNase II Nuclease Family. Mol. Cell *29*, 717–728.

Lu, H., Zawel, L., Fisher, L., Egly, J.M., and Reinberg, D. (1992). Human general transcription factor IIH phosphorylates the C-terminal domain of RNA polymerase II. Nature *358*, 641–645.

Lu, Y., Liu, P., James, M., Vikis, H.G., Liu, H., Wen, W., Franklin, A., and You, M. (2010). Genetic variants cis-regulating Xrn2 expression contribute to the risk of spontaneous lung tumor. Oncogene *29*, 1041–1049.

Luke, B., Panza, A., Redon, S., Iglesias, N., Li, Z., and Lingner, J. (2008). The Rat1p 5′ to 3' exonuclease degrades telomeric repeat-containing RNA and promotes telomere elongation in Saccharomyces cerevisiae. Mol. Cell *32*, 465–477.

Lund, E., Güttinger, S., Calado, A., Dahlberg, J.E., and Kutay, U. (2004). Nuclear export of microRNA precursors. Science *303*, 95–98.

Luo, W., Johnson, A.W., and Bentley, D.L. (2006). The role of Rat1 in coupling mRNA 3′-end processing to transcription termination: implications for a unified allosteric-torpedo model. Genes Dev. *20*, 954–965.

Macrae, I.J., Zhou, K., Li, F., Repic, A., Brooks, A.N., Cande, W.Z., Adams, P.D., and Doudna, J. a (2006). Structural basis for double-stranded RNA processing by Dicer. Science *311*, 195–198.

MacRae, I.J., Zhou, K., and Doudna, J.A. (2007). Structural determinants of RNA recognition and cleavage by Dicer. Nat. Struct. Mol. Biol. *14*, 934–940.

MacRae, I.J., Ma, E., Zhou, M., Robinson, C. V, and Doudna, J. a (2008). In vitro reconstitution of the human RISC-loading complex. Proc. Natl. Acad. Sci. U. S. A. *105*, 512–517.

Malecki, M., Viegas, S.C., Carneiro, T., Golik, P., Dressaire, C., Ferreira, M.G., and Arraiano, C.M. (2013). The exoribonuclease Dis3L2 defines a novel eukaryotic RNA degradation pathway. EMBO J. *32*, 1842–1854.

Mandel, C.R., Kaneko, S., Zhang, H., Gebauer, D., Vethantham, V., Manley, J.L., and Tong, L. (2006). Polyadenylation factor CPSF-73 is the pre-mRNA 3′-end-processing endonuclease. Nature *444*, 953–956.

Maniatis, T., and Reed, R. (2002). An extensive network of coupling among gene expression machines. Nature *416*, 499–506.

Mathews, D.H., Disney, M.D., Childs, J.L., Schroeder, S.J., Zuker, M., and Turner, D.H. (2004). Incorporating chemical modification constraints into a dynamic programming algorithm for prediction of RNA secondary structure. Proc. Natl. Acad. Sci. U. S. A. *101*, 7287–7292.

Mathys, H., Basquin, J., Ozgur, S., Czarnocki-Cieciura, M., Bonneau, F., Aartse, A., Dziembowski, A., Nowotny, M., Conti, E., and Filipowicz, W. (2014). Structural and Biochemical Insights to the Role of the CCR4-NOT Complex and DDX6 ATPase in MicroRNA Repression. Mol. Cell *54*, 751–765.

Mattick, J.S. (2001). Non-coding RNAs: The architects of eukaryotic complexity. EMBO Rep. *2*, 986–991.

Mattick, J.S., and Makunin, I. V. (2006). Non-coding RNA. Hum. Mol. Genet. *15 Spec No*, 17–29.

Meister, G., Landthaler, M., Peters, L., Chen, P.Y., Urlaub, H., Lührmann, R., and Tuschl, T. (2005). Identification of novel argonaute-associated proteins. Curr. Biol. *15*, 2149–2155.

Mi, S., Cai, T., Hu, Y., Chen, Y., Hodges, E., Ni, F., Wu, L., Li, S., Zhou, H., Long, C., et al. (2008). Sorting of Small RNAs into Arabidopsis Argonaute Complexes Is Directed by the 5′ Terminal Nucleotide. Cell *133*, 116–127.

Midtgaard, S.F., Assenholt, J., Jonstrup, A.T., Van, L.B., Jensen, T.H., and Brodersen, D.E. (2006). Structure of the nuclear exosome component Rrp6p reveals an interplay between the active site and the HRDC domain. Proc. Natl. Acad. Sci. U. S. A. *103*, 11898–11903.

Miki, T.S., and Großhans, H. (2013). The multifunctional RNase XRN2. Biochem. Soc. Trans. *41*, 825–830.

Miki, T.S., Rüegger, S., Gaidatzis, D., Stadler, M.B., and Großhans, H. (2014a). Engineering of a conditional allele reveals multiple roles of XRN2 in Caenorhabditis elegans development and substrate specificity in microRNA turnover. Nucleic Acids Res. 1–12.

Miki, T.S., Richter, H., Rüegger, S., and Großhans, H. (2014b). PAXT-1 promotes XRN2 activity by stabilizing it through a conserved domain. Mol. Cell *53*, 351–360.

Minagawa, A., Takaku, H., Takagi, M., and Nashimoto, M. (2004). A novel endonucleolytic mechanism to generate the CCA 3′ termini of tRNA molecules in Thermotoga maritima. J. Biol. Chem. *279*, 15688–15697.

Muhlrad, D., Decker, C.J., and Parker, R. (1994). Deadenylation of the unstable mRNA encoded by the yeast MFA2 gene leads to decapping followed by 5′-->3' digestion of the transcript. Genes Dev. *8*, 855–866.

Murthy, K.G.K., and Manley, J.L. (1995). The 160-kD subunit of human cleavage-polyadenylation specificity factor coordinates pre-mRNA 3′-end formation. Genes Dev. *9*, 2672–2683.

Myer, V.E., and Young, R. a (1998). RNA polymerase II holoenzymes and subcomplexes. J. Biol. Chem. *273*, 27757–27760.

Nagarajan, V.K., Jones, C.I., Newbury, S.F., and Green, P.J. (2013). XRN 5′→3' exoribonucleases: Structure, mechanisms and functions. Biochim. Biophys. Acta - Gene Regul. Mech. *1829*, 590–603.

Neil, H., Malabat, C., D'Aubenton-Carafa, Y., Xu, Z., Steinmetz, L.M., and Jacquier, A. (2009). Widespread bidirectional promoters are the major source of cryptic transcripts in yeast. Nature *457*, 1038–1042.

Newbury, S.F. (2006). Control of mRNA stability in eukaryotes. Biochem. Soc. Trans. *34*, 30–34.

Newbury, S., and Woollard, A. (2004). The 5′-3' exoribonuclease xrn-1 is essential for ventral epithelial enclosure during C. elegans embryogenesis. RNA *10*, 59–65.

Nirenberg, M., Caskey, T., Marshall, R., Brimacombe, R., Kellogg, D., Doctor, B., Hatfield, D., Levin, J., Rottman, F., Pestka, S., et al. (1966). The RNA code and protein synthesis. Cold Spring Harb. Symp. Quant. Biol. *31*, 11–24.

Nissan, T., Rajyaguru, P., She, M., Song, H., and Parker, R. (2010). Decapping Activators in Saccharomyces cerevisiae Act by Multiple Mechanisms. Mol. Cell *39*, 773–783.

Nissen, P., Hansen, J., Ban, N., Moore, P.B., and Steitz, T. a (2000). The structural basis of ribosome activity in peptide bond synthesis. Science *289*, 920–930.

O'Sullivan, R.J., and Karlseder, J. (2010). Telomeres: protecting chromosomes against genome instability. Nat. Rev. Mol. Cell Biol. *11*, 171–181.

Oeffinger, M., Zenklusen, D., Ferguson, A., Wei, K.E., El Hage, A., Tollervey, D., Chait, B.T., Singer, R.H., and Rout, M.P. (2009). Rrp17p Is a Eukaryotic Exonuclease Required for 5′ End Processing of Pre-60S Ribosomal RNA. Mol. Cell *36*, 768–781.

Ohno, S. (1972). So much "junk" DNA in our genome. Brookhaven Symp. Biol. *23*, 366–370.

Okamura, K., Liu, N., and Lai, E.C. (2009). Distinct Mechanisms for MicroRNA Strand Selection by Drosophila Argonautes. Mol. Cell *36*, 431–444.

Otero, L.J., Ashe, M.P., and Sachs, A.B. (1999). The yeast poly(A)-binding protein Pab1p stimulates in vitro poly(A)-dependent and cap-dependent translation by distinct mechanisms. EMBO J. *18*, 3153–3163.

Pall, G.S., and Hamilton, A.J. (2008). Improved northern blot method for enhanced detection of small RNA. Nat. Protoc. *3*, 1077–1084.

Pena, V., Rozov, A., Fabrizio, P., Lührmann, R., and Wahl, M.C. (2008). Structure and function of an RNase H domain at the heart of the spliceosome. EMBO J. *27*, 2929–2940.

Peters, L., and Meister, G. (2007). Argonaute Proteins: Mediators of RNA Silencing. Mol. Cell *26*, 611–623.

Petfalski, E., Dandekar, T., Henry, Y., and Tollervey, D. (1998). Processing of the precursors to small nucleolar RNAs and rRNAs requires common components. Mol. Cell. Biol. *18*, 1181–1189.

Piao, X., Zhang, X., Wu, L., and Belasco, J.G. (2010). CCR4-NOT deadenylates mRNA associated with RNA-induced silencing complexes in human cells. Mol. Cell. Biol. *30*, 1486–1494.

Poole, T.L., and Stevens, A. (1995). Comparison of features of the RNase activity of 5'-exonuclease-1 and 5'-exonuclease-2 of Saccharomyces cerevisiae. Nucleic Acids Symp. Ser. 79–81.

Poole, T.L., and Stevens, A. (1997). Structural modifications of RNA influence the 5' exoribonucleolytic hydrolysis by XRN1 and HKE1 of Saccharomyces cerevisiae. Biochem. Biophys. Res. Commun. *235*, 799–805.

Qu, L.H., Henras, A., Lu, Y.J., Zhou, H., Zhou, W.X., Zhu, Y.Q., Zhao, J., Henry, Y., Caizergues-Ferrer, M., and Bachellerie, J.P. (1999). Seven novel methylation guide small nucleolar RNAs are processed from a common polycistronic transcript by Rat1p and RNase III in yeast. Mol. Cell. Biol. *19*, 1144–1158.

Rabl, J., Leibundgut, M., Ataide, S.F., Haag, A., and Ban, N. (2011). Crystal structure of the eukaryotic 40S ribosomal subunit in complex with initiation factor 1. Science *331*, 730–736.

Ratcliff, F., Harrison, B.D., and Baulcombe, D.C. (1997). A similarity between viral defense and gene silencing in plants. Science *276*, 1558–1560.

Rebbapragada, I., and Lykke-Andersen, J. (2009). Execution of nonsense-mediated mRNA decay: what defines a substrate? Curr. Opin. Cell Biol. *21*, 394–402.

Rehwinkel, J., Behm-Ansmant, I., Gatfield, D., and Izaurralde, E. (2005). A crucial role for GW182 and the DCP1:DCP2 decapping complex in miRNA-mediated gene silencing. RNA *11*, 1640–1647.

Ritchie, D.B., Schellenberg, M.J., Gesner, E.M., Raithatha, S. a, Stuart, D.T., and Macmillan, A.M. (2008). Structural elucidation of a PRP8 core domain from the heart of the spliceosome. Nat. Struct. Mol. Biol. *15*, 1199–1205.

Rivas, F. V, Tolia, N.H., Song, J.-J., Aragon, J.P., Liu, J., Hannon, G.J., and Joshua-Tor, L. (2005). Purified Argonaute2 and an siRNA form recombinant human RISC. Nat. Struct. Mol. Biol. *12*, 340–349.

Schimmel, P., Giegé, R., Moras, D., and Yokoyama, S. (1993). An operational RNA code for amino acids and possible relationship to genetic code. Proc. Natl. Acad. Sci. U. S. A. *90*, 8763–8768.

Schirle, N.T., and MacRae, I.J. (2012). The crystal structure of human Argonaute2. Science *336*, 1037–1040.

Schmeing, T.M., and Ramakrishnan, V. (2009). What recent ribosome structures have revealed about the mechanism of translation. Nature *461*, 1234–1242.

Schmitt, M.E., and Clayton, D. a (1993). Nuclear RNase MRP is required for correct processing of pre-5.8S rRNA in Saccharomyces cerevisiae. Mol. Cell. Biol. *13*, 7935–7941.

Schneider, C., and Tollervey, D. (2013). Threading the barrel of the RNA exosome. Trends Biochem. Sci. *38*, 485–493.

Schoenberg, D.R. (2011). Mechanisms of endonuclease-mediated mRNA decay. Wiley Interdiscip. Rev. RNA *2*, 582–600.

Schürmann, N., Trabuco, L.G., Bender, C., Russell, R.B., and Grimm, D. (2013). Molecular dissection of human Argonaute proteins by DNA shuffling. Nat. Struct. Mol. Biol. *20*, 818–826.

Schwarz, D.S., Hutvágner, G., Du, T., Xu, Z., Aronin, N., and Zamore, P.D. (2003). Asymmetry in the assembly of the RNAi enzyme complex. Cell *115*, 199–208.

Sedano, C.D., and Sarnow, P. (2014). Hepatitis C virus subverts liver-specific miR-122 to protect the viral genome from exoribonuclease Xrn2. Cell Host Microbe *16*, 257–264.

Shadel, G.S., Buckenmeyer, G. a., Clayton, D. a., and Schmitt, M.E. (2000). Mutational analysis of the RNA component of Saccharomyces cerevisiae RNase MRP reveals distinct nuclear phenotypes. Gene *245*, 175–184.

Shatkin, a J. (1976). Capping of eucaryotic mRNAs. Cell *9*, 645–653.

Sheth, U., and Parker, R. (2003). Decapping and decay of messenger RNA occur in cytoplasmic processing bodies. Science *300*, 805–808.

Sinturel, F., Pellegrini, O., Xiang, S., Tong, L., Condon, C., and Bénard, L. (2009). Real-time fluorescence detection of exoribonucleases. RNA *15*, 2057–2062.

Sinturel, F., Bréchemier-Baey, D., Kiledjian, M., Condon, C., and Bénard, L. (2012). Activation of 5′-3' exoribonuclease Xrn1 by cofactor Dcs1 is essential for mitochondrial function in yeast. Proc. Natl. Acad. Sci. U. S. A. 3–8.

Song, J., Smith, S.K., Hannon, G.J., and Joshua-Tor, L. (2004). Crystal structure of Argonaute and its implications for RISC slicer activity. Science *305*, 1434–1437.

Stalder, L., and Mühlemann, O. (2009). Processing bodies are not required for mammalian nonsense-mediated mRNA decay. RNA *15*, 1265–1273.

Steiner, F. a, Hoogstrate, S.W., Okihara, K.L., Thijssen, K.L., Ketting, R.F., Plasterk, R.H. a, and Sijen, T. (2007). Structural features of small RNA precursors determine Argonaute loading in Caenorhabditis elegans. Nat. Struct. Mol. Biol. *14*, 927–933.

Steitz, T. a, and Steitz, J. a (1993). A general two-metal-ion mechanism for catalytic RNA. Proc. Natl. Acad. Sci. U. S. A. *90*, 6498–6502.

Stevens, A., and Poole, T.L. (1995). 5'-exonuclease-2 of Saccharomyces cerevisiae. Purification and features of ribonuclease activity with comparison to 5'-exonuclease-1. J. Biol. Chem. *270*, 16063–16069.

Timmons, L., and Fire, A. (1998). Specific interference by ingested dsRNA. Nature *395*, 854.

Tinoco, I., and Bustamante, C. (1999). How RNA folds. J. Mol. Biol. *293*, 271–281.

Tishkoff, D.X., Rockmill, B., Roeder, G.S., and Kolodner, R.D. (1995). The sep1 mutant of Saccharomyces cerevisiae arrests in pachytene and is deficient in meiotic recombination. Genetics *139*, 495–509.

Tomecki, R., Kristiansen, M.S., Lykke-Andersen, S., Chlebowski, A., Larsen, K.M., Szczesny, R.J., Drazkowska, K., Pastula, A., Andersen, J.S., Stepien, P.P., et al. (2010). The human core exosome interacts with differentially localized processive RNases: hDIS3 and hDIS3L. EMBO J. *29*, 2342–2357.

Uhlén, M., Fagerberg, L., Hallström, B.M., Lindskog, C., Oksvold, P., Mardinoglu, A., Sivertsson, Å., Kampf, C., Sjöstedt, E., Asplund, A., et al. (2015). Tissue-based map of the human proteome. Science *347*, 1260419–1260419.

Valadkhan, S., Mohammadi, A., Wachtel, C., and Manley, J.L. (2007). Protein-free spliceosomal snRNAs catalyze a reaction that resembles the first step of splicing. RNA *13*, 2300–2311.

Voorhees, R.M., Weixlbaumer, A., Loakes, D., Kelley, A.C., and Ramakrishnan, V. (2009). Insights into substrate stabilization from snapshots of the peptidyl transferase center of the intact 70S ribosome. Nat. Struct. Mol. Biol. *16*, 528–533.

Wachtel, C., and Manley, J.L. (2009). Splicing of mRNA precursors: the role of RNAs and proteins in catalysis. Mol. Biosyst. *5*, 311–316.

Wagschal, A., Rousset, E., Basavarajaiah, P., Contreras, X., Harwig, A., Laurent-Chabalier, S., Nakamura, M., Chen, X., Zhang, K., Meziane, O., et al. (2012). Microprocessor, Setx, Xrn2, and Rrp6 co-operate to induce premature termination of transcription by RNAPII. Cell *150*, 1147–1157.

Wahle, E. (1991). A novel poly(A)-binding protein acts as a specificity factor in the second phase of messenger RNA polyadenylation. Cell *66*, 759–768.

Wang, M., and Pestov, D.G. (2011). 5'-end surveillance by Xrn2 acts as a shared mechanism for mammalian pre-rRNA maturation and decay. Nucleic Acids Res. *39*, 1811–1822.

Wang, W., Carey, M., and Gralla, J.D. (1992). Polymerase II promoter activation: closed complex formation and ATP-driven start site opening. Science *255*, 450–453.

Wasmuth, E. V, and Lima, C.D. (2012). Exo- and Endoribonucleolytic Activities of Yeast Cytoplasmic and Nuclear RNA Exosomes Are Dependent on the Noncatalytic Core and Central Channel. Mol. Cell *48*, 133–144.

Wei, P.-C., Lo, W.-T., Su, M.-I., Shew, J.-Y., and Lee, W.-H. (2011). Non-targeting siRNA induces NPGPx expression to cooperate with exoribonuclease XRN2 for releasing the stress. Nucleic Acids Res. 1–10.

West, S., Gromak, N., and Proudfoot, N.J. (2004). Human 5′ --> 3' exonuclease Xrn2 promotes transcription termination at co-transcriptional cleavage sites. Nature *432*, 522–525.

Westheimer, F.H. (1987). Why nature chose phosphates. Science *235*, 1173–1178.

Wichtowska, D., Turowski, T.W., and Boguta, M. (2013). An interplay between transcription, processing, and degradation determines tRNA levels in yeast. Wiley Interdiscip. Rev. RNA *4*, 709–722.

Wightman, B., Bürglin, T.R., Gatto, J., Arasu, P., and Ruvkun, G. (1991). Negative regulatory sequences in the lin-14 3′-untranslated region are necessary to generate a temporal switch during Caenorhabditis elegans development. Genes Dev. *5*, 1813–1824.

Will, C.L., and Lührmann, R. (2011). Spliceosome structure and function. Cold Spring Harb. Perspect. Biol. *3*, 1–2.

Wormington, M., Searfoss, a M., and Hurney, C. a (1996). Overexpression of poly(A) binding protein prevents maturation-specific deadenylation and translational inactivation in Xenopus oocytes. EMBO J. *15*, 900–909.

Xiang, S., Cooper-Morgan, A., Jiao, X., Kiledjian, M., Manley, J.L., and Tong, L. (2009). Structure and function of the 5′-->3' exoribonuclease Rat1 and its activating partner Rai1. Nature *458*, 784–788.

Xiao, S., Houser-Scott, F., and Engelke, D.R. (2001). Eukaryotic ribonuclease P: Increased complexity to cope with the nuclear pre-tRNA pathway. J. Cell. Physiol. *187*, 11–21.

Xue, Y., Bai, X., Lee, I., Kallstrom, G., Ho, J., Brown, J., Stevens, A., and Johnson, a W. (2000). Saccharomyces cerevisiae RAI1 (YGL246c) is homologous to human DOM3Z and encodes a protein that binds the nuclear exoribonuclease Rat1p. Mol. Cell. Biol. *20*, 4006–4015.

Yan, K.S., Yan, S., Farooq, A., Han, A., Zeng, L., and Zhou, M.-M. (2003). Structure and conserved RNA binding of the PAZ domain. Nature *426*, 468–474.

Yang, W. (2011). Nucleases: diversity of structure, function and mechanism. Q. Rev. Biophys. *44*, 1–93.

Yang, K., Zhang, L., Xu, T., Heroux, A., and Zhao, R. (2008). Crystal structure of the beta-finger domain of Prp8 reveals analogy to ribosomal proteins. Proc. Natl. Acad. Sci. U. S. A. *105*, 13817–13822.

Yang, W., Lee, J.Y., and Nowotny, M. (2006). Making and Breaking Nucleic Acids: Two-Mg2+-Ion Catalysis and Substrate Specificity. Mol. Cell *22*, 5–13.

Yi, R., Doehle, B.P., Qin, Y., Macara, I.G., and Cullen, B.R. (2005). Overexpression of exportin 5 enhances RNA interference mediated by short hairpin RNAs and microRNAs. RNA *11*, 220–226.

Zabolotskaya, M. V, Grima, D.P., Lin, M.-D., Chou, T.-B., and Newbury, S.F. (2008). The 5'-3' exoribonuclease Pacman is required for normal male fertility and is dynamically localized in cytoplasmic particles in Drosophila testis cells. Biochem. J. *416*, 327–335.

Zakrzewska-Placzek, M., Souret, F.F., Sobczyk, G.J., Green, P.J., and Kufel, J. (2010). Arabidopsis thaliana XRN2 is required for primary cleavage in the pre-ribosomal RNA. Nucleic Acids Res. *38*, 4487–4502.

Zhang, K., Dion, N., Fuchs, B., Damron, T., Gitelis, S., Irwin, R., O'Connor, M., Schwartz, H., Scully, S.P., Rock, M.G., et al. (2002). The human homolog of yeast SEP1 is a novel candidate tumor suppressor gene in osteogenic sarcoma. Gene *298*, 121–127.

V Appendix

PAXT-1 Promotes XRN2 Activity by Stabilizing it through a Conserved Domain